Safety in Mines Research Advisory Committee

Final Project Report

Further Validation of Bracket Pillar Design Methodology

Fernando Vieira, Tufan Dede,

Roger Stewart, Anthony Ruskovich

Research agency : CSIR Mining Technology, Rock Engineering
Project No : GAP 516
Date : July 1998

Executive summary

Design charts for bracket pillar design were developed under a previous SIMRAC project GAP 223 to provide rock mechanics engineers with an initial estimate of bracket pillar sizes for clearly identified geological discontinuities, based on mining and geological factors that would be easily measured. A methodology for the application of such a design tool had then been proposed. The novel characteristic of this pillar design approach was the allowance to "tolerate" a certain level of seismic risk along the bracketed feature. Once an informed decision is made regarding the level of seismic risk to be accepted for a given layout, the rock engineer obtains from "design charts" a recommendable pillar width, assumed to keep the risk of "slip type events" below the pre-accepted level. It was felt that designing for an acceptable level of seismicity (e.g. for a tolerable event magnitude) would be less conservative but more realistic an approach than requiring, for instance, zero ESS, as had previously been practiced.

GAP 516, the current project, was concerned with the applicability of the above design approach to real mine geometries and has concentrated, therefore, on studying the behaviour of various closely monitored bracket pillars, including a validation, based on field data, of the bracket pillar design methodology. The methodology has also been reviewed.

To better understand the intrinsic behaviour of geological features as well as the failure mechanism of these when being bracketed, an underground site was identified, and a portable seismic system (PSS) installed. Based on the mining taking place in the area, eight different seismological regions were defined and summaries of mining and seismic information for each area were produced.

Seismic data from the selected site was processed and interpreted. Back analyses were carried out which attempted to compare modelling data and field seismic data for the actual bracket pillar layouts. Seismic moments calculated from seismograms for seismic events in the vicinity of actual geological structures and bracket pillars were compared with theoretical values produced under project GAP 223 from 2-D DIGS-based bracket pillar designs (i.e. the design charts) and from numerical modelling using MAP3D designs. Good agreement between seismic parameters from the field sites and those from equivalent numerical models was obtained.

The results from three-dimensional modelling were compared to those from two-dimensional DIGS models, given that the available pillar design charts were obtained

from DIGS two-dimensional bracket pillar models, under plain strain conditions. Differences were encountered and are discussed in this report.

In combining the seismic studies of the monitored features with modelling studies, reasonably good agreement was found between the occurrence of the larger seismic events and the positions of slip expected from the three-dimensional modelling. The larger events tended to locate along geological structure planes and, specifically, in the proximity of the expected slip positions on various discontinuities.

The cumulative seismic moment of field events and the cumulative seismic moment obtained from MAP3D modelling agreed well. It was evident that some geological features were better modelled by including the influences from the out-of-plane dimension. A wider scatter and, therefore, weaker association from the 2-D DIGS/design charts results relative to field data was observed. It was found that 2-D DIGS provides values of slip greater than those obtained by MAP3D, for all modelled geological features considered in the study.

It was felt that the results of this study give grounds for confidence in the usefulness of the type of numerical modelling conducted for designing layouts that incorporate geological discontinuities. The bracket pillar design methodology, in particular, developed during the course of SIMRAC Project GAP 223 and refined by 3D modelling as presented in this report, would appear to be a valid tool when applied judiciously by qualified rock mechanics practitioners. Designs derived from design charts alone, however, would appear to be more conservative than designs based on 3D modelling that allow for explicit displacement along discontinuities and irregular geometries. On the strength of this finding, therefore, it would be recommended that 3D modelling codes that allow for explicit displacement along discontinuities and irregular geometries (for example Map3D) should be used when modelling bracket pillar layouts.

Preface

SIMRAC project GAP 516 was formulated to expand on some research work conducted under Project GAP 223: Deep Mine Layout Design Criteria (Vieira et al., 1998). More specifically, only output No. 1 of GAP 223, specified as "Bracket Pillars", was to be considered for extended study. The intent of GAP 516, as stated in the project proposal, was to undertake a "Study on the behaviour of various closely monitored bracket pillars, including a validation, based on field data, of a proposed bracket pillar design methodology" (see copy of approved project definition on page 6). Two aspects of research, therefore, were to be taken into account under the scope of work of the current project: the first requiring some study on the behaviour of geological features from a pre-selected mining area (an area selected previously under GAP 223), and the second the validation of an existent bracket pillar design methodology (also previously defined under GAP 223).

The first part of the study would involve recording, processing and interpretation of seismic data obtained using a PSS network, which had already been installed in the area of interest. The second and most relevant part of the study involved the validation of the GAP 223 bracket pillar design methodology, summarily described in section 3.4. Such work was carried out by applying principles of bracket pillar design, proposed under GAP 223, to a "bracket pillar area" for which appropriate seismic coverage had been arranged. Pillars and structures were modelled numerically and the model results compared to field data, in order to determine associations between these.

The project proposal of GAP 516 indicates that this project has one major enabling output (see table below), namely the "Field monitoring of bracket pillars". A breakdown of the required sub-outputs, all of which are addressed and discussed in the body of this report, is as listed below:

Output No.	GAP 516 Enabling Output, as per accepted SIMRAC Project Proposal
1	**Field monitoring of bracket pillars**
1.1	Report on improved understanding of seismic behaviour of bracketed faults and dykes. → Reported in section 2.
1.2	Report on numerical modelling approaches that evaluate potential behaviour of bracketed features, including the use of numerical codes, which may assist in bracket pillar design. → Reported in section 3.
1.3	Combine analysis and findings from output 1.1 and 1.2 and report on improved bracket pillar design considerations, including validation of available design criteria. → Reported in section 4.

The outputs above were addressed by firstly conducting a study on the behaviour of various closely monitored bracketed features (i.e. sub-task 1.1, addressed in section 2), providing thereby the basis against which bracket pillar designs based on GAP 223 methodology would be validated. On monitoring the behaviour of geological features in the field it had been hoped, in addition, to arrive at an improved understanding of the behaviour of geological features when they are approached by mining operations, thus enabling the identification of adequate strategies to counter the incidence of damaging seismicity in complex geological mining environments.

The study incorporated an evaluation of the potential behaviour of bracketed faults and dykes, based on numerical modelling (i.e. sub-task 1.2, addressed in section 3). These two assessments were subsequently integrated (i.e. sub-task 1.3, addressed in section 4 and partly in section 2), in the hope that the combined analysis would address the validity of designing bracket pillar layouts by using design charts, as proposed in the GAP 223 project. Such verification was effected by means of two- and three-dimensional modelling in the form of a back analysis that considered field seismic data from actual bracket pillar layouts.

Three appendices are included which contain detailed results that have been discussed in the body of the report.

In order to make this report reasonably self-contained, the bracket pillar design methodology which was developed during the course of SIMRAC Project GAP 223 has been summarized in this report (see section 3). The inclusion in this report of material published in a previous SIMRAC publication has been at the request of the GAPREAG committee, which suggested that, as far as practicable, a self-contained final report for GAP 516 should be produced and edited in such a way so that the reader would not be submitted to unnecessary cross references to the GAP 223 final report.

As a partial extension of the GAP 223 work, this report should be seen, therefore, as a supplement to Volume 2 of the final report of GAP 223 project: "Deep Mine Layout Design Criteria, Bracket Pillars" (Vieira et al., 1998). The latter should be consulted should further details on the development of the bracket pillar design methodology, beyond the ones presented here, be required.

Approved project proposal

SIMRAC 1

DEPARTMENT OF MINERAL AND ENERGY AFFAIRS
PROPOSAL FOR A PROJECT TO BE FUNDED IN TERMS OF THE MINERALS ACT
Section I CONFIDENTIAL –

DMEA REFERENCE NUMBER _____ (FOR OFFICIAL USE ONLY)	PROPOSAL TO BE HANDED IN AT MINERALIA, 6th FLOOR RECEPTION, cnr DE BEER/DE KORTE STREETS, BRAAMFONTEIN BEFORE 12:00 ON 30 JULY 1997

1. PROJECT SUMMARY

PROJECT TITLE: Further validation of bracket pillar design methodology

PROJECT LEADER: F.M.C.C. Vieira

ORGANIZATION: CSIR: Division of Mining Technology

ADDRESS: P.O. Box 91230, Auckland Park, 2006

TELEPHONE: (011) 3580000 TELEFAX: (011) 726-5405 TELEX: 4-26070

PRIMARY OUTPUT[1]:	Study on the behaviour of various closely monitored bracket pillars, including a field validation of a proposed bracket pillar design methodology .
HOW USED?[2]:	For assisting the design of mine layouts which have to negotiate discontinuities. To quantify the effects of geologic features on mine layout stability in order to negotiate them safely.
BY WHOM?[3]:	Rock mechanics engineers, Mine planning engineers and Government Mining Engineer.
CRITERIA FOR USE[4]:	Must provide for improved safety and optimal extraction of geologically affected mine layouts.
POTENTIAL IMPACT[5]:	Understanding the behaviour of geological features when approached by mining operations will enable the definition and implementation of adequate strategies to counter the incidence of seismicity, including the frequency of rockbursts and, thus, improve safety.

Figure 1 GAP 223 Project proposal as approved by SIMRAC (Page 1; project definition and major output).

Acknowledgements

The authors of this document gratefully acknowledge that the work reported here results entirely from funding provided by SIMRAC as Project GAP 516. Gratitude is extended to the members of SIMRAC, SIMGAP and GAPREAG for their support of the research programme.

The work has enjoyed the co-operation of the staff at Vaal Reefs Gold Mine 5 Shaft where the research site was situated. The authors would like to thank the management of the mine for their willingness to allow the field work to take place on the mine.

In addition, we would like to express our gratitude to all the personnel on the mine who have provided much needed assistance during the course of the field experiment. Without their help, none of this work would have been possible.

Fruitful discussions were held with the staff of the rock mechanics and seismology departments of Vaal Reefs Gold Mine, and we gratefully acknowledge their provision of seismic data recorded by the mine-wide seismic network from the 5 Shaft area. Lastly, we thank the members of these departments who have sent their comments on the contents of a draft copy of this report. Their views have been noted and they have contributed, therefore, to the improvement of this report.

Table of contents

Page

Page

List of figures

Page

List of tables

Glossary of abbreviations, symbols and terms

Abbreviations

Data Acquisition Unit	DAU
Excess Shear Stress	ESS
Integrated Seismic System	ISS
Peak Particle Velocity	PPV
Portable Seismic System	PSS
Safety in Mines Research Advisory Committee	SIMRAC
Three dimensional	3D
Two dimensional	2D

Symbols

Area of slip	A
Average slip	D
Slip	R
Volume of slip	V
Start of slip pitch	a
End of slip pitch	b
Shear stiffness, modulus of rigidity	G
Max peak particle velocity	V_{max}
Hypocentral distance	r
Seismic moment	M_o

Seismic energy	E
Seismic event magnitude	M
Maximum magnitude	M_{max}
Friction coefficient	μ
Stress : normal	σ_n
: shear	τ_s
: maximum principal	σ_1
Strength, uniaxial compressive	σ_c
Ratio of horizontal to vertical stress	k
Backfill : characteristic stress	a
: ultimate strain	b
Stope span	S
Width of stope	W

Terminology

DAU

Data Acquisition Unit – controls triggering and digitisation for a Portable Seismic System

DIGS

Discontinuity Interaction and Growth Simulation – based on Displacement Discontinuity Method. DIGS is a modelling package capable of fracture growth simulation.

ESS

Excess Shear Stress – a measure of the difference between the sliding forces acting on an interface and the frictional resistance acting on the same. It can be written as: ESS = τ_s - $\sigma_n\mu$, where τ_s = shear stress, σ_n = normal stress and μ = friction coefficient.

MAP3D

Boundary element program based on Indirect Boundary Element Method. MAP3D is a comprehensive three-dimensional rock stability analysis package, used to construct models and analyse, then display displacements, strains, stresses and strength factors. Zones of different moduli may be entered.

KMMA

Klerksdorp Mine Managers Association. An association of mine management of neighbouring mines that owns the Klerksdorp Regional Seismic Network.

1 General introduction

It has been well established that the stress changes associated with deep-level underground mining can induce sudden slip movements on fault and dyke structures. These slip events can result in the occurrence of damaging rockbursts, which impact on excavations in the vicinity, possibly causing equipment damage and, more seriously, injury and loss of life. A number of alternatives exist for designing mine layouts at depth in the vicinity of fault and dyke structures. These range from mining straight through the structure to bracketing it along its length by leaving a certain amount of unmined ground on either side of the structure, in order to inhibit movement on the structure and reduce the seismic risk. More broadly, these strips of unmined ground (i.e. bracket pillars) are also left *in situ* to prevent "daylighting" of a structure or of a reef intersection, as well as to apply confinement to discontinuities and thereby to eliminate or reduce the effects of bursting (Dukes, 1998).

Currently, designed bracket pillars vary in shape from long strips of unmined ground to irregular blocks of ground left at variable intervals to reduce the potential for failure in the enclosed structure. In some cases, these pillars were designed as ground control pillars, approximately 5 m wide and simply intended as a protective layer around the poor ground associated with the geological structure. In other cases, 30 m wide pillars have been used to ensure that the mining-induced stresses would be kept sufficiently far from the structure itself (Handley et al, 1997). At certain mines in the Klerksdorp region it has been claimed that 30 m pillars would not be used against specific structures and that 10 to 15 m pillars have been used successfully in the improvement of site response (Dukes, 1998).

A significant perceived disadvantage associated with the use of bracket pillars is the loss of potential ore reserves. Improved design criteria for bracket pillars could facilitate the enhancement of worker safety by controlling slip movements while avoiding over-design which locks up ore reserves unnecessarily.

Bracket pillars that are under-designed can cause serious problems, though. A narrow pillar left against one side of a fault can temporarily lock up slip movement. However, when the other side of the fault loss is stripped out, large, damaging seismic events can take place, effectively exchanging a series of small and relatively innocuous events, for one large and more damaging one. It is therefore imperative to estimate worst case conditions when designing bracket pillars (Anon, 1989). Note, though, that the above

theory (idea) remains untested. In effect, smaller events with magnitude 1,0 and above appear to cause more casualties than larger events (Spottiswoode, 1998).

In some cases, the size of a pillar that is required to prevent slip on a geological structure has been estimated from the rockbursts precipitated by mining close to that structure. Based on this criterion it would appear that 20-50 m wide pillars are required to ensure safe mining in the vicinity of certain faults and dykes (Gay et al, 1993).

Hemp (1994a) indicated in a literature review that bracket pillar design is assisted by strategies based on practical underground experience, a basic understanding of what makes a geological feature rockburst prone or not and the interpretation of numerical modelling results which are used when mining in the vicinity of hazardous geological structures.

Unfortunately, the design of bracket pillars is an extremely complex problem in that it is influenced by so many independent factors. All geological structures are different in terms of their physical and geometrical properties. In addition, no two mining layouts are the same and the way in which the mining-induced stresses will interact with individual structures is very difficult to predict.

A number of tools are, however, available for use in addressing this problem. The most important of these are geological data, seismic data and numerical modelling programs. Through information gathered using these different tools it may be possible to devise improved criteria or, at least, guidelines for better designing bracket pillars.

Numerical modelling can provide some insight into the effects of different layout sequences and pillar size combinations. However, in general, it is difficult to ensure that no movement whatsoever can occur on the bracketed structure. This suggests that a layout sequence which moves along or away from the potentially hazardous structure should be employed together with appropriate local support systems and backfill placement (Hemp, 1994b).

2 The seismic behaviour of faults and dykes from a pre-selected mine site

2.1 Introduction

A Portable Seismic System (PSS) was installed at the bracket pillar research site on Vaal Reefs 5 Shaft (Figure 2) in order to monitor the seismic response of the geological structure to the mining activity in the area and the behaviour of the bracket pillars during their formation. The installation began in January 1996, under the scope of work defined in GAP 223, and the first seismic events were recorded in April of that year. The PSS network initially consisted of five triaxial geophone sites on 68 and 70 Levels, surrounding an area of about 450 by 300 m. The geophones were grouted into the ends of 5 m boreholes drilled into tunnel walls. With the steady deterioration of ground conditions in the area, some of the initial geophone sites went out of order and were replaced by other sites where the ground conditions were somewhat better. The network configuration was also changed from time to time in an attempt to monitor the changing areas of mining activity better, particularly towards the end of the project. The focus of the network remained fairly consistent, however. At the end of the monitoring period allowed by GAP 516 (i.e. end of July, 1998), the network consisted of four triaxial sites and two biaxial sites; the triaxial geophones were installed in boreholes, while the biaxial geophones were pasted to the skin of the rock (data from these geophones were used only for event location and were not used for source parameter determinations).

Preliminary analysis of the seismic data recorded from events occurring in the immediate vicinity of the various discontinuities (in an attempt to relate differences in source parameter characteristics to differences in mining method in distinct areas) gave some insight into the seismic response of the features. It seemed clear that the mining method (i.e. the use of bracket pillars versus stripping against or mining through the discontinuities) strongly influenced the observed behaviour. A discussion of the results of this analysis was included in the Final Report for SIMRAC Project GAP 223 (Vieira et al, 1998).

While the sensitivity and location accuracy of the project seismic network was satisfactory, so that production blast sequences in the vicinity of the network were recorded and clusters of seismicity associated with discrete mining areas were adequately resolved, maintaining the network in an operational state proved rather

challenging, particularly in the early stages of the field work, so that some periods of data loss were experienced.

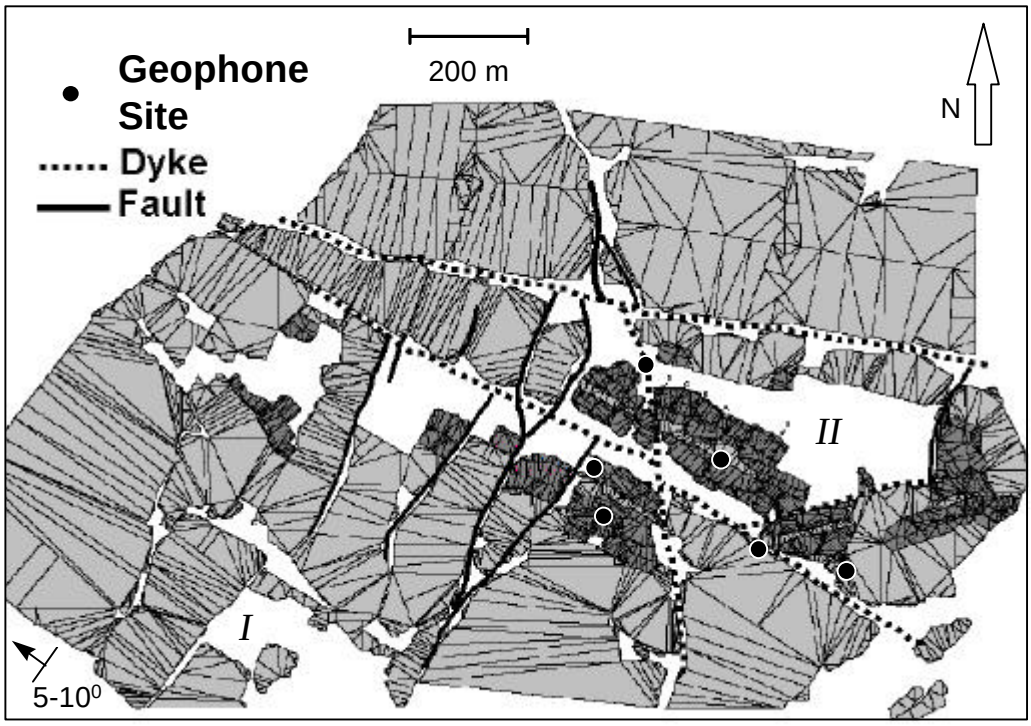

Figure 2 Plan of Vaal Reefs 5 Shaft bracket pillar research site, showing PSS geophone positions. Mined-out ground is shown in grey, with areas mined during the study period shown in darker grey. Zones I and II are referenced in the text.

In addition, it appears that the use of top-compression amplifiers at the recording sites (to increase the dynamic range of the system) interfered with the triggering logic, which resulted in a failure to capture a number of the larger seismic events that occurred in the area. Regrettably, this problem was identified only at a late stage of the monitoring (after comparison with data recorded by the mine-wide seismic network). A further difficulty that was encountered manifested itself as a lack of sensitivity to seismic activity from beyond the bounds of the PSS network. It was postulated that this is due to the absorption of seismic energy by the highly fractured rock mass surrounding the excavations in the area. The concept was, however, not tested.

2.2 Interpretation of seismic data from a monitored area

Figure 3 is a plan of seismicity recorded by the project network during a period of three months.

Owing to the shortcomings mentioned above in the PSS data set, the mine's seismology department was approached regarding the possibility of examining the seismic data recorded by the mine-wide ISS network.

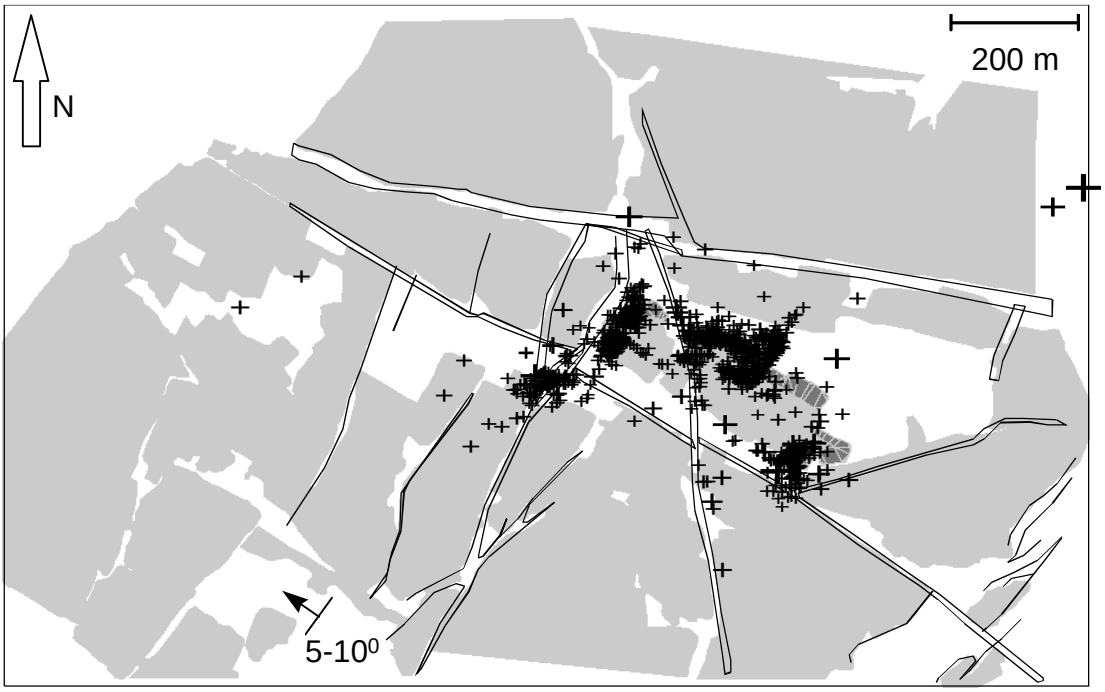

Figure 3 Plan of PSS data (crosses – scaled to seismic moment) recorded from 9/97 to 12/97. Areas mined during this period are shown in darker grey. Clustering of seismicity in areas of active mining is evident, as is the lack of sensitivity to seismicity from outside the bounds of the network.

The staff of the department were given permission by the mine management to share their data with the project staff, which they did. ISS data recorded from the project site during much of the period during which the PSS had been in place were obtained from the mine. The two data sets proved to be consistent with each other, so that data from the one set could be translated in terms of that from the other when necessary. The results of a comparison exercise which was conducted on the data sets are given in Appendix A.

The far more extensive station distribution of the ISS network ensured that data were reliably recorded from seismic events scattered throughout far more of the region of interest than was the case with the PSS network (although the seismic activity from the easternmost parts of the study area were under-represented during the first half of the study period even in the ISS data set, due to the configuration of that network at the

time). On the other hand, the spatial resolution of the ISS data was clearly somewhat lower than that of the PSS data, due to the lower station density of the ISS network (resulting from the requirement of monitoring seismicity for the whole mine and, thus, the inability to achieve the same degree of focus as the much smaller dedicated PSS network). Figure 4 is a plan of seismicity recorded by the mine-wide network during a period of three months.

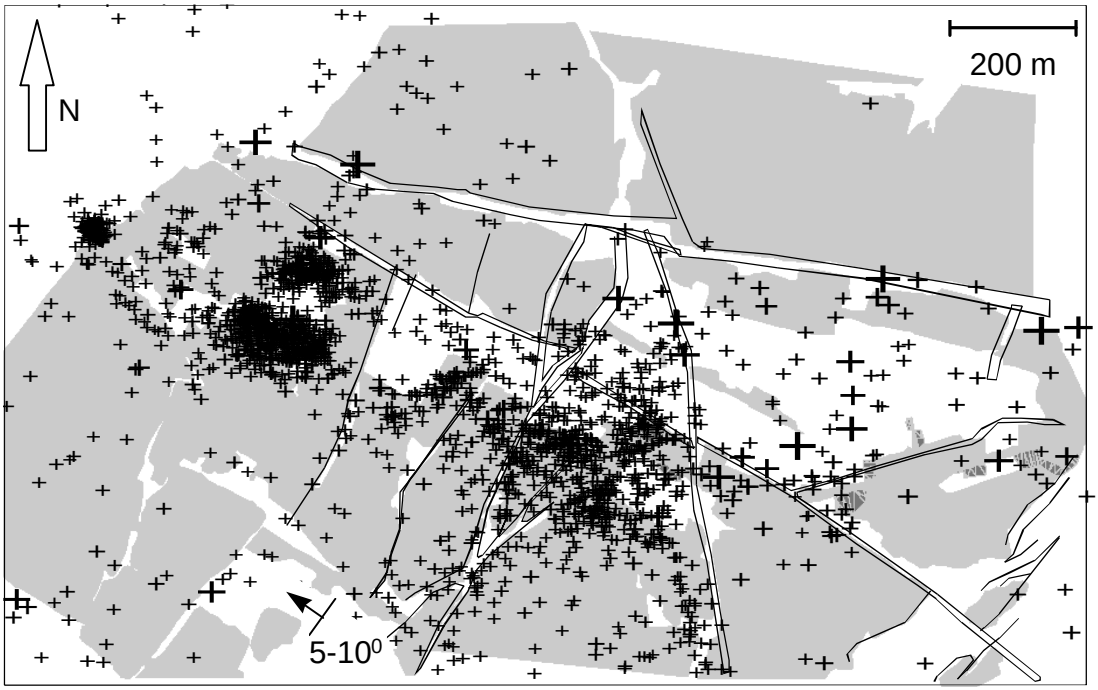

Figure 4 Plan of ISS data (crosses – scaled to seismic moment) recorded from 6/96 to 9/96. Areas mined during this period coincide with the areas where event density is higher. Less well-defined clustering of seismicity in areas of active mining is evident, as is the relatively complete coverage of seismicity from the area (compare with Figure 3, over a different time period).

The project site featured a complex geological structure, comprising numerous closely spaced faults and dykes with differing orientations and physical properties, intersecting one another at various angles. The area had also been extensively mined out and the ground conditions were generally rather poor. Such mining as was still taking place was scattered throughout the area, generally in close proximity to more than one discontinuity and advancing at various angles with respect to neighbouring features.

2.3 Seismicity in zones of "expected slip": discussion

Owing to the difficulties inherent in interpreting seismic data recorded from a complex environment such as described above, an attempt was made to use the results from a 3D numerical modelling study, which ran concurrently as a requirement of sub-task 1.2 of this project (see section 4), in order to simplify and focus the seismic investigation. The analysis centred around a comparison of the expected (modelled) slip on discontinuities during each three-month mining period with the actual recorded incidence of seismicity.

While it would be reasonable to assume that a very high proportion of the larger seismic events recorded from such an area as this (dominated as it is by the geological structure) resulted from slip on a discontinuity (an assumption that has been supported by the mine's seismology department in discussions between staff from that department and the project staff), a more general treatment would require a more robust means of discriminating between structural seismicity and seismicity associated with the advancing stope faces. A truly 3D seismic network with good location accuracy would provide for such discrimination through the location of structural seismic events on the discontinuities concerned. Typically, seismic networks employed in underground mining environments, such as those used in this study, are very planar and, thus, lack accuracy of location for the out-of-plane component, so that location information alone cannot be used to associate a recorded seismic event with a given discontinuity. In addition, events often locate close to the intersections between structures and, therefore, even the best locations can be of limited value in distinguishing which structure was involved.

Ebrahim Trollope and Glazer (1996) have proposed a bimodal distribution of mining-induced seismicity related to different source mechanisms. This distribution is thought to manifest itself as two different populations in moment-energy space, one population being associated with the zone of fracturing ahead of an advancing excavation, and the other with structural failure on a discontinuity (so that the observed physical properties of the rock mass are modified by the presence of a weak zone in the response to mining-induced stresses). Such a bimodal distribution was generally not found in the ISS data examined for this study. One exception arose from the inclusion of recorded development blasting (towards the West of the study area in the early stages of the study period, e.g. the very intense cluster at the extreme left of Figure 4) in the data set. For the most part, the seismic data tended to populate a single trend. This is thought to be due to the overwhelming influence of the geological structures, as well as to the highly fractured nature of the rock mass in the area.

Nevertheless, a reasonably good agreement was found between the occurrence of the larger seismic events and the positions of slip expected from the 3D modelling. The larger events tended to locate along lines defined by the geological structure and, specifically, in the proximity of the expected slip positions on various discontinuities. Scatter in the alignment can be explained by a combination of a relatively low location accuracy and by the fact that the discontinuities do not have vertical dip (so that events occurring off-reef on a discontinuity would not locate on the line defined by the intersection of the discontinuity with the reef plane). Also these events have source dimensions of 10 m and greater. The mapped geological features show a strike length of 200 m and greater. As in the case of seismic events, for every large fault (or event), there are many more small faults which are not shown on the maps. It is believed that slip on these smaller faults could also occur. Plans of larger seismic events recorded by the ISS network during two three-month intervals are shown in Figure 5 and Figure 6.

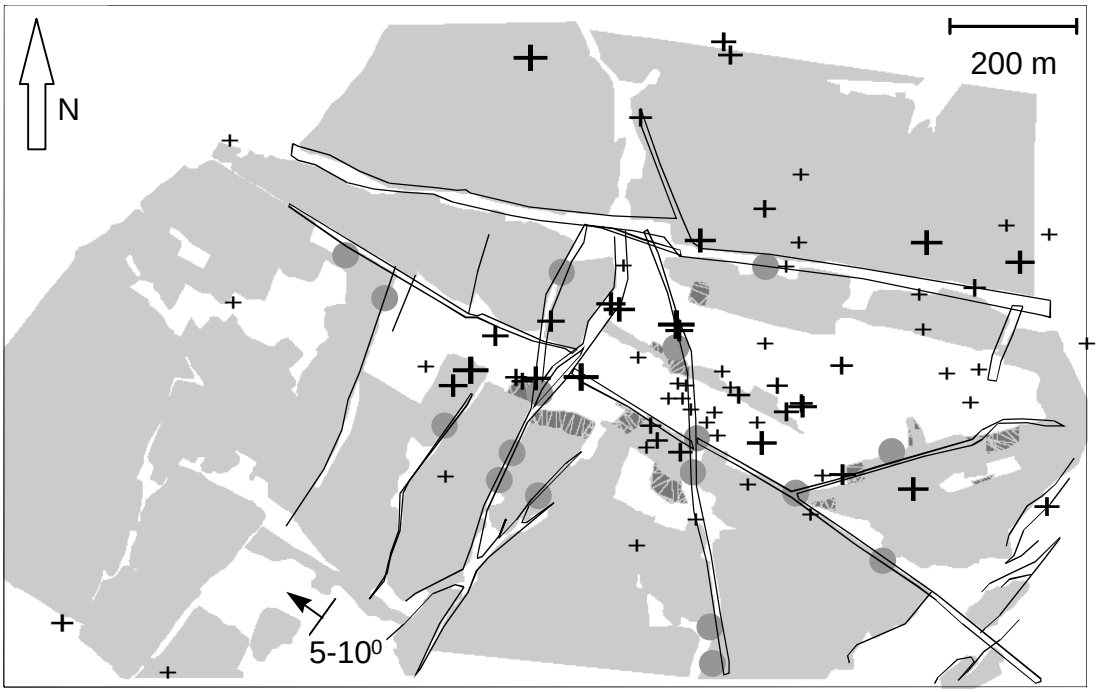

Figure 5 Plan of larger ($M_0 > 3 \cdot 10^9$ Nm) seismic events recorded by ISS from 9/96 to 12/96. Positions of discontinuity slip expected from 3D modelling are indicated by circles.

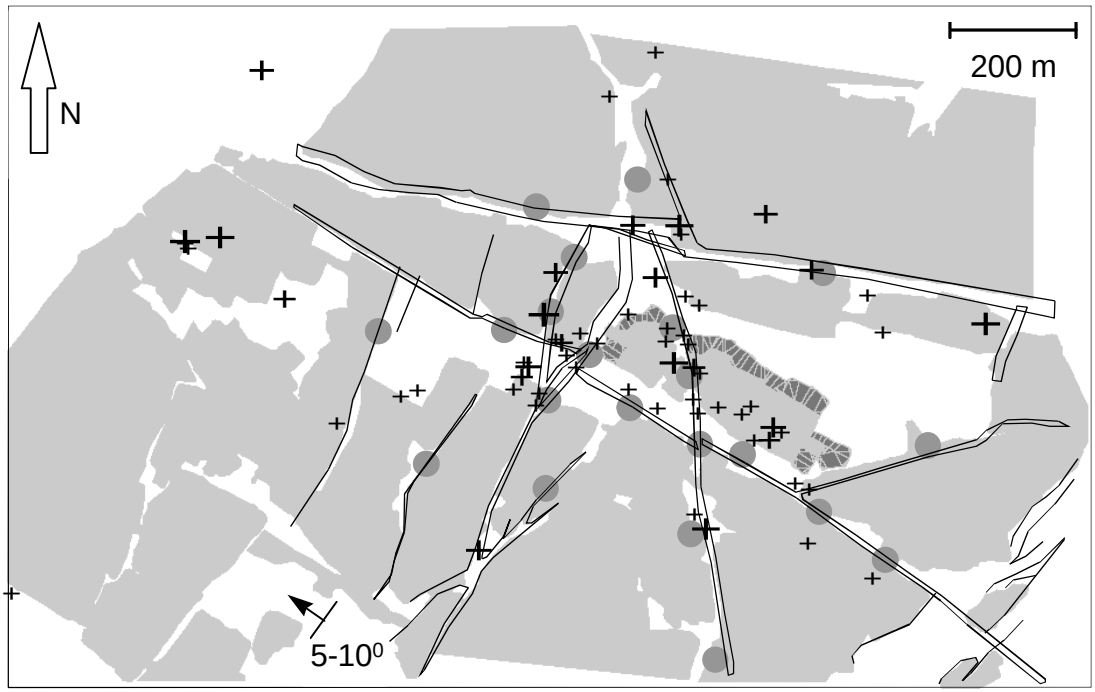

Figure 6 Plan of larger ($M_0 > 3´10^9$ Nm) seismic events recorded by ISS from 9/97 to 12/97. Positions of discontinuity slip expected from 3D modelling are indicated by circles.

A number of shortcomings in the modelling used in the above seismic investigation should be noted at this stage. Owing to limitations in the modelling package (e.g. limited number of boundary elements) and in available computing resources and run times, only a reduced number of discontinuities were modelled, and these were modelled individually (see explanation of model set up in section 4.4.2 on page 71; see also Figure 31, page 70, to verify which features were modelled).

The complex structure in the south-western portion of the area (to the West of and including the zone labelled ‘I’ in Figure 2) was not modelled, although, on later inspection, this was found to be seismically active. Also, the behaviour of each discontinuity was treated as a function of its physical properties and of its response to stress changes induced by mining activity in the area, so that any interaction between discontinuities (which very likely did take place, given the nature of the geological structure of the area) was not recognised in the modelling. At least one active discontinuity (to the West of the zone labelled ‘II’ in Figure 2) was also not included in the modelling, due to its presence not having being recognised at that stage.

The characteristics of seismicity generated ahead of advancing mining incorporate the effects of stope convergence and are modified by the presence of the stope and of the fracture zone around the stope, so that the failure has a significant non-shear component.

On the other hand, the characteristics of seismicity generated by slip on a discontinuity should be dominated by the shear movement. Thus, seismic events associated with structural failure should have significantly higher S- to P-phase ratios of seismic moment and seismic energy than those associated with advancing excavations. This approach to distinguishing structural seismicity from face seismicity allows for the use of a larger subset of the recorded seismic database, so that this type of analysis is not restricted to the use of only the largest events.

The occurrence of seismic events with high S- to P-phase ratios recorded by the PSS was compared with the slip positions expected from the 3D modelling, and a reasonable agreement was found between the recorded seismicity and the structural lineations and positions of expected slip on the discontinuities. This agreement was obviously limited largely to the immediate vicinity of the PSS network, due to the paucity of data from further afield. Scatter in the agreement resulted from the non-vertical dip of the discontinuities and from the presence of at least one unmapped active feature in the area. This analysis was not carried out on the ISS data, as separate P- and S-phase data were not received. Plans of seismic events with high S- to P-phase moment and/or energy ratios recorded by the PSS network during four consecutive three-month intervals are shown in Figure 7 through Figure 10.

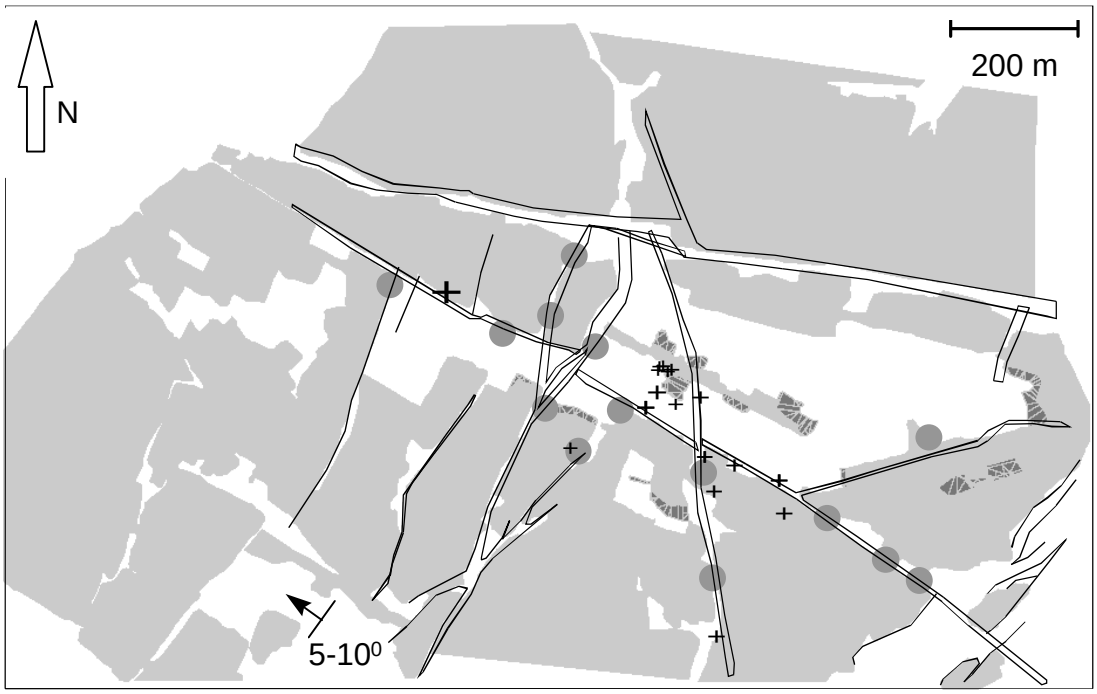

Figure 7 Plan of seismic events with high S- to P-phase ratios of moment and/or energy recorded by PSS from 12/96 to 3/97. Positions of discontinuity slip expected from 3D modelling are indicated by circles.

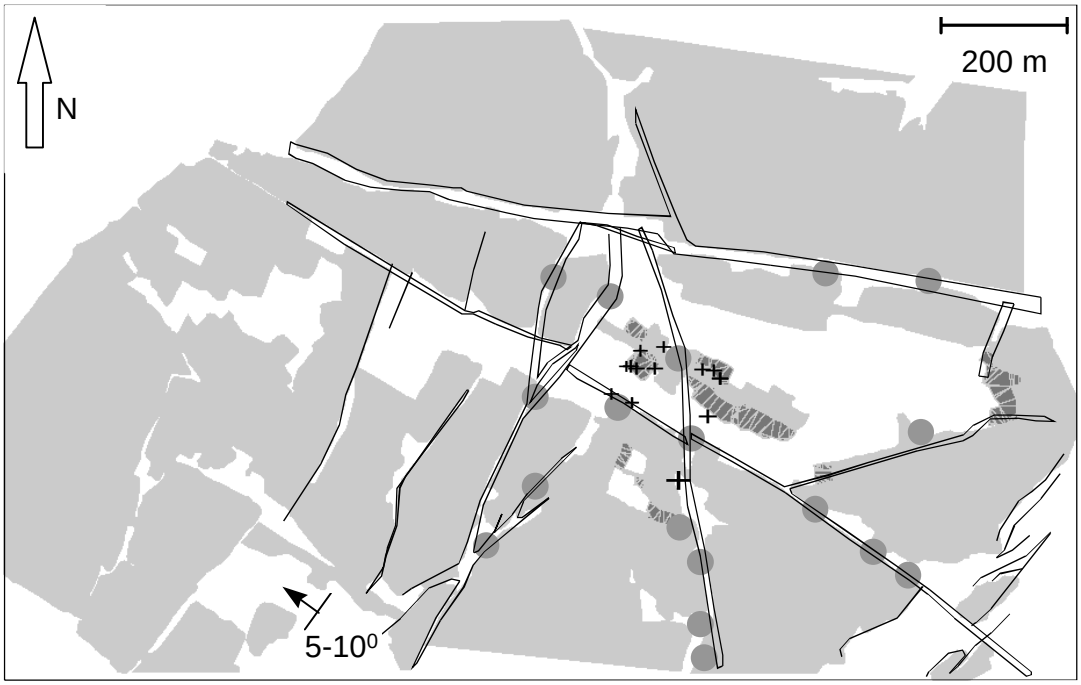

Figure 8 Plan of seismic events with high S- to P-phase ratios of moment and/or energy recorded by PSS from 3/97 to 6/97. Positions of discontinuity slip expected from 3D modelling are indicated by circles.

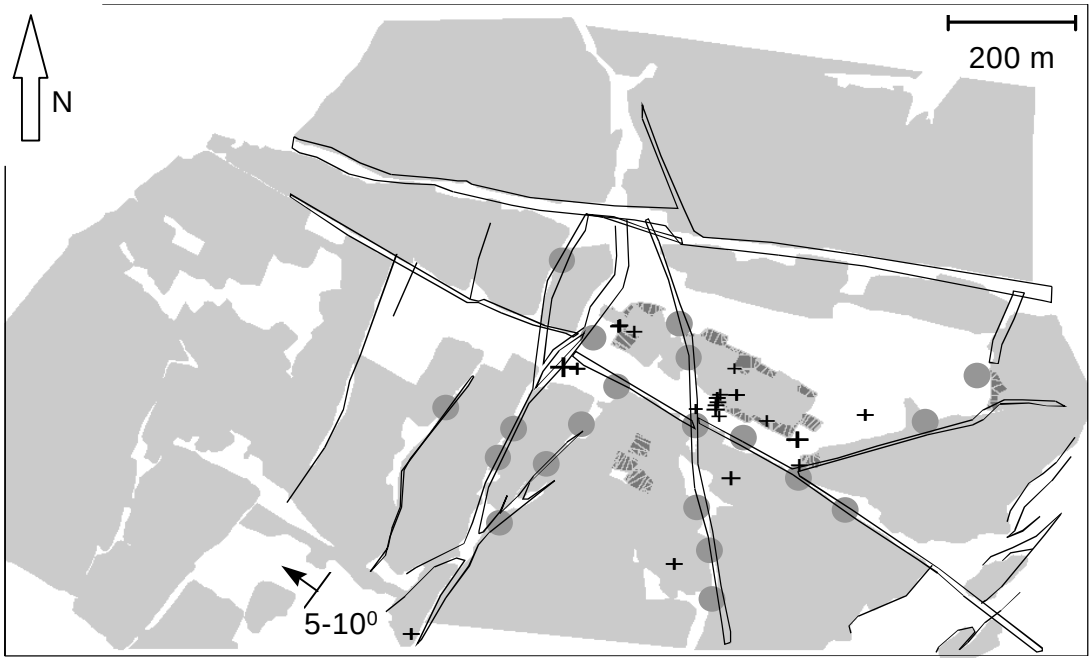

Figure 9 Plan of seismic events with high S- to P-phase ratios of moment and/or energy recorded by PSS from 6/97 to 9/97. Positions of discontinuity slip expected from 3D modelling are indicated by circles.

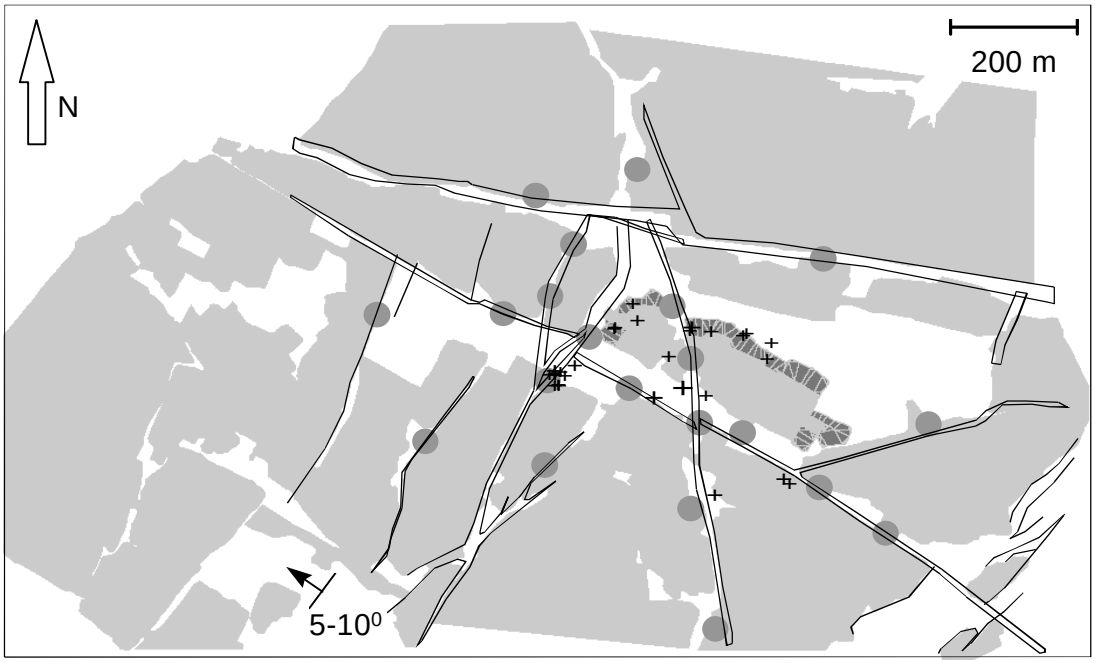

Figure 10 Plan of seismic events with high S- to P-phase ratios of moment and/or energy recorded by PSS from 9/97 to 12/97. Positions of discontinuity slip expected from 3D modelling are indicated by circles.

3 Numerical approach to evaluate potential behaviour of bracketed features and to assist in bracket pillar design.

3.1 Introduction

Napier and Ryder (1986) carried out some numerical modelling of bracket pillars in order to explore the effects of different layout sequences and pillar size combinations. They found that bracket pillars limit fault plane movements in the zone between the intersection of two reef planes and a fault. However, for faults that dip at between 45º and 60º, they do not restrict hangingwall and footwall movements unless they are very wide, i.e. wider than 100 m. This would obviously be an unacceptable layout. At steeper dips (i.e. structure dips greater than 75º) the dimensions of pillars would become more acceptable.

For certain dip values of structures, if bracket pillars are used, it may be possible to reduce fault movements to moderate levels. Napier and Ryder (1986) found also that if backfill ribs were used in place of bracket pillars, slip movement in the hangingwall and footwall would also be reduced, although motion on the fault plane between the two reef plane intersections would NOT be inhibited. From Napier and Ryder's (1986) work it is apparent that slip movements on discontinuities may not be inhibited completely by the use of bracket pillars. A better approach to design bracket pillars would be to limit the maximum slip which can be calculated from the area of the potential slip surface, and the average slip or ride. Such an approach is implicit in the methodology evaluated in this work (see section 3.3).

Dukes (1998) comments, however, that from a practical point of view stability analyses of geological discontinuities based on planar fault planes, a practice usually considered in numerical analyses, severely over estimate the hazard related to slip. He deduces that, in such cases, countering the slip hazard with bracket pillars of sizeable dimensions results in ore reserves being extensively sterilised.

It appears from the above that a large number of considerations and numerical conditions have to be taken into account by a rock engineering practitioner when designing bracket pillars, when using numerical models. To assist in this regard, a methodology was developed that attempts to rationalise such a design process, by means of "design charts". This methodology was developed under SIMRAC project Gap 223 (Vieira et al, 1998). Since the testing of such a methodology constitutes the objective of this study, an explanation of the rationale behind its development is presented in the following two sections.

3.2 Two dimensional numerical models of bracket pillar layouts

Numerical models were prepared to interpret the influence of certain parameters on the stability of both a bracket pillar as well as the discontinuity being bracketed. Tabular reefs cut through by planar faults were considered. Numerical approaches have been considered because stresses arising from tabular excavations, as well as slip movements on discontinuity planes, can easily be modelled by numerical methods (Napier, 1987). The possible hazard on a given discontinuity plane, for instance, has usually been interpreted in terms of excess shear stress and determined numerically. This is not, however, the approach of this work.

Note that the stress patterns surrounding real mine layouts are complex and for that reason the structures are best modelled separately, for reasons of clarity and ease of interpretation of results. Initially, only 2D models were considered using DIGS (Napier, 1990). Later, however, 3D analyses were carried out for comparison, the results of which are discussed in section 4.4 of this report. Here, the steps leading to the development of GAP 223 "bracket pillar design methodology" are briefly explained.

Two possible bracket pillar layouts were studied. In the first layout, layout (a) in Figure 11, the mining faces were assumed to approach a discontinuity from one side only, i.e. with no previous mining on the other side. In the second studied layout, layout (b) in Figure 11, mining would take place on both sides of the discontinuity simultaneously. The two reef horizons on the second layout were considered vertically displaced by a fault, over a distance of 150 m. Mining faces were modelled to advance symmetrically away from a central gully on each stope and towards the discontinuity.

To best understand the interrelation between the various likely bracket pillar layouts, and to assess each parameter's influence on the stability of the bracketed structure (as well as on the size of a bracket pillar), the influence of a number of "design" parameters was of interest. The parameters evaluated included depth of layout, local k-ratio, the discontinuity angle, the stope dip, the pillar width and mining span. Table 1 and Table 2 show the respective values considered.

Combinations of these model parameters in respect of the two bracket pillar scenarios of Figure 11 (i.e. combinations of all parameters indicated in Table 1 and Table 2, respectively) led to more than 8000 independent numerical runs, from where a considerable amount of data was generated. Such data, subsequently, was used to draw bracket pillar "design charts" (Vieira et al., 1998).

In all numerical runs carried out under this study the same values of elastic constants were applied, i.e. a Young's Modulus of 70 GPa and a Poisson's Ratio of 0.21. The geological discontinuities on both layouts (layout (a) and (b) in Figure 11) were numerically modelled as a single crack, with a friction angle of 30^{o} and zero cohesion.

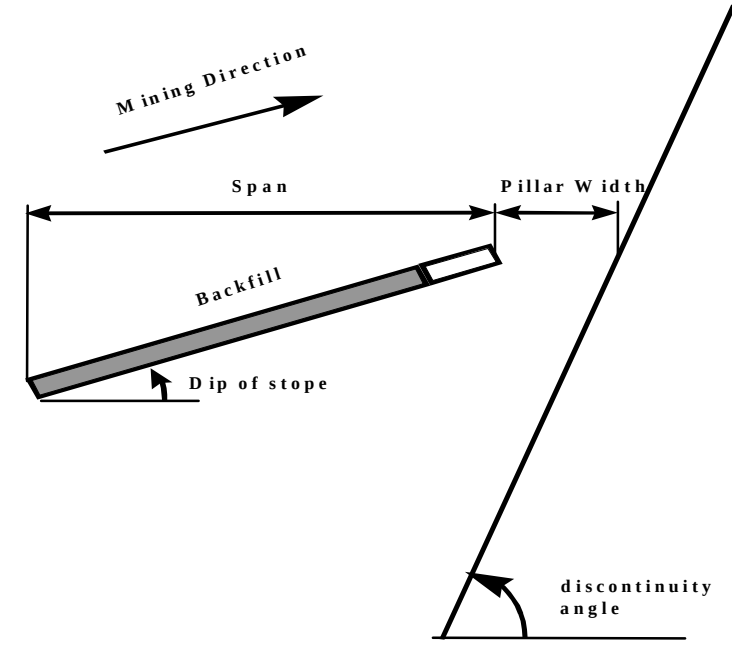

(a)

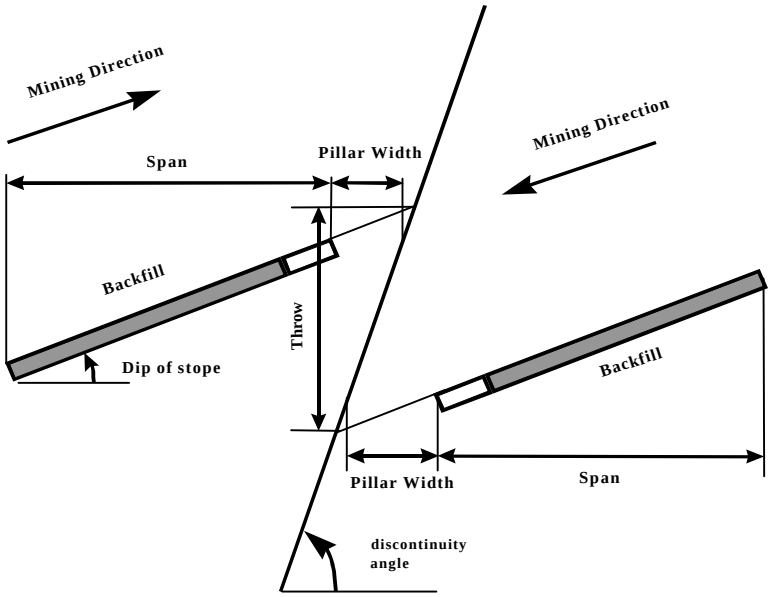

(b)

Figure 11 Layout geometry for hypothetical bracket pillar layouts modelled with DIGS. (a) denotes a layout where mining approaches the discontinuity from one side, and (b) denotes a layout where mining takes place on both sides of a discontinuity.

Table 1 Model parameters applied to numerical runs that considered layout (a) shown in Figure 11.

depth (m)	k-ratio	discont. angle	stope dip	pillar width (m)	span (m)
2000	0.5	60^o	0^o	100	100
3000	1	68^o	15^o	50	200
	2	75^o	30^o	30	300
		83^o		20	400
		90^o		10	500
		97^o		5	
		105^o			
		112^o			
		120^o			

Table 2 Model parameters applied to numerical runs that considered layout (b) shown in Figure 11. A given model run consisted of combinations of each parameter type.

depth (m)	k-ratio	discont. angle	stope dip	pillar width (m)	span (m)
2000	0.5	60^o	0^o	100	100
		68^o	15^o	50	200
		75^o	30^o	30	300
		83^o		20	400
		90^o		10	500
		97^o		5	
		105^o			
		112^o			
		120^o			

A given model run would consist of a specific combination of the six parameter types shown on Table 1 and Table 2, respectively. For example, a different model would be set up for every combination of dip, stope span, pillar width, discontinuity dip, stress state (k-ratio) and depth (this, as said, resulted in 8000 DIGS independent runs).

The solution from each modelled combination would estimate the size of a potential seismic event which, hypothetically, would have occurred due to slip along the discontinuity. Numerous sets of preliminary “pillar size” design charts (e.g. Figure 12) were then drawn up based on the results from the population of all numerical runs resulting from combinations of the parameters in Table 1 and Table 2.

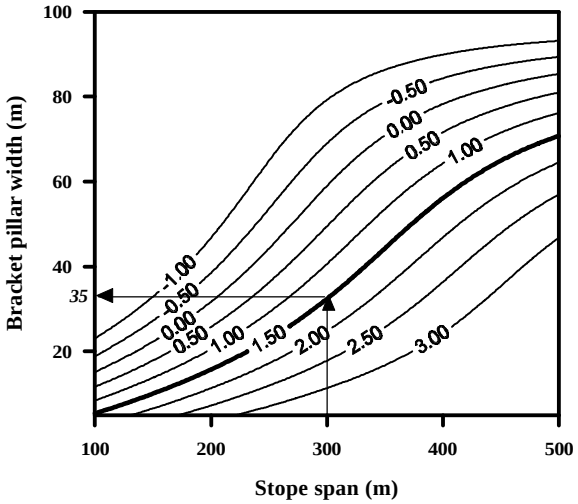

Figure 12. Example of a design chart to be used for a bracket pillar layout at a depth of 2000 m, k-ratio=0.5, with a discontinuity dipping 75^o, and a stope dip of 0^o. Each plotted line corresponds to estimated maximum seismic magnitude contours of slip type seismic events, for varying stope spans and pillar widths.

For each model run the calculation of the size of a potential seismic event along a bracketed discontinuity was of interest. The magnitude of such events was calculated according to established relationships, based on a given model, as explained in section 3.3. Sets of bracket pillar design charts were then drawn up based on the "expected" event magnitudes for given layout conditions. The charts were constructed by contouring the seismic hazard potential (i.e. the maximum magnitude expected for a given geometry combination) against two other variables, e.g. pillar width and mining span. Different charts would be developed for varying stope and discontinuity dips, and for different depths as well. See the complete collection of bracket pillar design charts in the Appendixes of the GAP 223 Final Project Report, Volume 2, (Vieira et al, 1998).

3.3 Rationale behind the development of "bracket pillar design charts"

It is important to stress that design charts for bracket pillar are intended to provide only initial estimates of required bracket pillar widths, based on mining and geological constraints that are easily measured. This new philosophy of pillar design requires that the rock engineer decide on a "tolerable" event magnitude that could take place on geological features in the area of interest. The decision on what constitutes tolerable magnitudes falls under the field of risk assessment, after considering serious seismic and

accident statistical analyses. Elaboration on this matter, however, falls outside the scope of this project and will not be discussed. Designing for an "acceptable level of seismicity" (e.g. for a tolerable event magnitude) is a less conservative but more realistic an approach than requiring zero ESS, as had previously been practised (Hemp, 1994a).

Bracket pillar design charts rest on a methodology based on a conceptual model that assumes seismic emissions along bracketed discontinuities. In the applied rationale, a seismic event is considered to be the result of a shear movement along the fault or dyke being bracketed. The induced seismicity due to slip is measured by means of a calculated seismic parameter (e.g. seismic moment or event magnitude).

In this rationale presented, the seismic moment (M_0) is calculated based on a relationship given by Aki and Richards (1980), such that:

$$M_0 = G \int R \, dA \quad (Nm)$$ Equation 1

where G = modulus of rigidity (Pa)

A = area of slip = area of circle (m^2)

R = slip (m)

Owing to the use of a 2D code (DIGS) in our analysis, the plane strain model applied provides only a slip profile, which is constant in the out-of-plane direction. The area of integration is assumed to be a Brune-type circle, the diameter of which is the dip length undergoing slip. Equation 1 can then be written as:

$$M_0 = G \, A \, D \quad (Nm)$$ Equation 2a

$$= G \, V \quad (Nm)$$ Equation 2b

where A = area of slip = area of circle (m^2)

$D = \int_a^b R \, dx$ = average slip (m)

$V = \frac{\pi}{4} (b - a)^2 \, D$ = volume of slip (m^3)

a, b = start / end of slip pitch

The distribution of slip provided by the plane strain model is numerically integrated over the length (i.e. along dip) of the discontinuity undergoing slip, and the average slip is calculated by dividing the integrated slip value by the dip length undergoing slip. The area of the circle is calculated and multiplied by the average slip. This can then be thought of as the *volume* of slip (*V* in Equation 2b). The greatest amount of slip, either in the hangingwall or in the footwall, is obviously considered in the calculation of the modelled seismic moment, in that the "worst case scenario" (Anon, 1988) would have in this way been taken into consideration.

The maximum potential seismic event magnitude (M), the one included on the various design charts, is then obtained from the empirical relation derived by Hanks and Kanamori (1979):

$$M = \frac{2}{3}[\log(M_o) - 9.1] \qquad \text{Equation 3}$$

3.4 Some considerations on the practical usage of bracket pillar design charts

Bracket pillars designed so as to result in “no seismicity” in the vicinity of bracketed features are impractical, as they would have to be very wide (Napier, 1987) and result, consequently, in totally uneconomical layouts. The new approach is that pillars could be designed by taking into account a tolerable level of seismicity in their vicinity. This design involves the use of pillar “design charts” and, for its correct application, the following needs to be taken into consideration:

1. The seismic hazard (represented by the seismic moment or event magnitude and defined in section 3.3) along a bracketed geological structure is assumed to be dependent on the amount of arbitrary slip displacement on the discontinuity only.

2. Based on an adequate rockburst risk assessment, the largest tolerable seismic magnitude for the region of interest is set. Events of a lower magnitude should have a low probability of causing rockburst in the nearby stopes. In this case, therefore, the local stope support would also be designed to control the expected effects of events below the tolerable seismic magnitude. For example, if for a given mine region experience shows that the conditions in the nearby stopes remain acceptable when seismic events of magnitude 2.0 and less occur at a particular distance then the maximum tolerable event on a structure would presumably be one of magnitude 2.0. The rock mechanics engineer at a mine will have to determine, statistically, and by

risk assessment the tolerable seismic magnitude for a geotechnical area where bracket pillars are intended.

3. Knowing the planned span of mining and having established a tolerable seismic magnitude for the respective mine region, the pillar width required may be read off from the appropriate chart that characterises the prevailing mining conditions (i.e. stope dip, stope span, discontinuity dip, depth, k-ratio, backfill).

This process of application of design charts is illustrated in the diagram in Figure 13.

Note, however, that bracket pillar design should not seen to be complete at this point. A rock mechanics engineer would probably need to model a layout in greater detail for very complex mining configurations, by using 3D modelling tools. Such an approach would allow for the inclusion of effects of the third spatial dimension, as well as other factors, such as realistic mining sequence in the vicinity of the structure. These are not accounted for in the plain strain conditions of the design charts.

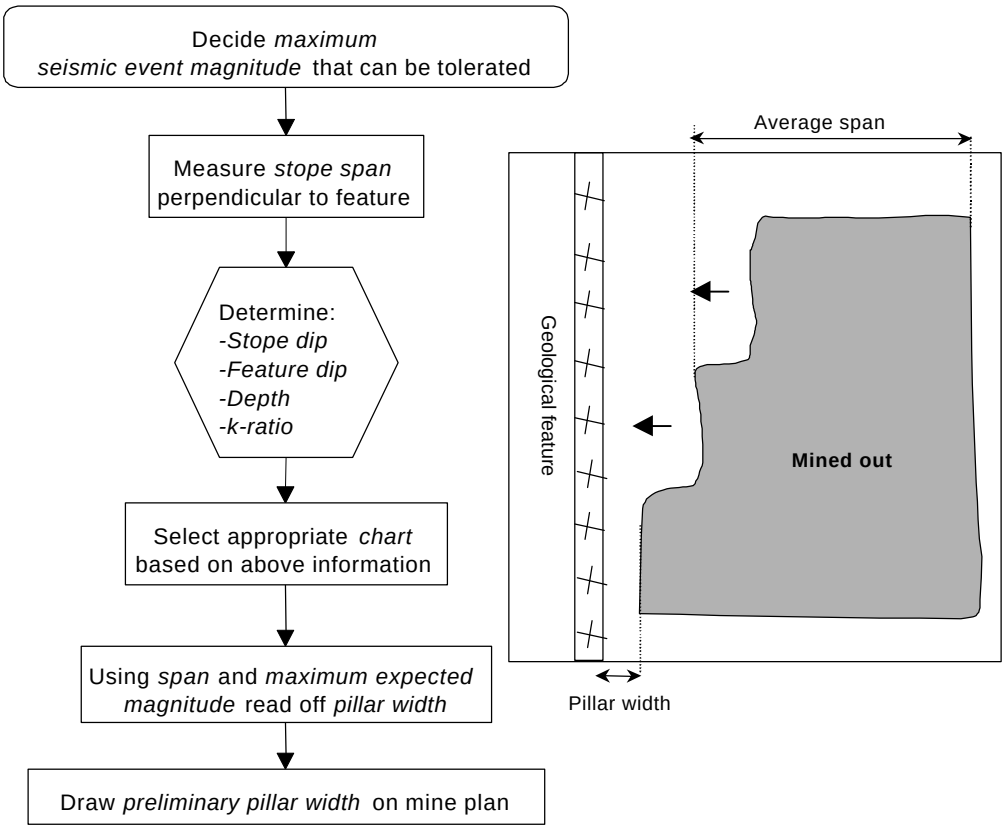

Figure 13 Flowchart indicating the process of designing bracket pillars using bracket pillar design charts.

3.5 The effect of various mine layout parameters on the maximum expected magnitude ranges of bracket pillar design charts.

3.5.1 The effect of mining span

It was verified that the parameter "mining span", i.e. the amount of mining in the vicinity of a bracketed feature (see Figure 11), has a significant effect on the "maximum expected magnitude" of a seismic event due to slip along a discontinuity. To illustrate such influence, an example based on the layout (a) in Figure 11 is drawn in Figure 14. Take the case of a stope that increases its span by about 50 m, adjacent to a geological feature controlled by a bracket pillar of 30 m wide. Using the appropriate design chart (e.g. Figure 14), and assuming that the stope span would have increased, say, from 250 m to 300 m by mining the abutment of the stope away from the structure (i.e. maintaining the pillar size but mining the panels furthest away from the discontinuity), it could be verified that the "maximum expected magnitude" on the chart would have jumped from 1.8 to 2.3 (follow arrows shown in Figure 14 that intercept the iso-magnitude lines). If the amount of mining increases to reach spans of 300 m or greater, then the expected magnitude on the bracketed feature would have approached values M_o=2.3 or greater. The greater the span, the greater the seismic magnitude for the same pillar width.

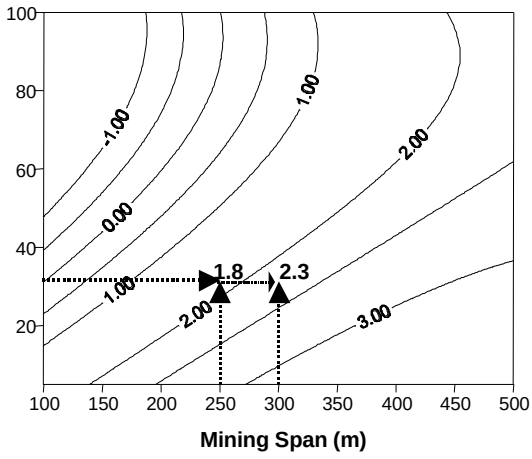

(a)

Figure 14 Example of variation in the maximum expected magnitude for the case of a layout in which the k-ratio is 0.5 (i.e. the ratio s_H/s_V is 27/54 MPa), the stope dip is 0^o (i.e. flat reef) and a discontinuity dips at 112^o.

Note, however, that an increase in the expected magnitude would not be caused by a change of span alone. A reduction in pillar width would contribute to promote the same effect. The latter would in fact be a more likely practical scenario in real mining conditions, i.e. one where pillar sizes are reduced through mining nearer to discontinuities. In this instance, take for example the case of a stope that has a mined out span of approximately 250 m and a pillar width of about 60 m (layout (a) in Figure 11). If the pillar size is to be reduced from, say, 60 m down to 30 m the expected magnitude on the bracketed feature would have increased from 0.7 up to 1.8 (follow arrows shown in chart (a) of Figure 15). In reducing the pillar size, the mined out span would have increased correspondingly from 350 m to 280 m, the effect of which would result in an additional increase in the expected magnitude value from 1.8 to 2.3.

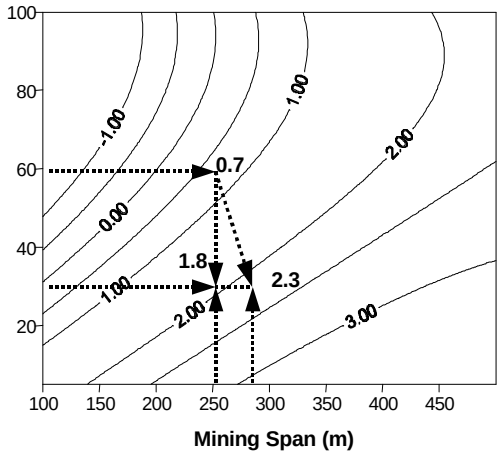

(a)

Figure 15 Example of variation in the maximum expected magnitude due to reduction of pillar size and increase in span, for the case of a layout in which the k-ratio is 0.5 (i.e. the ratio s_H/s_V is 27/54 MPa), the stope dip is 0^o (i.e. flat reef) and a discontinuity dips at 112^o.

If the tolerable seismic event magnitude had been set at 2.0 then the seismic risk under these mining conditions would be unacceptable. To allow for the additional 30 m mining (and maintaining the tolerable magnitude value at no more than 2.0) the pillar width would have to be of the order of 39 m, approximately (follow arrows in Figure 16). Thus, in designing bracket pillars an overall view of the mining layout needs to be taken.

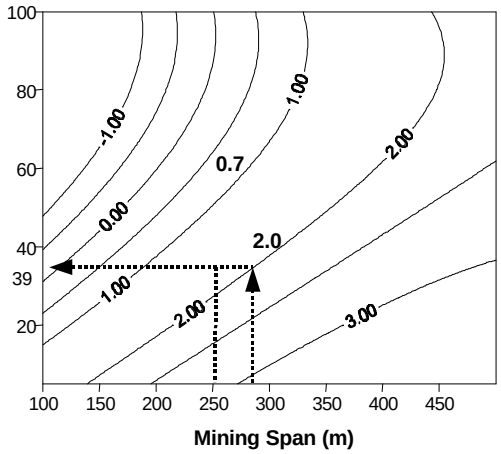

Figure 16 Required pillar size for 30 m increase in mining, for the case of a layout in which the k-ratio is 0.5, the stope dip is 0^{o} (i.e. flat reef) and a discontinuity dips at 112^{o}.

3.5.2 The effect of reef/stope dip

The effect of stope dip (i.e. reef dip) on the "maximum expected magnitude" along a bracketed discontinuity can be observed in the same manner as for the case above. Given the same geometric conditions of a certain bracket pillar layout and varying only the dip of the reef, it can be seen that the maximum expected magnitude along the bracketed discontinuity would vary accordingly (see Figure 17). Three examples are shown in respect of a layout with a mined out span of 250 m adjacent to a geological feature and where a 30 m pillar is used. From Figure 17 it can be seen that for the case where the reef is flat (i.e. reef dip = 0º, (a) chart), the maximum expected magnitude is 0.9. This magnitude increases to 1.8 when the reef/stope dip is 15^{o}, chart (b), and further increases to 2.8 when the reef/stope dip is 30^{o}, chart (c) in Figure 17.

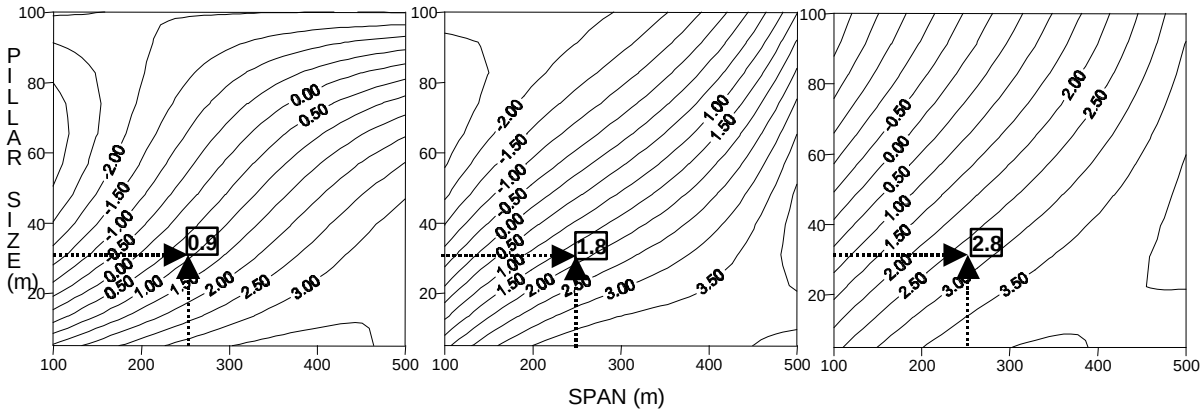

Figure 17 ***The effect of reef/stope dip on the maximum expected magnitude, for the case of a layout in which the k-ratio is 0.5 (i.e. the ratio s_H/s_V is 27/54 MPa), the discontinuity dips at an angle of 105^o and has varying reef/stope dips: 0^{o}or flat reef, case (a), 15^o, case (b), and 30^o, case (c).***

3.5.3 The effect of discontinuity dip

Note also that the dip of the discontinuity, i.e. the angle of inclination of the bracketed geological discontinuity, affects significantly the maximum expected magnitude of events caused by slip (Figure 18). From all the studies conducted, i.e. taking into account all considered model cases studies referred to in Table 1 and Table 2, it appears that the most favourable discontinuity dip is between 75^o and 83^o. The most dangerous from a seismic risk point of view is when the discontinuity dips around 105^o, for the case where the reef dip is 15º. These conditions would change for different reef dips.

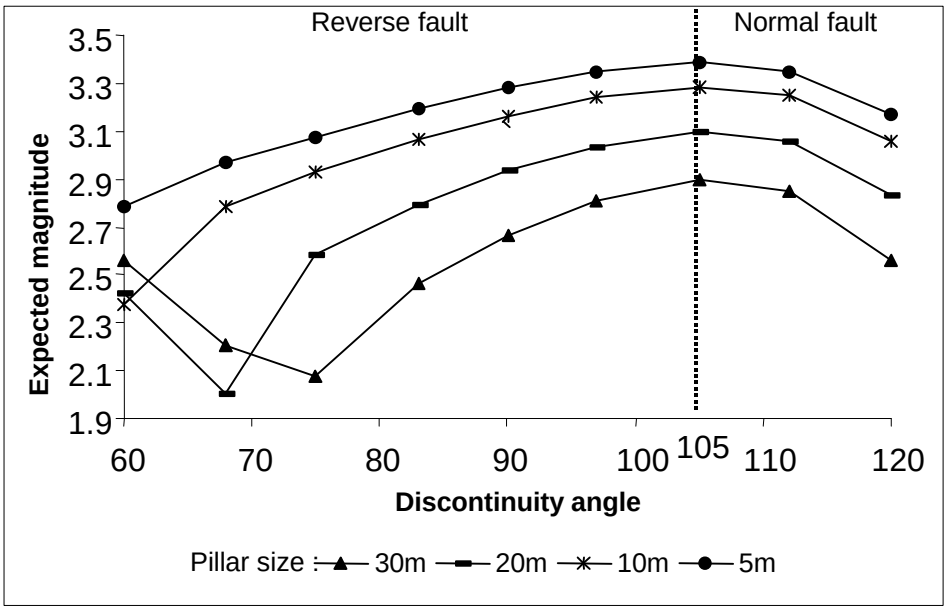

Figure 18 The effect of discontinuity dip on seismicity, for the case of a layout in which the k-ratio is 0.5 (i.e. the ratio s_H/s_V is 27/54 MPa), with a span of 300 m and a reef/stope dip of 15^o.

3.5.4 The effect of depth of the layout

When mining in the vicinity of a geological discontinuity that is assumed to have potential to slip, the maximum seismic moment caused by slip on such a discontinuity is directly proportional to the depth below surface (Figure 19a). Consequently, the seismic event magnitude will be logarithmically proportional to the depth of the mining (Figure 19b). These trends become more pronounced with increasing dip, confirm in Figure 19 a) and b).

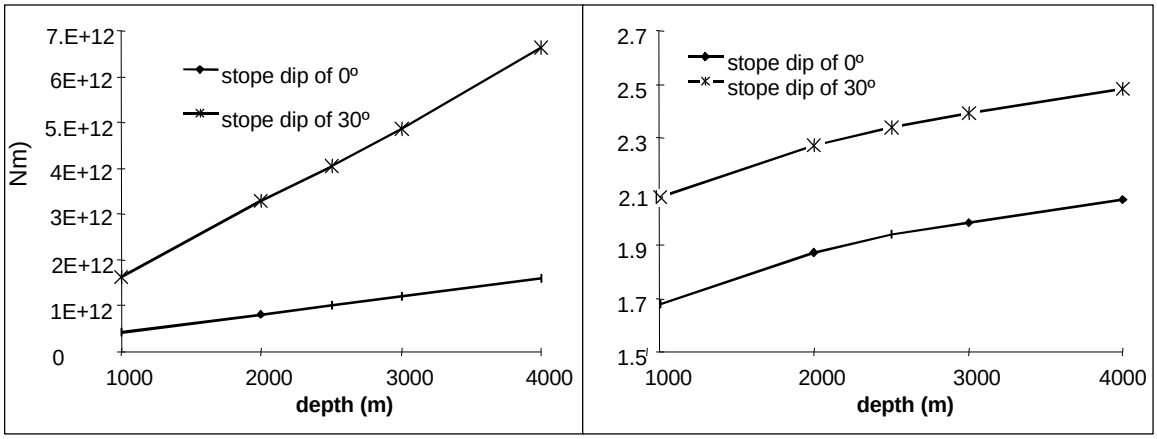

(a) (b)

Figure 19 The effect of depth on the seismic moment (a) and event magnitude (b), for a layout where the k-ratio is 0.5, the span of mining is 200 m, and incorporates a 20 m wide bracketing pillar against a discontinuity.

3.5.5 The effect of local k-ratio

From a numerical modelling point of view, the horizontal-to-vertical stress ratio, i.e. the k-ratio, is one of the most important parameters controlling slip along a discontinuity. Note that in reality rock masses are subject to anisotropy values of k. It should be pointed out that the component of stress normal to a structure to be bracketed is the most important. The most favourable situation is for a k-ratio of 2.0 as far as the geometries in Figure 11 and stress conditions are concerned.

The effect of the k-ratio on the expected magnitude on the bracket pillar design charts is shown in Figure 20. In this figure three cases of k-ratio variation are shown; case (a) of a layout where k-ratio is 0,5, case (b) of a layout where the k-ratio is 1, and case (c) of a layout where the k-ratio is 2. It can be observed, all other parameters being equal, that the maximum expected event magnitude along a bracketed discontinuity would decrease for increasing values of k-ratio.

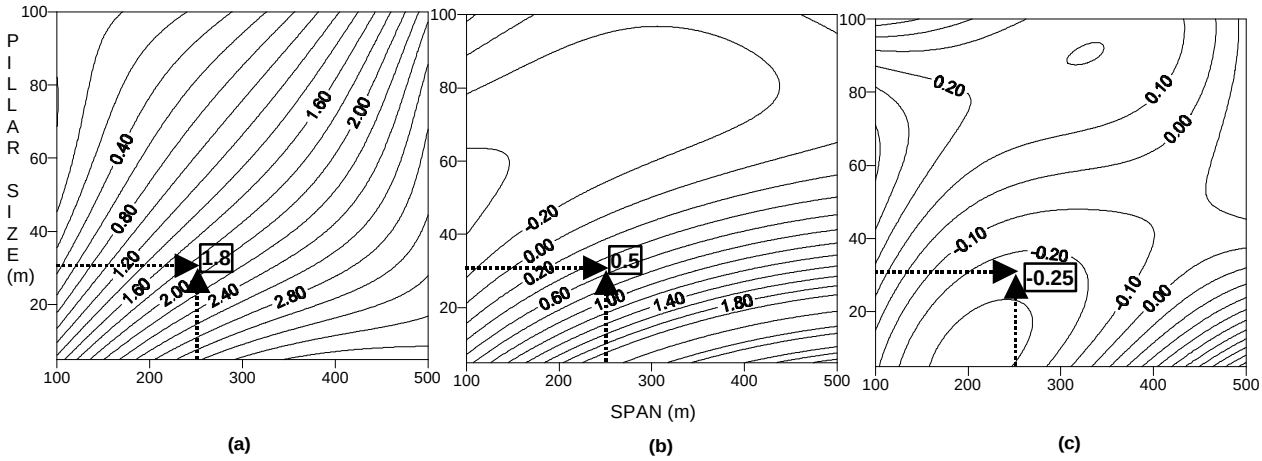

Figure 20 Effect of k-ratio on the maximum expected magnitude relative to a bracket pillar layout that has a reef/stope dip of 15°, a discontinuity angle of 75°, and a k-ratio=0.5 (a), i.e. s_H/s_V = 40/80 MPa); k-ratio = 1 (b), i.e s_H/s_V = 80/80 MPa; and a k-ratio=2 (c), i.e. s_H/s_V = 160/80 MPa.

3.5.6 Further effects of the layout geometry on the seismic hazard of a bracketed feature: the throw of discontinuity

In the case of the studied layout where mining takes place on both sides of a discontinuity (see Figure 11.b), it could be hypothesised that fault movements in the hangingwall and footwall areas would not be prevented by bracket pillars, although movement within the fault loss area should be considerably reduced (Napier, 1987). This consideration could be relevant for the location of off-reef tunnels in the layout considered. Note, however, that the siting of footwall tunnels should not be governed by rock mass movement considerations alone, as stress conditions in the fault loss are also important.

The throw of a discontinuity, i.e. the amount of reef/stope displacement, has a significant effect on the maximum expected magnitude of the design charts (see Figure 21). When designing a bracket pillar for a given layout, therefore, the discontinuity throw should be taken into consideration. Note, though, that a parameter "throw" was not directly included in the overall design methodology of Figure 13, given that the design charts were developed for a constant value of throw of 120 m. Generally, however, this parameter should be considered.

Note that the inclusion of one more parameter to the solution of the models studied (i.e. add one more to the parameters listed in Table 1 and Table 2) would require an additional 10000 runs, on top of the nearly 8000 processed. The effort required would not be justifiable, given the resources available to the project. The effect of throw, therefore, was interpreted in specific cases individually (e.g. Figure 21).

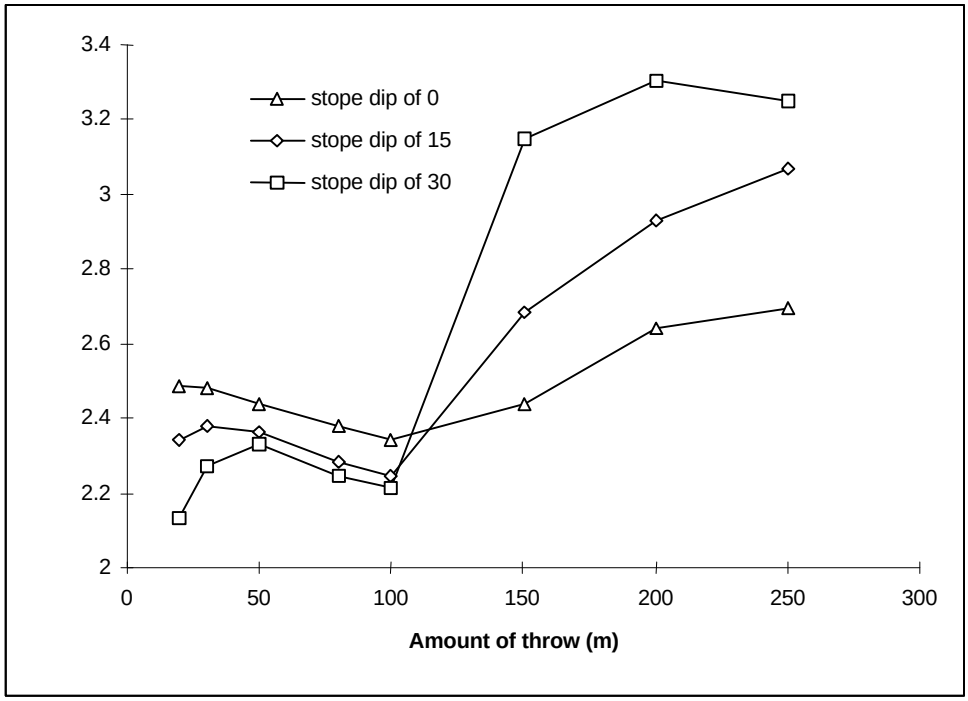

Figure 21 The effect of throw on the maximum expected magnitude, for a layout where mining takes place on both sides of a discontinuity (e.g. Figure 11.b). This layout has a discontinuity that dips 120^o, a mining span of 200 m, and a k-ratio of 0.5 (i.e. s_H/s_V=27/54 MPa).

As mentioned earlier, the models representing mining towards a discontinuity from one side and from both sides (Figure 11.a and Figure 11.b) were also run with variable initial spans. The stope dip for the respective cases were varied between 0^o and 30^o, for a constant k-ratio of 0.5 at a depth of 2000 m below surface.

Mining steps were considered in such a way that the bracket pillars formed in the models would have widths of 100, 50, 40, 30, 20, 10 and 5 m. On obtaining the various solutions for each run, the values of the maximum expected magnitude were tabulated (Table 3). In this table the cumulative magnitude values along the discontinuity, obtained for each pillar width, are shown. These magnitude values are obtained assuming that no slip takes

place prior a current mining step. Data in Table 3 is presented in chart format in Figure 22 and Figure 23.

It can be seen from these figures that the maximum expected magnitude is most dependent on pillar size and on initial span. However, it is interesting to note that in the case of a flat dipping layout where mining occurs on both sides of a discontinuity which is bracketed by a pillar less than 40 m wide, the maximum expected magnitude is approximately the same for all the modelled layout spans Figure 22 (b).

The above also appears to be true for layouts with stopes dipping 15^{o} and 30^{o} and that have discontinuities bracketed by pillars of 30 and 20 m (Figure 23a and Figure 23b) respectively). Other charts demonstrating the above interdependencies are available from the SIMRAC Final Report of GAP 223 and will not be referred to further.

Table 3 ***Maximum expected magnitude from mining sequentially: (a) mining a reef dipping 15^o on one side of the discontinuity only, (b) mining on both sides of a flat stope (0^o), (c) mining on both sides of a stope dipping 15^{o,} (d) mining on both sides of a stope dipping 30^o. For these layouts a discontinuity that dips 90^o , has a throw of 120 m and a local k-ratio of 0.5 (s_H/s_V=27/54 MPa) were considered.***

(a)

PILLAR SIZE	NEW SPAN	INITIAL SPAN 100 m	200 m	300 m	400 m
		100	200	300	400
100	x	0	0	0	0
50	x+50	0	0	2.41	2.95
40	x+60	0	2	2.76	3.22
30	x+70	1.23	2.5	3.01	3.38
20	x+80	2.15	2.91	3.27	3.57
10	x+90	2.73	3.16	3.51	3.72
5	x+95	2.85	3.32	3.66	3.83

(b)

PILLAR SIZE	NEW SPAN	INITIAL SPAN 100 m	200 m	300 m	400 m
		100	200	300	400
100	y	0	0	0	0
50	y+50	0	0.48	1.71	2.2
40	y+60	1.62	2.02	2.2	2.27
30	y+70	2.28	2.5	2.65	2.7
20	y+80	2.64	2.83	3.27	3.39
10	y+90	2.93	3.33	3.54	3.64
5	y+95	3.22	3.47	3.67	3.82

(c)

PILLAR SIZE	NEW SPAN	INITIAL SPAN 100 m	200 m	300 m	400 m
		100	200	300	400
100	y	0	0	0	0
50	y+50	0	0.0615	1.9	2.33
40	y+60	1.52	1.64	1.98	2.33
30	y+70	2.33	2.37	2.44	2.42
20	y+80	2.7	3.07	3.18	3.3
10	y+90	3.14	3.4	3.57	3.65
5	y+95	3.31	3.56	3.73	3.82

(d)

PILLAR SIZE	NEW SPAN	INITIAL SPAN 100 m	200 m	300 m	400 m
		100	200	300	400
100	y	0	0	0	0
50	y+50	0.99	1.94	2.21	2.6
40	y+60	0.99	2.03	2.26	2.6
30	y+70	1.96	2.03	2.26	2.6
20	y+80	2.6	2.59	2.64	2.6
10	y+90	3.22	3.39	3.54	3.55
5	y+95	3.4	3.59	3.76	3.83

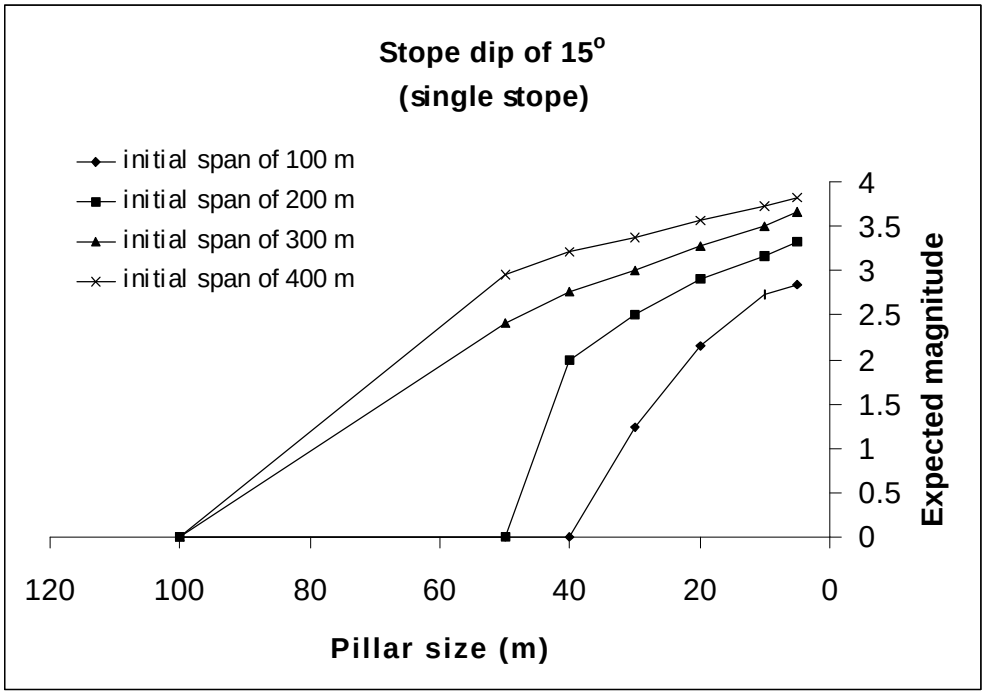

(a)

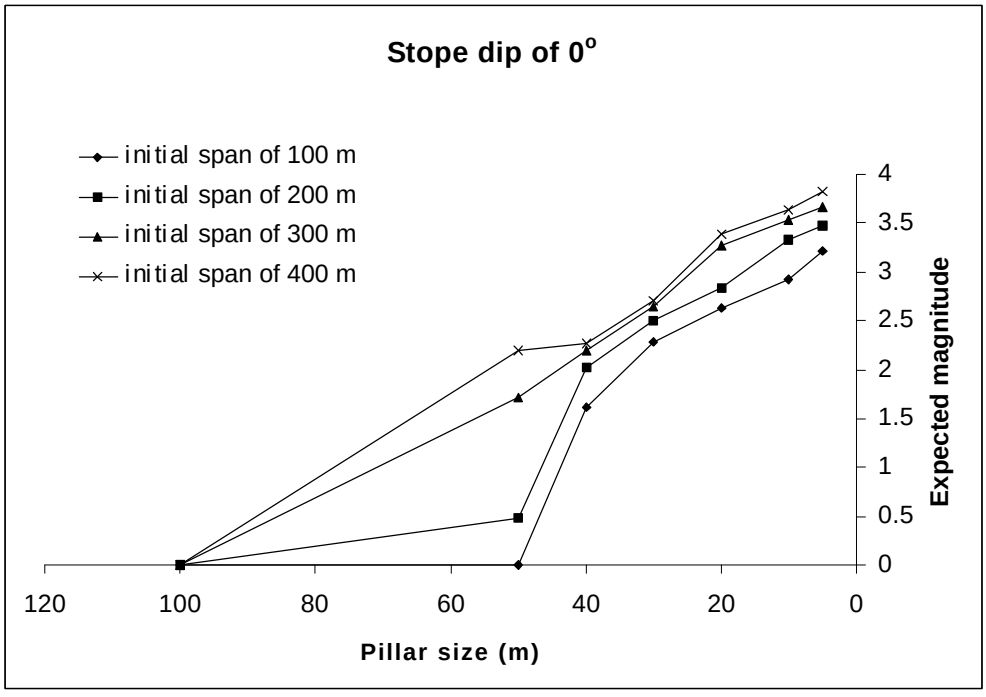

(b)

Figure 22 Maximum expected magnitude from mining sequentially: (a) mining a reef dipping 15º from one side of the discontinuity only, (b) mining a flat (0º) reef from both sides of a discontinuity. A discontinuity dipping 90º and a local k-ratio of 0.5 (s_H/s_V=27/54 MPa) were considered in both cases.

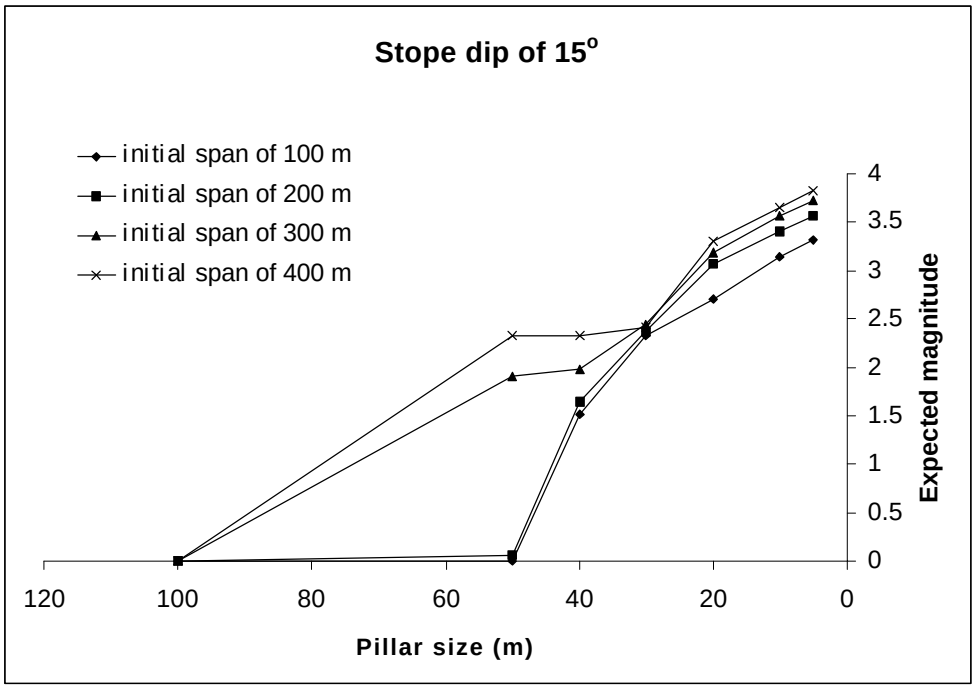

(c)

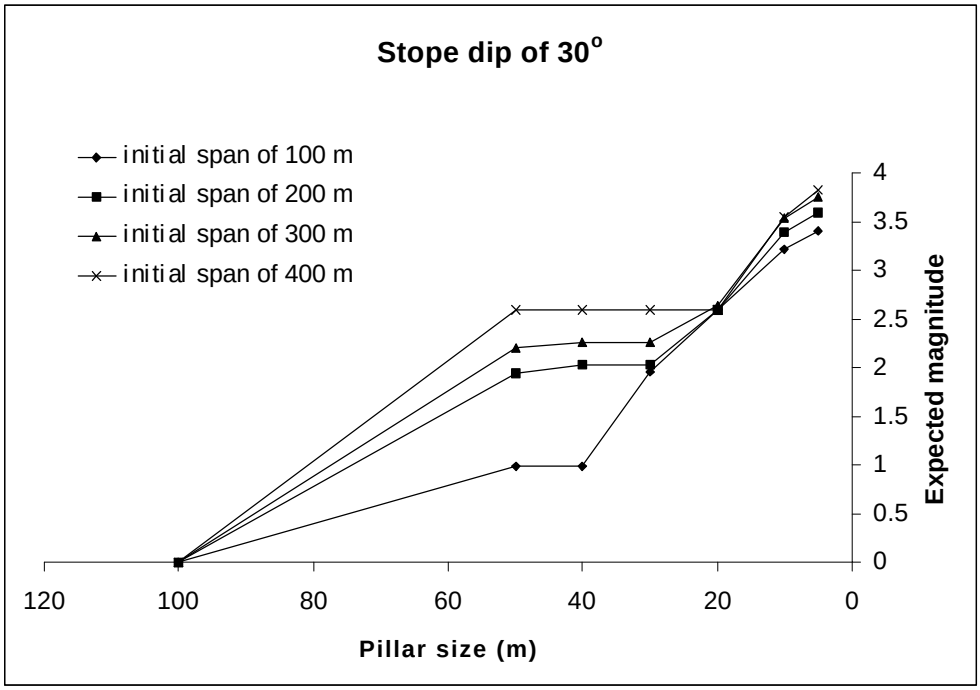

(d)

***Figure 23** Maximum expected magnitude from mining sequentially: (c) mining a stope dipping 15° on both sides of a discontinuity and (d) mining a stope dipping 30° on each side. A discontinuity dipping 90° and a local k-ratio of 0.5 (s_H/s_V=27/54 MPa) were considered in both cases.*

3.5.7 The effect of backfilling a stope adjacent to a bracketed discontinuity

The model cases described in 3.5.6 in respect of studies designed to establish the interdependencies in bracket pillar layouts (e.g. these in Figure 11) were further used to evaluate the effect of backfill on the stability of a bracketed discontinuity plane. The modelled stopes, therefore, were considered subsequently to be filled with a "good quality" backfill material, the mechanical properties of which followed a hyperbolic stress-strain relationship, with a characteristic stress parameter, *a,* of 5 MPa and an ultimate strain, *b,* of 0.3. The fill width was assumed to be 0.9 m in a stope width of 1 m. Figure 24 (a) shows the characteristic behaviour of the backfill material considered.

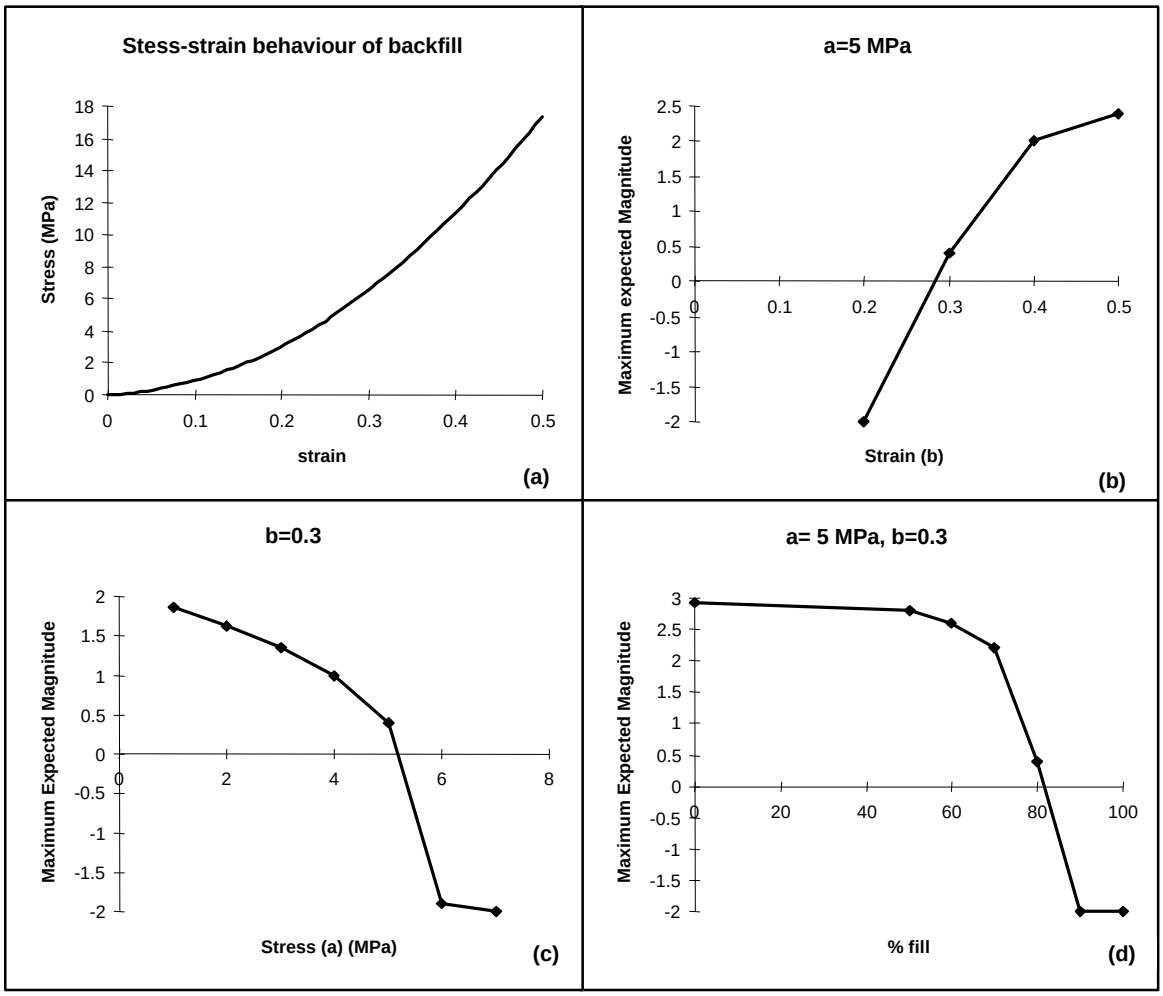

Figure 24 The effects of backfill on the seismic hazard of a bracketed discontinuity: (a) characteristic stress-strain curve of modelled backfill material, (b) the effect of the ultimate strain parameter, (c) the effect of stress, (d) the effect of percentage of fill.

Note, though, that the effects of the physical properties of the backfill on the maximum expected magnitude along a discontinuity that slips were obtained using plane strain modelling. Figure 24b shows the influence of the *b* value (i.e. the ultimate strain of the backfill) on the potential seismic hazard, measured as the maximum expected magnitude caused by slip.

When the ultimate strain (b) is increased while the “a” value is kept constant, e.g. a = 5 MPa, the maximum expected magnitude will increase. However, when the stress parameter “a” is increased under constant ultimate strain, the maximum expected magnitude is reduced (see Figure 24c). Figure 24d shows how the percentage of backfill used affects the potential seismic hazard along a discontinuity, indicating that for higher percentage fill (e.g. > 70 %), the hazard potential may be reduced rapidly. This rapid decrease in hazard potential is more pronounced in certain geometries than others.

In general, a layout that uses backfill as the support medium causes the bracket pillar design curves to flatten, which may imply a reduction in the potential seismic hazard. For example, for the case of a horizontal stope with a k-ratio of 0.5 at a depth of 3000 m and a discontinuity angle of 112^{o}, the maximum expected magnitude along such a discontinuity using a bracket pillar size of 30 m would be 2.3 (this value could be obtained from the design charts, GAP 223 Final Report, Vieira et al, 1998). Should that stope be backfilled, however, with 90 per cent fill, the magnitude would be reduced to 1.4.

In addition, the usage of backfill in bracket pillar layouts would allow, conceptually, for a increase in span from 250 to 500 m with almost no change in maximum event magnitude. This is a result of the fact that the presence of backfill leads to a build up of horizontal stress in the hangingwall and footwall and also reduces the volume of stope closure.

Design charts for bracket pillar layouts that use backfill as the support medium are available in Volume 2 of the SIMRAC Final Report for GAP 223 (Vieira et al, 1998). These specific charts were developed for layouts that consider a k-ratio of 0.5 and may be mined at depths of 3000 m. For geometries and stress conditions that differ from these, certain corrections need to be made. For further information on this the section "DIGS Design Charts" of the GAP 223 Final Report should be studied.

4 Studies on the validation of the methodology that uses "design charts" for bracket pillar design

4.1 Introduction

As was evident from the previous sections, preliminary design charts were obtained from numerical modelling of bracket pillar layouts considered under plain strain, i.e. 2D conditions.

Subsequently to such development, some amount of back analysis was carried out which attempted to compare modelling related seismic data (e.g. maximum expected magnitude from design charts) with seismic data available from real bracket pillar layouts (e.g. local seismic magnitude obtained from seismic systems) from a number of bracket pillar areas both on the Vaal Reefs Nº 5 Shaft and Western Deep Levels South mines.

Some agreement between the seismic parameters from the field and those from the models was found. These aspects are now discussed below.

4.2 Comparison between seismic magnitudes from field sites and expected magnitudes obtained from 2-D DIGS models (i.e. design charts)

Seismic records from two mines where bracket pillars were established were used for back-analysis purposes. These records were from bracket pillar areas on the Vaal Reefs no. 5 Shaft and on the Western Deep Levels South mines.

The following back analysis procedure was followed: bracket pillar sites were selected from the mines mentioned and for which adequate historic seismic information was available (example of one selected site is shown in Figure 25). The respective bracket pillar layouts were scrutinised from mine plans and the amount of mining over three-month intervals was marked off.

For each bracket pillar stope selected and for a given date, the distance of mining (i.e. the span) and the respective pillar size, would be recorded. The seismic magnitudes from events that occurred in the vicinity of the bracketed features during that exact period of

mining were also recorded. A database of field data and mine plan data was established that related, for various periods, the mining span, the bracket pillar size, the seismic magnitude of all events that occurred within that period of mining, the depth of mining and the width of mining. This data is available from the GAP 223 Final Report (Vieira et al, 1998).

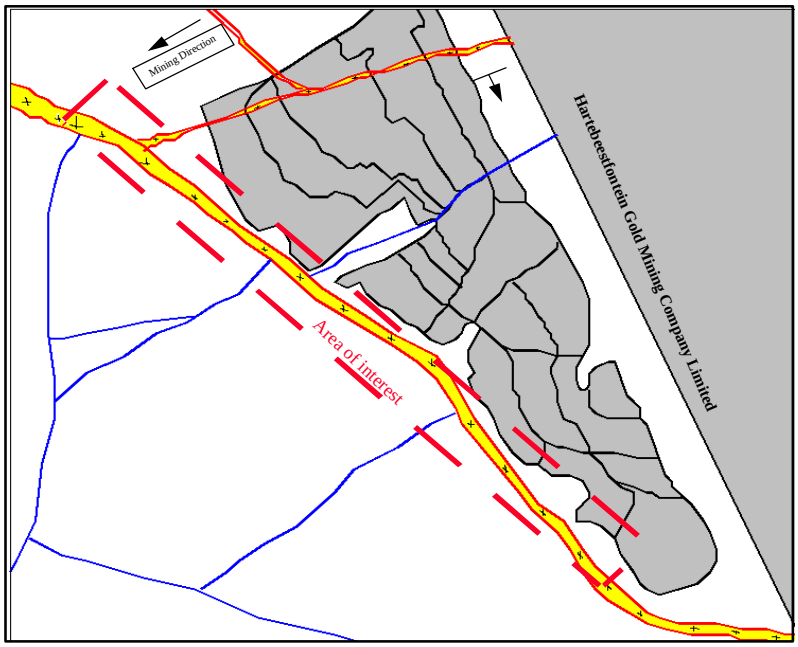

Figure 25 Example of a one side bracket pillar layout on the Vaal Reefs mine, which was back-analysed for the purpose of relating field seismic data with modelling data.

All recorded bracket pillar sizes and related event magnitudes that occurred on all layouts selected, obtained as above, were plotted against are another. Figure 26 shows the association that resulted from the combination of pillar size and field seismic magnitude as a very scattered, fuzzy plot. Note, though, that all magnitude sizes for all seismic events recorded were combined on the same chart.

Should only the events of larger magnitudes be included, however, one would obtain a relatively good association between bracket pillar size and event magnitude (see the dashed correlation line for the larger events in Figure 26).

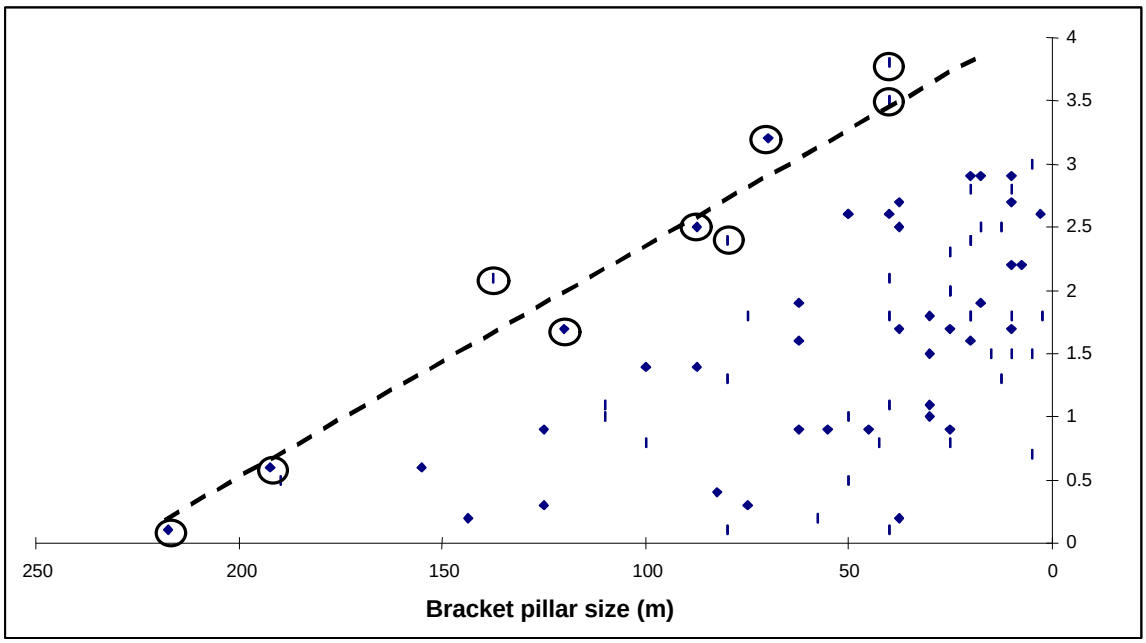

Figure 26 Association between magnitude of seismic events that occurred on bracket pillars from selected bracket pillar layouts, versus bracket pillar size at a correspondent time of event occurrence. Plotted data refer to all back-analysed bracket pillar layouts from Vaal Reefs and Western Deep Levels mines combined. Note that a strong association is possible when the biggest events that occurred for a given pillar size are taken into consideration (dashed line).

Further comparisons were made between expected magnitude values from 2D DIGS modelling (i.e. design charts data) and seismic data from true bracket pillar layouts.

This comparative study was done in the following manner: firstly, from all mentioned back-analysed layouts, relevant layout geometry data would be extracted, namely pillar size, mining span and seismic magnitude of actual field events recorded during each correspondent period of mining. These layout data were used as entries in bracket pillar design charts (e.g. Figure 12) from which correspondent maximum expected (modelled) seismic magnitude values would be derived for the layout. The most critical discontinuity dip would be assumed, a condition accepted to ensure that the expected magnitude value derived from the charts would be the largest possible (i.e. to design for the worst case scenario).

In a second phase, the dip of the discontinuity would be changed to represent the most favourable conditions for the layout and, entering the same "real" data on the design charts, the lowest value of the expected magnitude event for the layout would be derived.

Lastly, the two obtained design chart-based values of "expected seismic magnitude", one representing the most critical discontinuity dip condition and the other the least critical, would be compared against seismic magnitudes of field events that located on the actual discontinuity. Results from two of these comparative studies are shown in Figure 27.

From Figure 27 it can be seen that, for the various layout cases considered, the magnitude of the field events were between the largest and the smallest "maximum expected magnitude" obtained from the DIGS modelling. It is also indicated that as the pillar width decreases the correlation between the actual maximum sized event and that predicted, improves.

Based on the limited results of the case studies conducted, it can cautiously be said that a bracket pillar layout derived from DIGS based design charts would probably not underestimate the maximum size event by default. The observation arises from the fact that the values of seismic magnitude in all bracket pillar design charts developed under GAP 223 are "maximum expected" values, i.e. the top lines of charts a) and b) in Figure 27. Although for the cases back-analysed field seismic magnitudes were below the "maximum expected" magnitudes, the observation is not a definite conclusion, as further verification and proof are required.

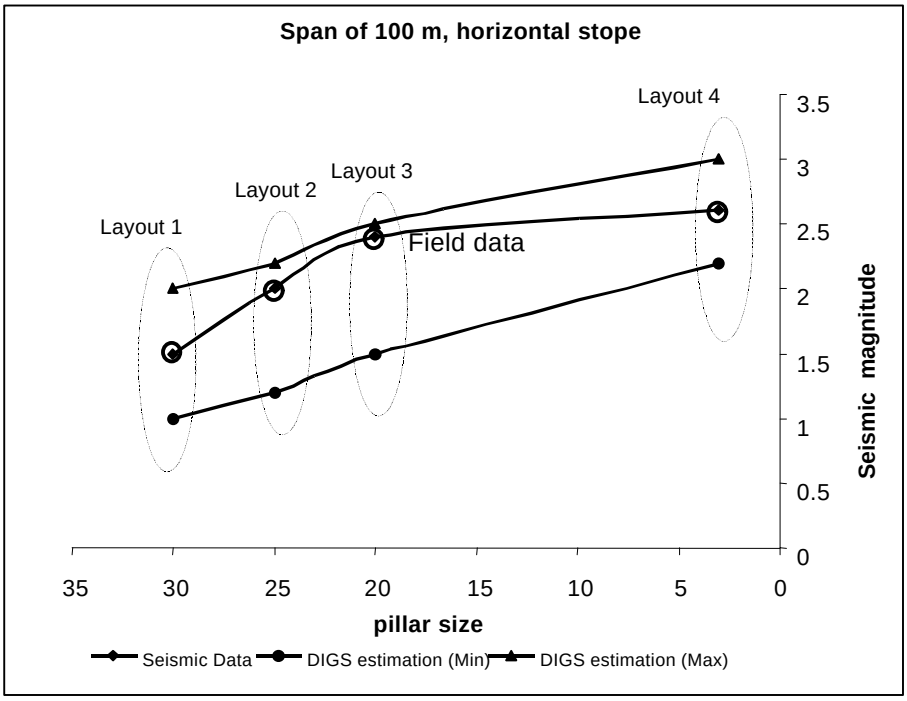

(a)

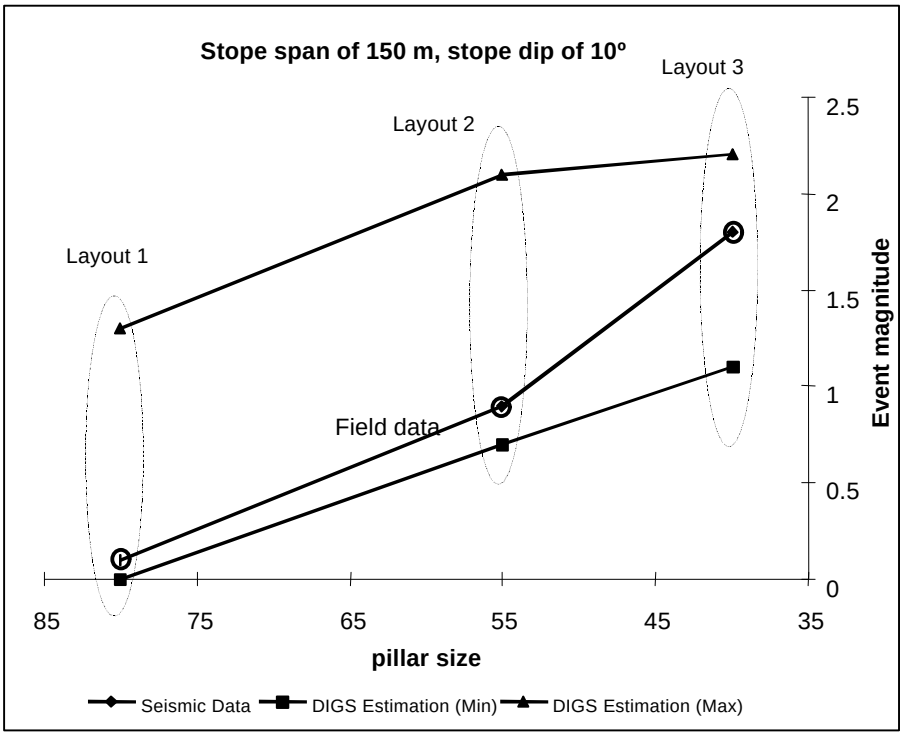

(b)

Figure 27 Comparison between maximum and minimum expected magnitude of events along bracketed discontinuities from design charts and event magnitude actually recorded at selected field sites where bracket pillar have been used. Note that design charts results were obtained from 2D-DIGS.

4.3 Comparison between seismic event magnitudes from field sites and maximum expected magnitudes obtained from equivalent three-dimensional MAP3D models

Layouts designed using bracket pillar design charts were further assessed against layouts prepared as 3D models run in MAP3D. Initially, simple geometries were considered, not necessarily depicting the realistic mine layouts (e.g. Figure 28). This procedure would maintain the similarities between the plain strain models from DIGS, apart from the inclusion of the third spatial dimension. Realistic layout assessment was also carried out, but is reported in section 4.4, page 69.

A series of runs was carried out in order to establish whether the extent of mining in the out of plane dimension would have considerable effect on the values of the "maximum expected magnitude" along a bracketed discontinuity. This condition could have not been taken into consideration using DIGS. In effect, this was the principal reason why 3D modelling was carried out.

MAP3D has been used extensively for 3D modelling of bracket pillar layouts (Wiles, 1996) as it is capable of explicitly calculating the amount of slip on discontinuities. In our case, the modelled discontinuities studied were represented as 'displacement discontinuity' elements with zero cohesion and 30^{o} friction angle.

Ultimately, it had been intended that the results obtained from 3D modelling would be compared against data from the bracket pillar design charts, as well as from seismic data recorded at given field sites.

The general model geometry used in these MAP3D analyses is shown in Figure 28. Variations of various modelling parameters were considered, similar to those discussed in section 3.2 for the 2D case study. One example of a MAP3D solution showing the spatial influence of the resultant slip on the discontinuity is also shown in Figure 28.

Once slip on a discontinuity is determined three-dimensionally, the maximum expected magnitude along the plane of slip (i.e. the bracketed discontinuity) may be determined. The procedure would involve similar steps as defined for the 2D cases, in section 3.3. This would be done using Aki and Richards (1980) Equation 1, on page 42. Subsequently, Equation 4 could be used to relate expected magnitude and size of the mining opening. Such relationship would be defined as:

$$\text{Magnitude} = \frac{2}{3}\log\,[W.\ \min(W,\ S)^2] + c \qquad \text{Equation 4}$$

where *W* is the width of mining in the third dimension, *S* is the mining span and *min* stands for the minimum of the two. '*c*' is a constant (Hanks and Kanamori, 1979) and Spottiswoode, 1996). In fact, various '*c*' values have been calculated from various sets of data, the results of which are (Table 4):

Table 4. **'c'** ***values obtained from different sets of data. The data from which to generate 'c' values include: event magnitude at a discontinuity, width of mining and mining span.***

Data Base	c values
Western Deep Levels	-4.53
Vaal Reef	-3.41
MAP3D	-4.2
DIGS	-4.33

A possible explanation as to why the Vaal Reef '*c*' value was found to be considerably different from the others considered may be due to the limited and somehow inadequate number of data available from the respective database.

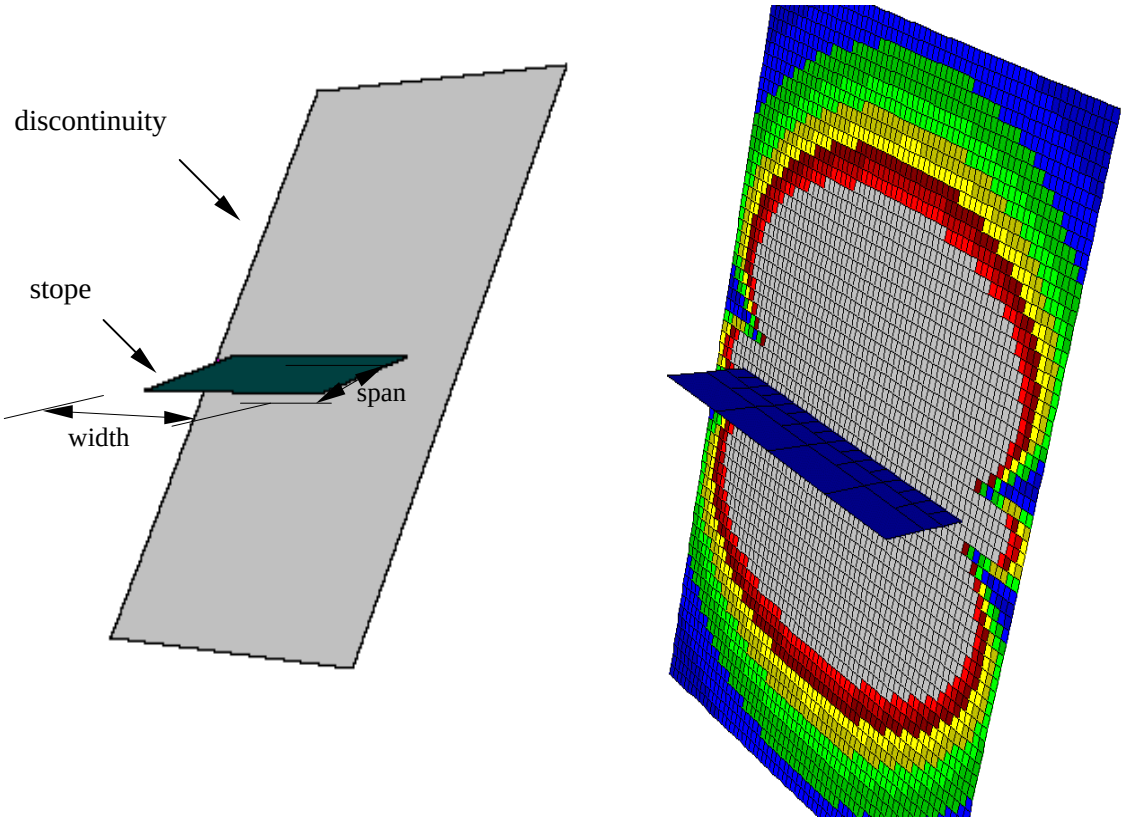

Figure 28 MAP3D model geometry used in 3D analyses (left). Note that the "width" of mining is now being considered, a factor not possible to account for using 2D DIGS. A typical spatial distribution of the extent of slip on a modelled discontinuity for a specific run (right) is also shown.

Modelling parameters adopted in the 3D model studies were kept the same as for the 2D DIGS models referred to in section 3.2. These included a Young's Modulus of 70 GPa and a Poisson's Ratio of 0.21.

Different mining geometries derived from combinations of stope width, span and discontinuity angle have been modelled. Table 5 lists the mining geometry dimensions considered in these models and shows, at the same time, correspondent values of the maximum expected magnitude calculated from MAP3D and DIGS analyses, for each given layout geometry.

Comparisons can, therefore, be made between the 2D and 3D modelling results, as is the example of the chart on Figure 29. It may be seen from this figure that the results from the two sets of analyses are coincident for lower ratios of mining width/mining span. On comparing model results obtained from design charts (2D DIGS based) against model

results from MAP3D runs (3D) for the same layout geometries (see Figure 30) indicates that where the expected magnitude is > 1.5 the correlation between the two models is good, with DIGS providing slightly lower values.

Table 5 ***List of mining geometry dimensions considered in MAP3D models (span, stop dip, pillar size, discontinuity dip, ratio of mining width to mining span). Also shown are the correspondent values of the maximum expected magnitude calculated from MAP3D and from DIGS analyses for each give layout geometry.***

span	stope dip	pillar size (m)	discont. dip	width: span	maximum expected magnitude	
					MAP3D	DIGS
100	0	100	90	500:100	0.87	0
150	0	50	90	500:150	1.07	0.1
160	0	40	90	500:160	1.12	0.2
170	0	30	90	500:170	1.18	0.5
180	0	20	90	500:180	1.68	1.55
190	0	10	90	500:190	2.6	2.4
195	0	5	90	500:195	2.78	2.66

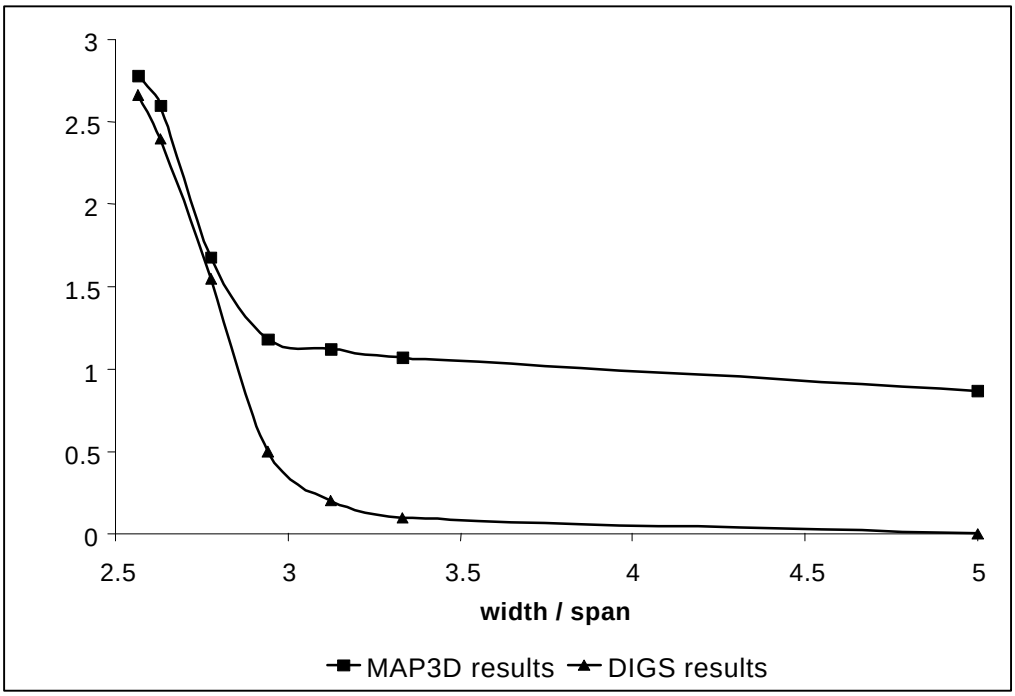

Figure 29 Comparison between MAP3D results and DIGS results. These appear coincident for the lower ratios of mining width/ mining span (i.e. for layouts that have relatively small mining widths in respect to relatively larger mining span).

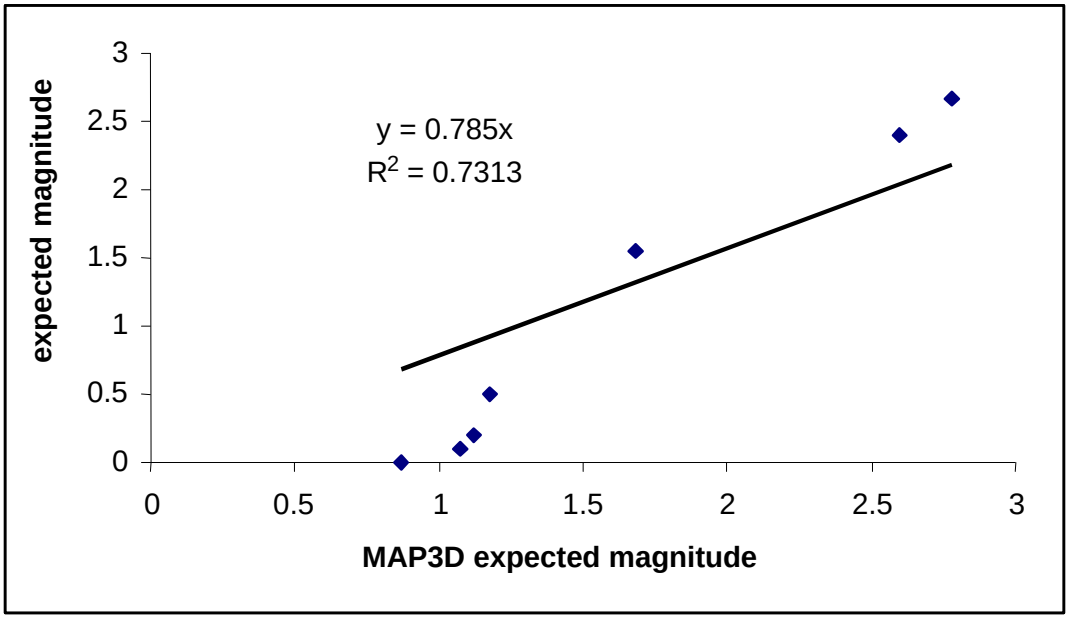

Figure 30 Association between MAP3D results (3D) and design charts, DIGS results (2D) for the same analysed bracket pillar layout geometries. There appears to be strong association between these two.

4.4 Comparison between cumulative seismic moment from structures at a selected field site and from these structures when modelled three-dimensionally using MAP3D.

4.4.1 Introduction

In this part of the work, further assessment toward the verification/validation of the methodology that uses design charts for bracket pillar design was carried out. A back-analysis was again conducted, but contrasts with the study in section 4.3 (e.g. Figure 28) in that the layouts now studied through modelling were less hypothetical, and based on realistic mining outlines of face advance (e.g. Figure 31). The study was focused on a complex bracket pillar area on the former No. 5 Shaft of Vaal Reefs Exploration and Mining Company. The geological and mining characteristics of this site have already been described in section 2.1, page 27. It is important to recall that the rock mass in the area of interest is quartzite in the footwall and argillaceous quartzite/shale in the hangingwall of the Vaal Reef and that the average stoping width ranges from 1 and 1.5 m. Mining takes place at a depth below datum between 2500 and 2615 m.

As mentioned in section 2.1, the mining area of interest was covered by a Portable Seismic System (PSS) (Figure 2), which had been installed in order to monitor the seismic response of geological structures to the mining activity and the behaviour of the various bracket pillars during their formation. The seismic data acquired from the field site was used and compared to seismic data from numerical modelling. This was necessary in order to determine the confidence to be gained from three-dimensional modelling of realistic bracket pillar layouts. DIGS based designs for the same bracket pillar site would be compared against the MAP3D results and ISS seismic records.

The number of fault and dyke structures existing in the area of interest make this a very complex mining layout to be modelled. Giving the impossibility with current resources of building a model that would replicate most of the layout structures in one single model, the relevant discontinuities were subdivided into various sections (see Figure 31).

The Tribute dyke (structure divided into section 3 and 18 in Figure 31) is to the north of the site, the area beyond this dyke having been mined out extensively. The Strike dyke (structure divided into sections 7, 8, 19 and 20 in Figure 31) runs parallel to the reef strike and is intersected by the Vos dyke (structure divided into sections 4, 5, 6 and 9 in Figure 31). To the south of this intersection, the Ben dyke (structure numbered 11 in Figure 31)

intersects both the Vos and Strike dykes. A number of bracket pillars had been designed around these dykes and faults of this area.

The performance of the structures bracketed by these pillars was evaluated, both against recorded seismicity (i.e. the seismic data discussed in section 2.2), and modelled expected seismicity, measured as the seismic moment of events presumably caused by slip along bracketed discontinuities.

A calibration exercise was conducted to ascertain the level of confidence of the model. This consisted of comparing, in the given boundary conditions, whether there was equivalence between modelled displacements on the reef plane of a given stope and the actually displacement measured at the correspondent field site. A good agreement between the two was obtained.

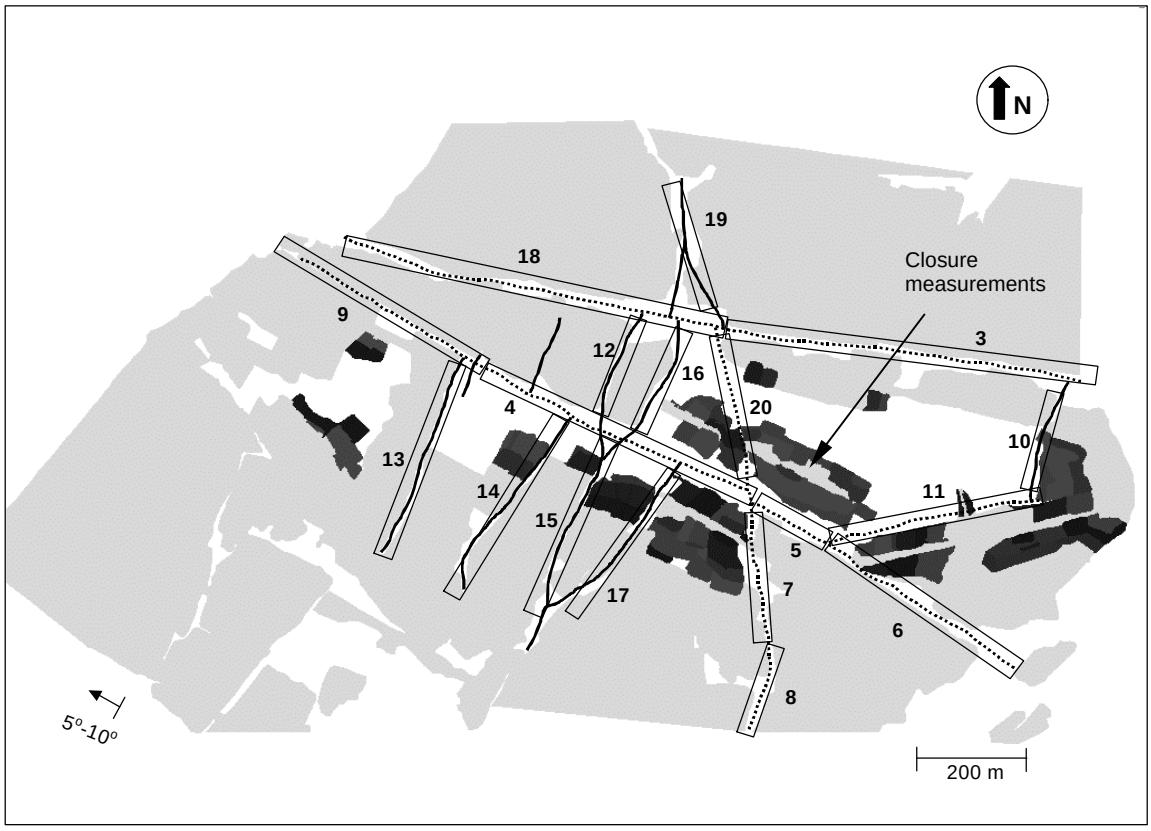

Figure 31 ***The Vaal Reefs No. 5 shaft region that was modelled. In this plan all major geological discontinuities are shown (enclosed in numbered rectangles). The extent of mining that occurred prior to the analysis start date is shown as grey and the recent mining is indicated in darker shades of grey. The stope where rock mass displacements were recorded is also indicated.***

4.4.2 Modelling settings and procedures

As stated, the region of interest from the Vaal Reefs mine (Figure 31) was modelled three-dimensionally using MAP3D. Ten mining steps were considered, correspondent to three-monthly interval of face advance. Mining face outlines were delineated for modelling starting from November 1995 until December 1997. Table 6 summarises the mining periods considered.

Table 6 The periods considered for MAP3D numerical analysis of the layout in Figure 31.

Mining step	Starting Date	Ending Date
1		Nov-95
2	Dec-96	Feb-96
3	Mar-95	May-96
4	Jun-96	Aug-96
5	Sep-96	Nov-96
6	Dec-96	Feb-97
7	Mar-97	May-97
8	Jun-97	Aug-97
9	Sep-97	Nov-97
10	Dec-97	Dec-97

Values for the elastic constants used in this model were the same as used for the DIGS models discussed in section 3.2, in which the Young's Modulus and Poisson's Ratio were 70 GPa and 0.21, respectively.

Owing to the complexity of the layout and the impossibility of running an equivalent model that includes all structures in one single numerical run (thus requiring large processing times for a limited number of boundary elements), it was decided that the discontinuities in the model would be subdivided into smaller sections, to be handled in separate but complementary runs (see boxes labelled from 3 to 20 in Figure 31). The discontinuities were assigned 30^{o} friction angles and very low cohesion.

At each mining step, the amount of slip along all modelled discontinuities is calculated. By using Equation 1 to Equation 3, a modelled maximum expected seismic moment or maximum expected magnitude along the discontinuity is determined.

The seismic records of the area modelled are then processed (those obtained from PSS and ISS field networks) in order to derive the field cumulative seismic moment for each

correspondent mining step. Lastly, a comparison between the seismic data and the modelling results is made in order to determine whether there was an association between these two.

4.4.3 Assessing the level of confidence of the MAP3D numerical model by comparing actual values of stope closure against equivalent data obtained from modelling.

Prior to undertaking the modelling exercises, it was felt necessary to assess the level of confidence that the MAP3D numerical model of the site would generate. The modelling settings mentioned above were considered, and the model geometry for all mining steps (i.e. the face outlines) were kept as realistic as possible. Use was made, therefore, of measurements of hangingwall/footwall displacements (i.e. stope closure) that were recorded at a stope within the region of interest.

Closure-ride stations had been installed in six panels of the "5 Shaft 68\57 West Stope" and measurements of displacements recorded three times per week. Figure 32 shows the relative positions of the closure stations.

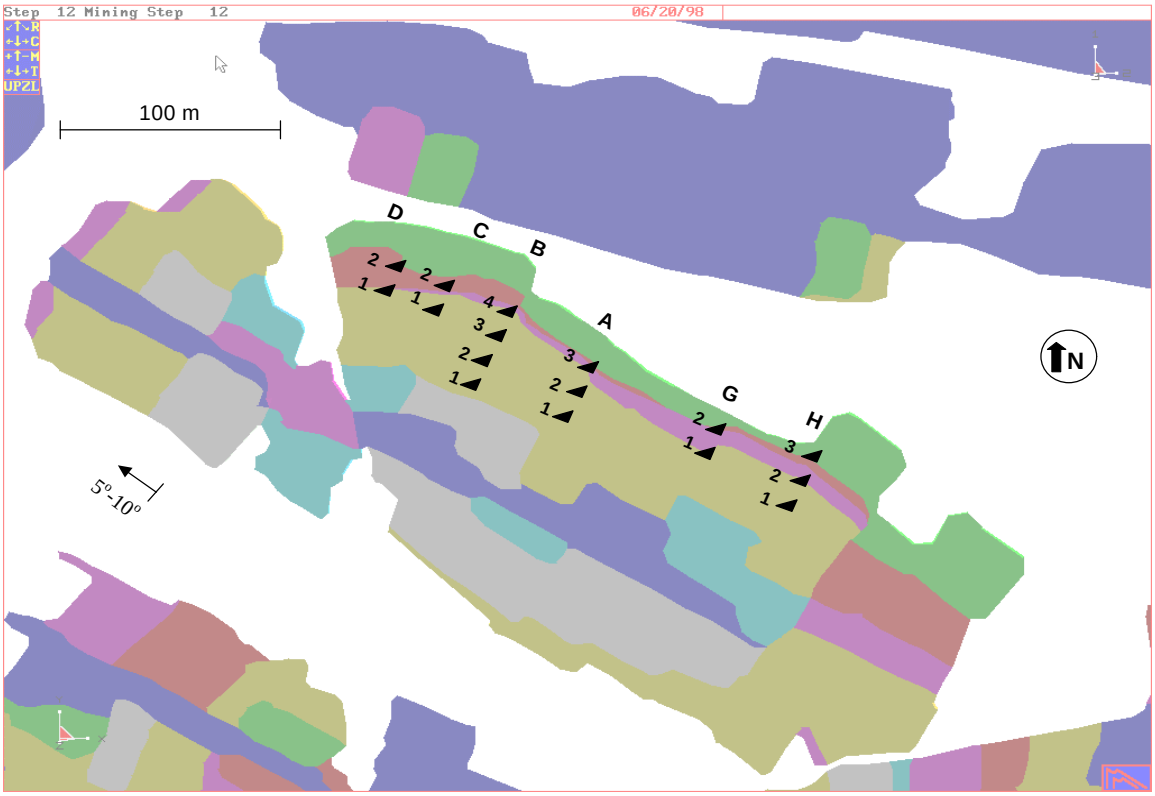

Figure 32 Relative positions of the closure-ride stations. Note that the stope where closure stations were installed (shown here) is the same as the central stope indicated by an arrow in Figure 31.

The hangingwall/footwall displacements on the reef obtained from the three-dimensional modelling were compared with the displacements measured at the field stations at correspondent periods of mining.

Two displacement profiles, i.e. modelled and measured, obtained for station A1 are shown in Figure 33 as an example. The upper profile represents the displacements measured in the field and the lower line the values obtained from modelling. Data from modelling emerged from the elastic solution of MAP3D. The area below the modelled results represents, therefore, the "elastic behaviour" of the layout at the specific site of station A1. On the other hand the field measurements include both inelastic and elastic influences. Consequently, the area between the two measurements will be indicative of the influence of non-elastic effects on the rock mass, which are not accounted for in the model. The narrower this band, the better the confidence that the model represents field conditions. In the case shown, approximately 63 per cent of the measured displacements were caused by elastic behaviour of the rock mass and 37 per cent by non-elastic (see Table 7 to justify these figures). The plot in Figure 33 may indicate that there is a strong qualitative agreement between modelled and measured rock displacement values for this station.

It was also observed that this trend is largely maintained for the majority of the remaining stations (confirm with charts presented in Appendix B). Such results support, with a significant degree of confidence, that the model conditions arranged for the planned modelling study were acceptable.

Table 7 Percentage elastic and non-elastic displacements (mm), accounted for station A1 during various mining steps.

Mining steps	Modelling result	Field data	% elastic	% non-elastic
8	99.03	167.09	59.27	40.73
9	252.52	397.82	63.47	36.53
10	271.87	409.60	66.37	33.63
11	284.24	455.24	62.44	37.56
12	321.30	502.48	63.94	36.06
		Average	*63.10*	*36.90*

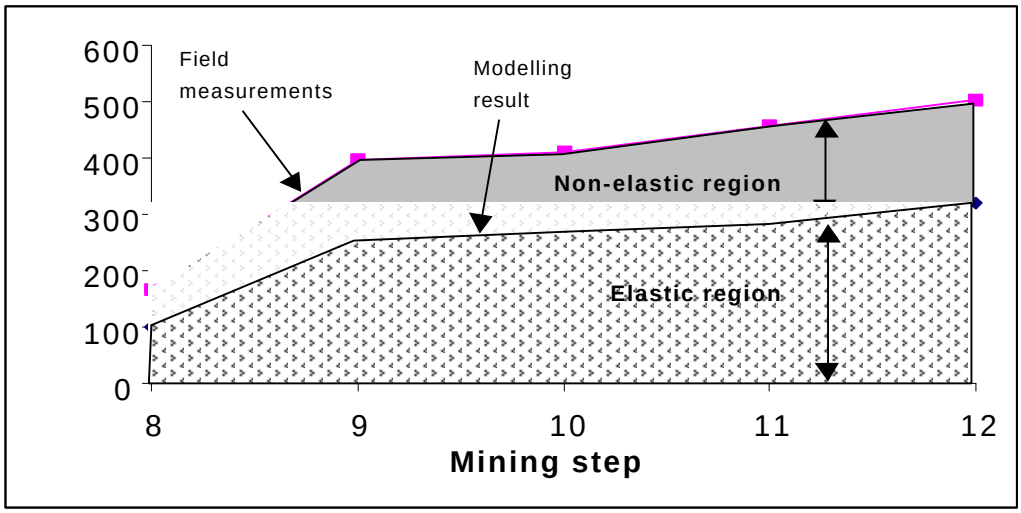

Figure 33 Two displacement profiles, i.e. modelled and measured, obtained for station A1. The upper profile represents the displacements measured in the field and the lower one the values obtained from modelling. The area between the two measurements is indicative of the influence of non-elastic effects on the rock mass, which are not accounted for in the model.

4.4.4 Presentation of modelling results

MAP3D solves explicitly the amount of slip along multiple geological features, an option not possible in MINSIM type codes. These features are represented as displacement discontinuity planes, within the limits of which solution variables are output.

Figure 34 (case a to e) shows examples of the extent of slip (marked as "area of slip") determined for a modelled discontinuity (numbered 20 in Figure 31) during the mining steps in **Error! Reference source not found.**, i.e. from December 1996 to December 1997. Also plotted in Figure 34 are all the events recorded for the correspondent modelling period. Note that no allowance was made in the modelling for the effect of slip of any recorded or predicted event on the slip calculation for the following mining step.

Although all discontinuities numbered in Figure 31 were modelled and their maximum slip values determined, the respective slip results are not presented here in terms of a shear displacement *per se,* but rather as transformed seismic moment (termed "seismic moment (MAP3D)", on graphs in Appendix C). This seismic moment, which has been determined for all features using the rationale explained in section 3.3, page 41, refers to the measure of a seismic event caused by slip along the bracketed discontinuity, during a given period of mining. This modelled parameter has been compared against the seismic moment of events actually recorded in the field. This is discussed in the next section.

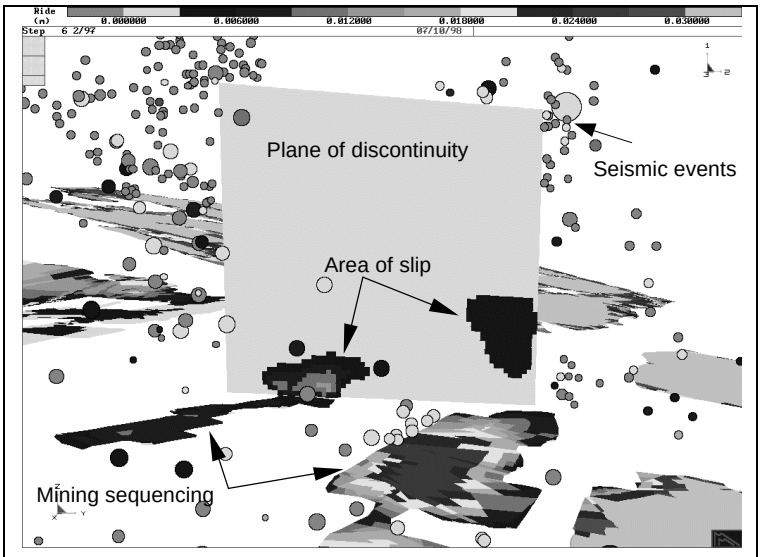

(a) Mining step 6 (from December 1996 to February 1997)

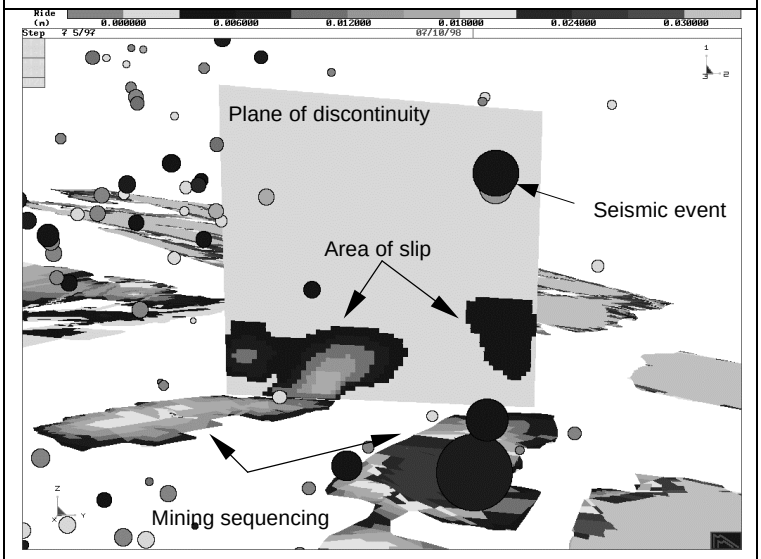

(b) Mining step 7 (from March 1997 to May 1997)

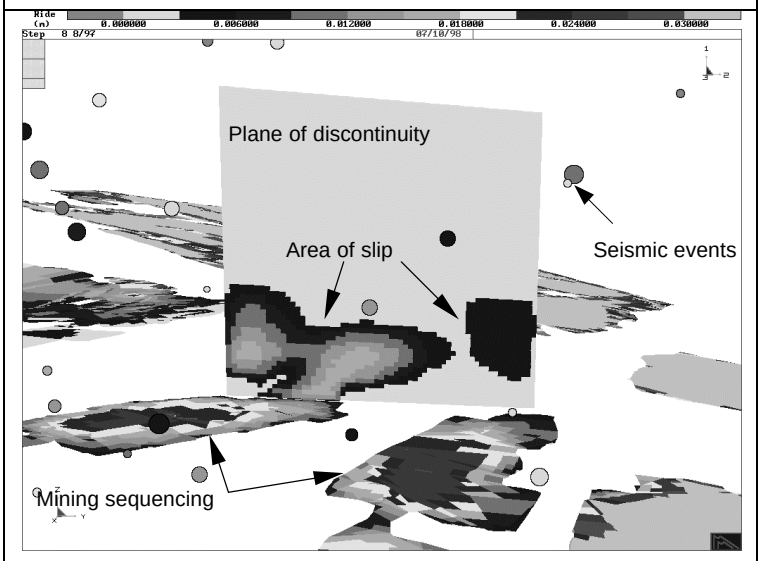

(c) Mining step 8 (from June 1997 to August 1997)

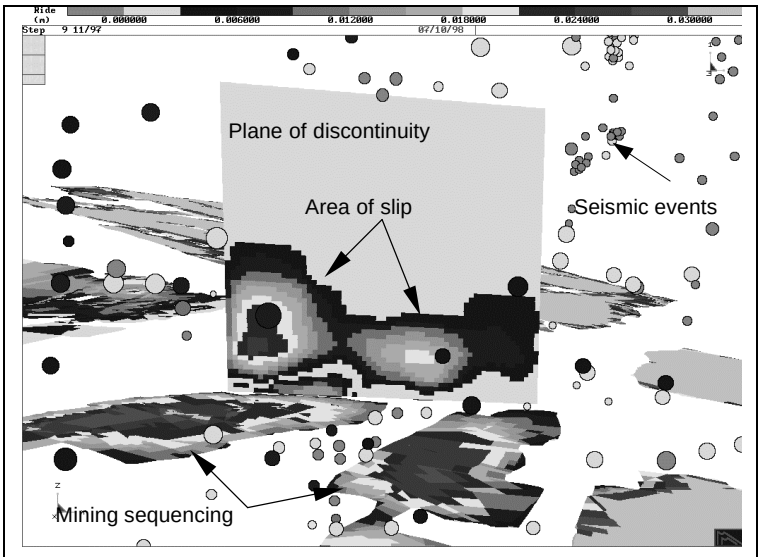

(d) Mining step 9 (from September 1997 to November 1997)

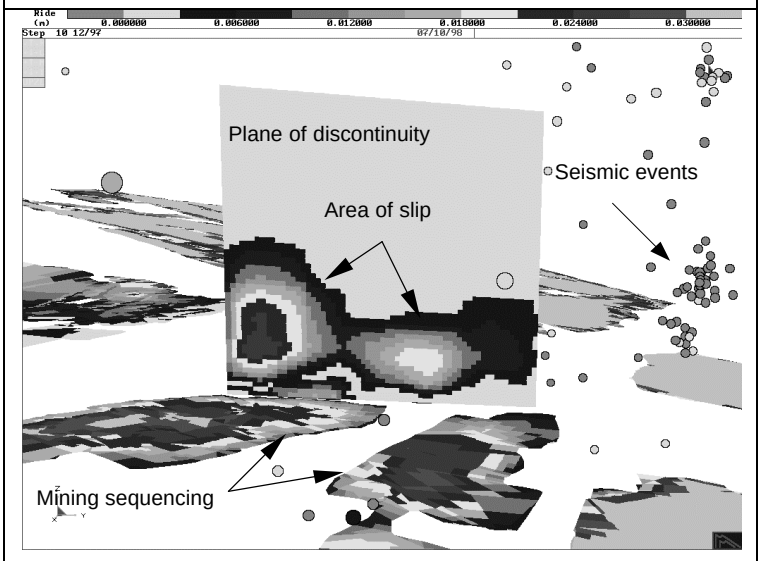

(e) Mining step 10 (December 1997)

Figure 34 Imaging of MAP3D solutions that illustrate the extent of slip along a modelled geological feature (feature numbered 20 in Figure 31) for various mining steps. The geological feature is represented as a displacement discontinuity plane (shown in light grey and marked as 'plane of discontinuity'). The extent of slip on the spatial domain of the feature is marked as 'area of slip'. The 3D spatial distribution of seismic events that occurred during the period of analysis are also included (shaded circles).

4.4.5 Modelling results: MAP3D vs. field measures of seismic hazard on bracketed features

The MAP3D derived seismic moments (e.g. 'maximum expected seismic moment' in Figure 35), in respect of modelled slip events that occurred on features during the mining periods in **Error! Reference source not found.**, were compared to the seismic moment of events actually recorded in the field, during the same period of mining (e.g. 'field seismic moment' in Figure 35. All features in Figure 31 were considered.

Overall, comparisons between the expected incremental moment (i.e. modelled seismic moment) and the seismic moment obtained from a seismic network showed reasonably good correlation for the majority of the features modelled. An example of the association between these two sets of data is shown in Figure 35, indicating the modelled seismic moment vs. field seismic moment along the discontinuity numbered 9, in Figure 31 (see other results for the remaining discontinuities in Appendix C of this report). It could be inferred, therefore, that the rationale presented in section 3.3, on which the determination of modelled seismic moments was based is reasonably valid. Results show over estimation by model of moment by 10 to 20%.

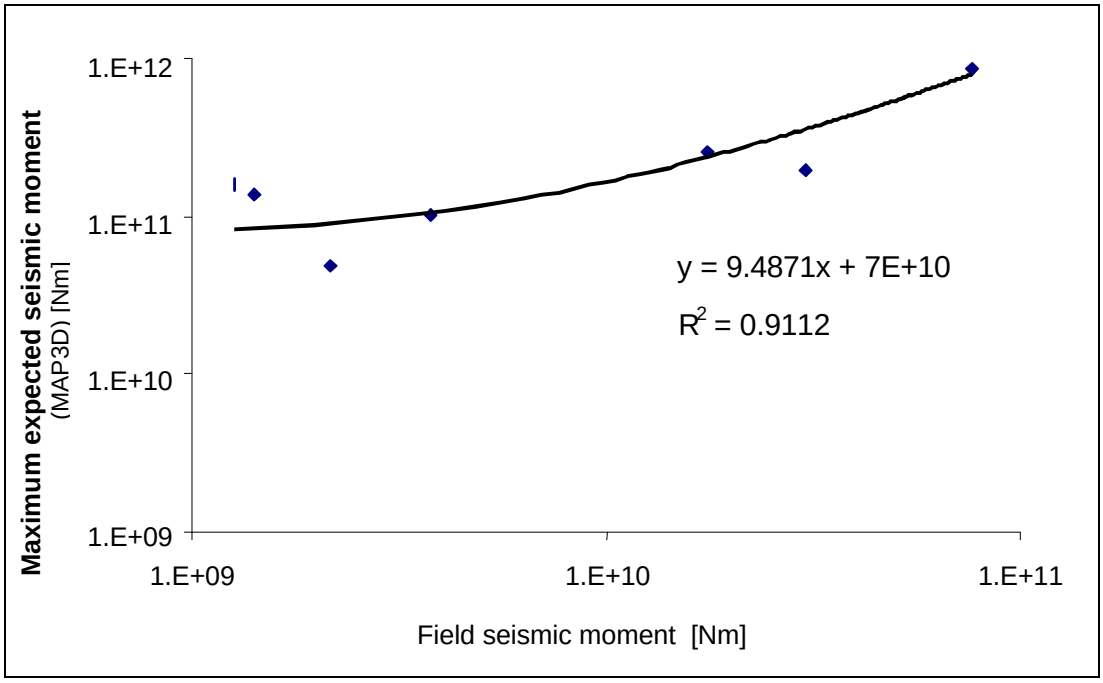

Figure 35 Correlation between field seismic moment and modelled seismic moment obtained for discontinuity numbered 9 in Figure 31.

Figure 36 illustrates further the qualitative level of agreement between the modelled seismic moment and the one obtained from the field seismic data for discontinuity no. 9, by comparing these two sets of data over various periods of mining (i.e. mining steps of **Error! Reference source not found.**).

Plots of comparisons similar to Figure 36 and referent to all studied geological features shown in Figure 31 have also been compiled in Appendix C of this report.

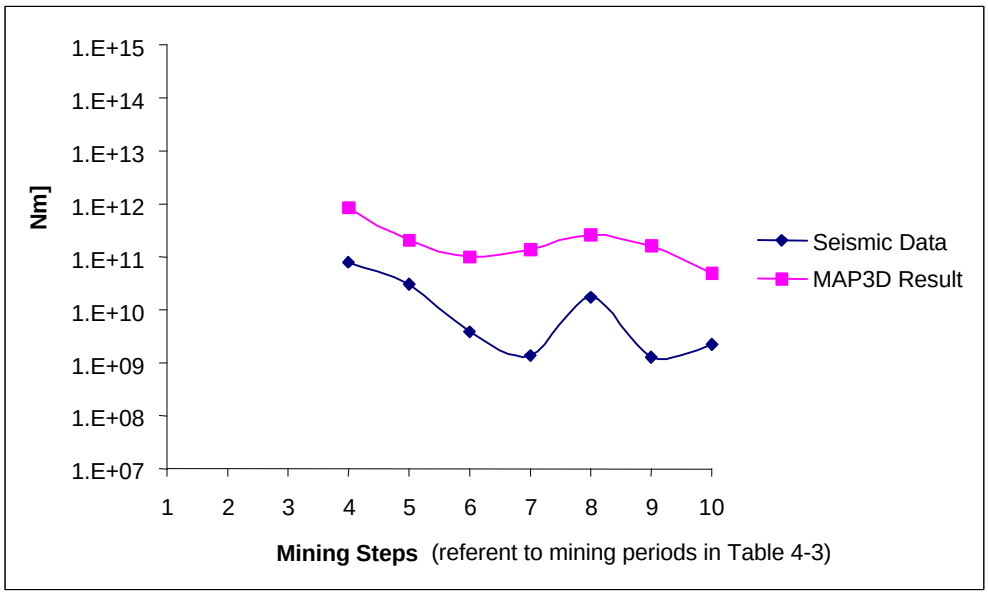

Figure 36 Comparison over various periods of mining, between the maximum expected incremental seismic moment (MAP3D modelled) and that from field seismic data for discontinuity numbered 9 in Figure 31.

4.5 Towards the validation of DIGS based design methodology: discussion

The remaining objective in sub-task 1.3 of the GAP 516 project proposal (see table in page 4), is concerned with validating the methodology discussed in section 3.4. In retrospect, the design methodology in question presupposes that pillars should be designed to take into account a tolerable level of seismicity in the vicinity of the bracketed discontinuity. This level of seismic hazard (represented by a seismic moment or event magnitude, as defined in section 3.3) along the bracketed geological structure is assumed to be dependent on the amount of arbitrary shear displacement along the discontinuity plane. Under this methodology, design charts (based on 2D DIGS

modelling) would be used to arrive at preliminary dimensions of a pillar required to bracket a given structure.

To test the validity of such a type of design using field data as a benchmark, as well as a 3D model to compare against inclusion of out-of-plane influences in the determination of the seismic hazard, the procedure in diagram of Figure 37 was followed.

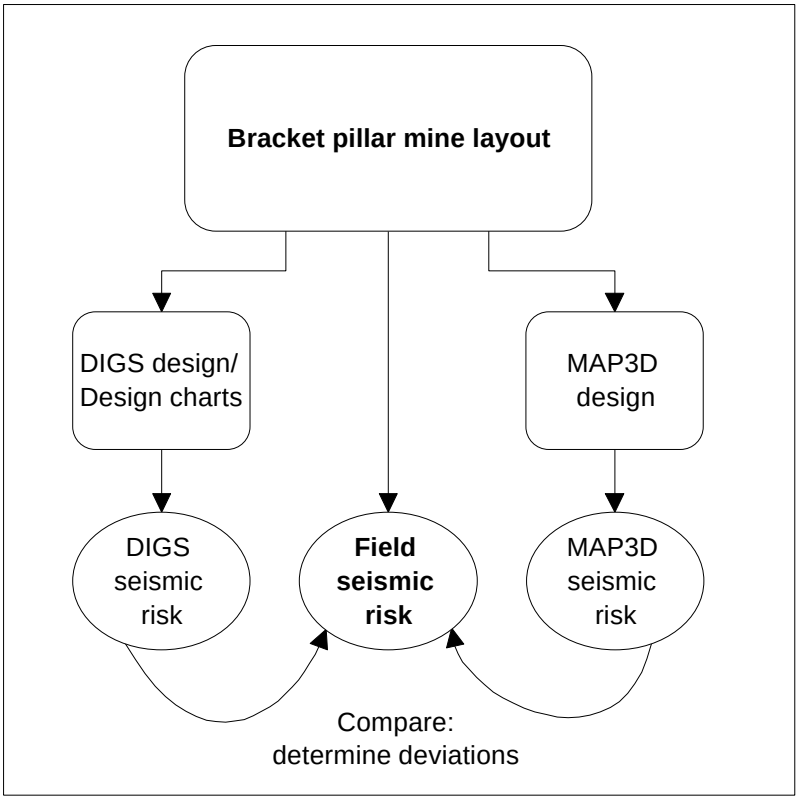

Figure 37 The process followed to validate the proposed methodology based on design charts for bracket pillar design.

The process would go as follows: from the seismic data gathered from the field site described in section 2.1, seismic moments of events in the vicinity of actual geological structures and bracket pillars should be determined. This data would be used as a benchmark against which DIGS based bracket pillar designs (i.e. based on design charts) would be compared. In addition, MAP3D modelling would be undertaken which would serve to verify whether significant differences would emerge from modelling the same layouts three-dimensionally. Differences were encountered and are discussed further.

The work discussed in the preceding sections of this report has addressed, in fact, the various legs of the procedure in Figure 37. Section 4.2 (which compares seismic

magnitudes from field sites and expected magnitudes from DIGS) addresses the phase of the above diagram concerned with the "DIGS designs" of bracket pillar mine layouts. Sections 4.3 and 4.4 (comparing seismic magnitudes from field sites and maximum expected magnitudes from equivalent and realistic MAP3D models) have addressed the phase of the diagram concerned with benchmarking DIGS designs against 3D modelling. This section discusses the results of these comparative studies.

4.5.1 Comparison between field and modelled cumulative seismic moment

The total seismic energy, measured as seismic moment, released on each modelled geological discontinuity during the entire period of monitoring was computed. Numerically, this corresponded to cumulating the seismic moment of all events that occurred in the vicinity of each discontinuity, over all the mining steps listed in **Error! Reference source not found.**. The exercise was done for both sets of data (MAP3D modelling and field data sets), for all geological discontinuities modelled.

Figure 38 shows the relationship that results from associating field and MAP3D data. Logarithmic scales are applied to both axes of the chart. Each point on the chart refers to the cumulative seismic moment along a given geological feature over the entire modelled period (number labels of each point on the chart refer to the feature number as given in Figure 31).

It is evident from Figure 38 that, when all features are considered, relative good correspondence exists between the two compared data sets. The line of symmetry shown is not the best-fit line, though. In the ideal case, however, perfectly related data points would be clustered along such a line. The majority of MAP3D results appear to cluster along the symmetry line of the chart presented, indicating that, for some of the modelled features, including the influences from the out-of-plane dimension was necessary.

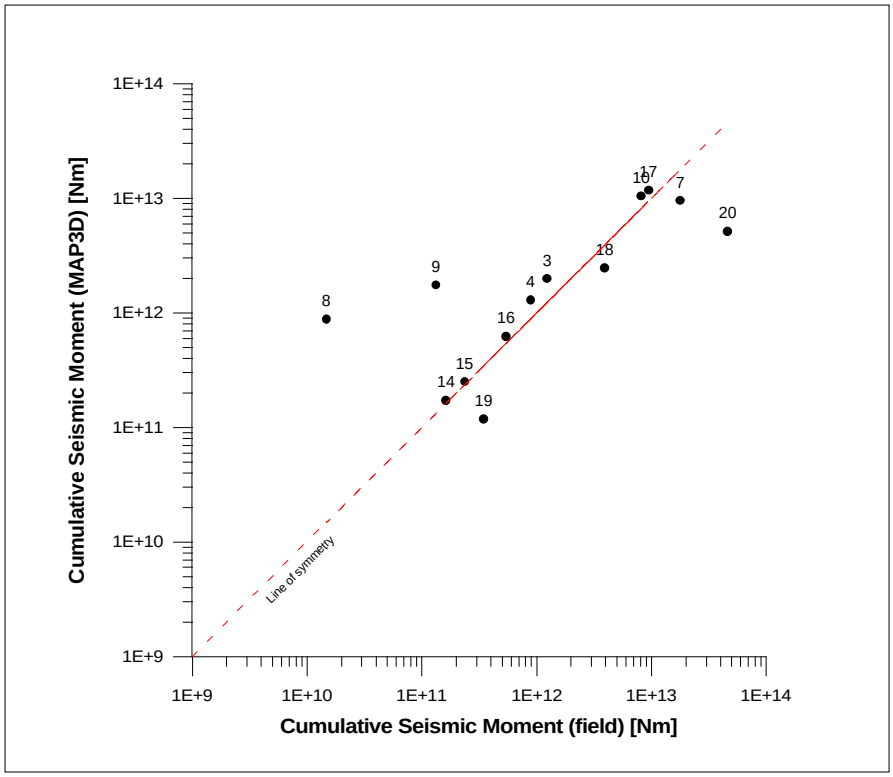

Figure 38 Association between cumulative seismic moment from events registered in the field and cumulative seismic moment from modelling (MAP3D), obtained for all modelled geological features over 10 mining steps (i.e. over all periods of mining in Table 6). Number labels of each point on the chart refer to the feature number, as given in Figure 31. Note that there is some relative agreement between MAP3D results and field results. The 'line of symmetry' is not the best-fit regression line, however.

A comparison similar to that of Figure 38 was made between the cumulative seismic moments obtained from 2D DIGS modelling, i.e. from design charts data, and the cumulative seismic moments from field seismic events. It was intended to give an indication of how well these two data sets were related, and thus obtain a feel for the respective deviations.

Figure 39 shows the relationship that results from associating such data. Logarithmic scales are also applied to both axes. Each point on the chart refers to the cumulative seismic moment along a given geological feature obtained from DIGS modelling (design charts) and from field data over the entire modelled period (number labels on each data point refer to the feature number given in Figure 31). It is striking to note that a similar

pattern of association exists between the DIGS generated and field obtained seismic data. There is, however, a wider scatter from DIGS/ design charts results relative to field data, than there was when MAP3D was used (compare with Figure 38). DIGS always overestimated the cumulative moment.

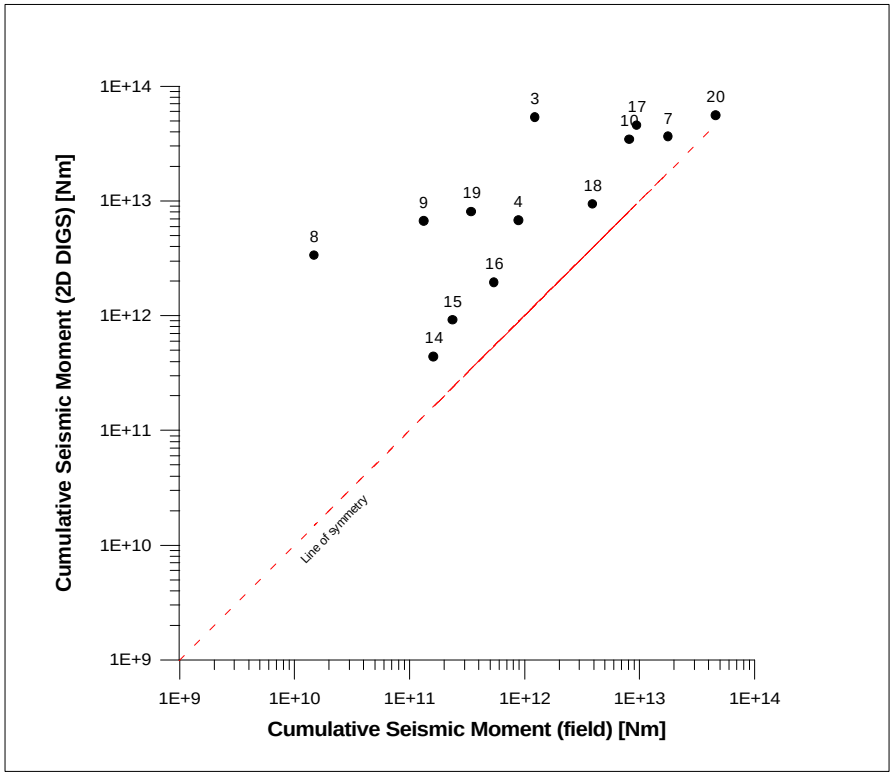

Figure 39 Association between cumulative seismic moment from events registered in the field and cumulative seismic moment from modelling (DIGS/i.e. design charts), obtained for all modelled geological features over 10 mining steps (i.e. over all periods of mining in Table 6). Number labels of each point on the chart refer to the feature number, as given in Figure 31. Note that DIGS results slightly overestimate field results. The 'line of symmetry' is not the best-fit regression line.

Overall, it appears from the above plots that the "seismic risk" of some features was better modelled using MAP3D than using DIGS. The difference may be attributed to the fact that MAP3D would have taken into account the irregular layout geometry in the third dimension, a condition not possible in DIGS. In other words, MAP3D allows the modelling of the actual mining sequence in the vicinity of the structure, in full 3D representation (note that MINSIM type codes would also account for such geometry

constrains, however, they would not allow for explicit slip along discontinuities to be determined). Figure 40 compares these two sets of data, MAP3D and DIGS. The extent to which DIGS cumulative seismic moments differ form those determined using MAP3D is shown in a graphic form. Deviations from the line of symmetry (which would have given perfect correspondence) measure the differences between the two sets of results. Note that, comparatively, DIGS solutions always over-estimated MAP3D solutions, for all modelled geological features.

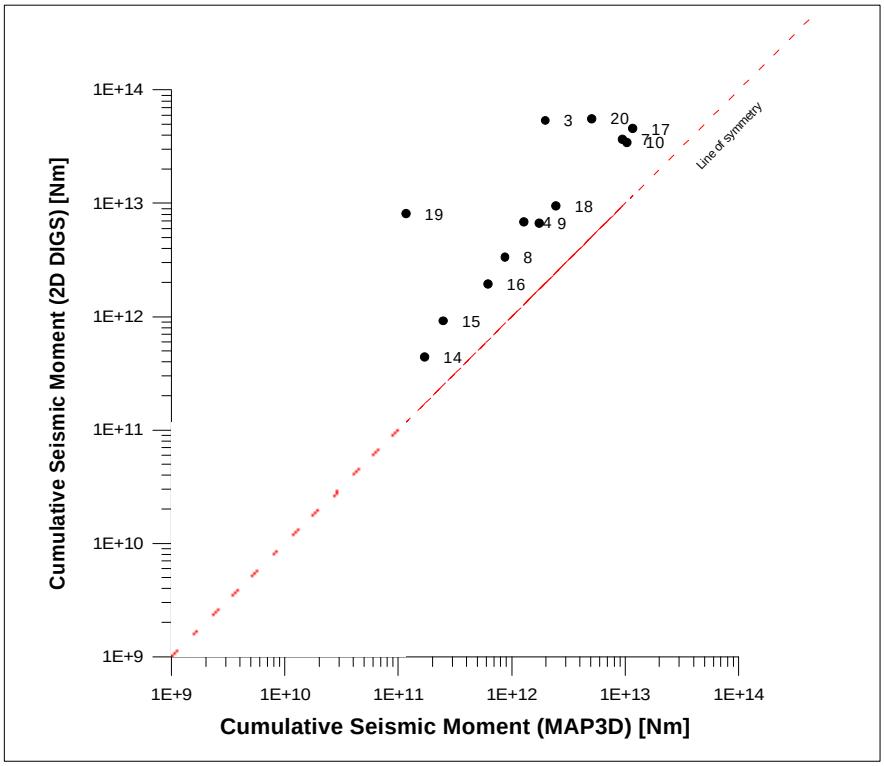

Figure 40 Association between cumulative seismic moment from 'slip type events' as determined using MAP3D, and cumulative seismic moment determined using DIGS (i.e. design charts), for all modelled geological features over 10 mining steps (i.e. over all periods of mining in Table 6). Number labels of each point on the chart refer to the feature number, as given in Figure 31. Note how DIGS results slightly overestimated MAP3D results. The 'line of symmetry' is not the best-fit regression line.

The comparison exercises revealed by Figure 38, Figure 39 and Figure 40 (MAP3D vs. Field, DIGS vs. Field and MAP3D vs. DIGS respectively), in respect of the determination of cumulative seismic moments of events along bracketed geological features, have shown the variation that exists between modelling results and field data. In some cases

relatively good agreements were obtained between these, in others the association is not strong.

The main conclusive observation appears to be the fact that the DIGS cumulative seismic moments were higher than those determined by MAP3D (confirm in Figure 40). This may imply that bracket pillar designs based on 'design charts' will be slightly conservative, when compared to MAP3D designs. If all results are combined in one chart which shows the differences among the various data sets for all geological discontinuities modelled (i.e. DIGS, MAP3D and field cumulative seismic moment), the same conclusion may be derived. For all cases studied, only in two instances did the DIGS results correlate better to field data than the MAP3D results (see seismic moment values for features numbered 7 and 20 in Figure 41).

However, it is not necessarily the case that the field data is a definite datum against which the modelling results need to be compared. There are errors in calculating Moment from seismograms, events may been missed or not located on the structure on which they occurred.

The latter three factors would under value the Moments calculated from field data. In addition, seismic data analysis carried out under SIMRAC project GAP 530 indicates that there can be a time lag between mining and the seismic response.

Thus, some events, which occurred on the structures after Dec. 97 should be included in the field data, set. Therefore, it can be concluded that the correlation between theoretical and measure parameters are better that indicated.

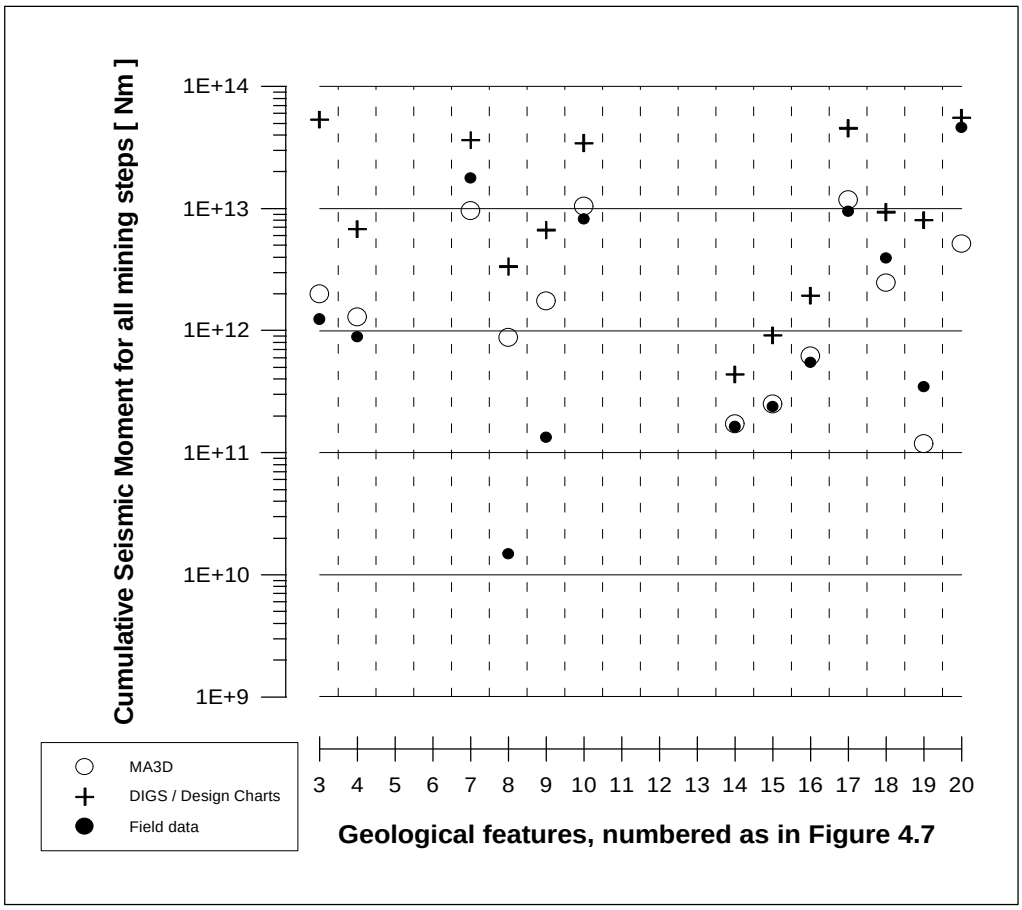

Figure 41 ***Comparison of results derived from modelling against those obtained from field data. The differences between DIGS, MAP3D and the field cumulative seismic moment for all modelled geological discontinuities are visible. Only in two instances did DIGS results correlate better to field data than MAP3D results (see moment values for features numbered 7 and 20 in Figure 31). Overall, DIGS cumulative seismic moments are relatively higher than MAP3D for the majority of the features.***

5 Conclusions

A methodology for bracket pillar width estimation that used "design charts" has been reviewed. This is based on numerical modelling with DIGS, and has been confirmed in three dimensions using MAP3D modelling and seismic data analysis.

In many instances, comparison between seismic data and both 2D and 3D modelling results gives good correlation as far as both the magnitude and the trends of the relationships are concerned. A reasonably good agreement was found between the occurrence of the larger seismic events and the positions of slip expected from the 3D modelling. The larger events tended to locate along lines defined by the geological structure and, specifically, in the proximity of the expected slip positions on various discontinuities.

The occurrence of seismic events with high S- to P-phase ratios recorded by the PSS was compared with the slip positions expected from the 3D modelling, and a reasonable agreement was found between the recorded seismicity and the structural lineations and positions of expected slip on the discontinuities. This agreement was obviously limited largely to the immediate vicinity of the PSS network, due to the paucity of data from further afield.

It appears that, in general, a layout that uses backfill as the support medium causes the bracket pillar design curves to be much flatter, which may imply a reduction in the potential seismic hazard. For example, for the case of a horizontal stope with a k-ratio of 0.5 at a depth of 3000 m and a discontinuity angle of 112^{o} relative to the horizontal plane, the maximum expected magnitude along such a discontinuity using a bracket pillar size of 30 m would be 2.3. Should that stope be backfilled, however, with 90 per cent fill over the available area, the value of the expected seismic magnitude would be reduced to 1.4.

Comparisons made between the 2D and 3D modelling indicated that the respective results appear to be coincident for lower ratios of mining width/mining span (i.e. for layouts that have relatively small mining widths for relatively larger mining spans).

A relative good association between the cumulative seismic moment of field events and the cumulative seismic moment obtained from MAP3D modelling was established. It was evident that some geological features were better modelled by including the influences from the out-of-plane dimension. A wider scatter and, therefore, weaker association from the DIGS/design charts results relative to field data was observed. Some discrepancies could also be explained by deficiencies in the seismic data.

In addition, DIGS solutions consistently over-estimated MAP3D solutions, for all modelled geological features. Note that modelling analyses were carried out independently from analyses of seismic data. The correlations that have been found between modelling results and recorded seismicity arose from unbiased analysis, therefore.

6 Recommendations

The results of this study give grounds for confidence in the usefulness of the type of numerical modelling conducted in this study for designing mine layouts that have to negotiate discontinuities. The bracket pillar design methodology developed during the course of SIMRAC Project GAP 223, refined by 3D modelling as presented in this report, would appear to be a valid tool that can assist in mine layout design when applied judiciously by qualified rock mechanics practitioners.

Designs derived from design charts alone (see Vieira et al, 1998) would appear to be more conservative than designs based on 3D modelling.

On the strength of this finding, therefore, it would be recommended that 3D modelling codes that allow for explicit displacement along discontinuities and irregular mining geometries (for example Map3D) could be used when modelling bracket pillar layouts. Note, however, that any 3D numerical code will not eliminate the uncertainty related to the geometric characteristics of the discontinuities in the three-dimensional space.

Note that numerical modelling provides simplifications of real systems. These must be seen as a tool in the process of assessing rock mass behaviour. In this respect, bracket pillar designs based on numerical modelling or on "design charts" should not be regarded as "final designs".

These designs are initial estimates that should be verified and/or modified to consider specific experiences and rock mass conditions of the site for which they are intended.

A possible design methodology on bracket pillars should involve:

- The use of design charts, to best estimate pillar size.
- 3D modelling of the area of interest, to account for influence of the third dimension and irregular mining faces.
- Modification of design from experience, when that exists, at users risk.

7 References

Aki K. and Richards P. G., 1980. Quantitative seismology: Theory and practice, Freeman, 1980.

Anon., 1988. An industry guide to methods of ameliorating the hazards of rockfalls and rockbursts. Johannesburg, Chamber of Mines of South Africa Research Organisation.

Dede, T. and Handley M.F., 1997. Bracket pillar design charts. SIMRAC Interim Project Report. Johannesburg.

Dukes, G.B.,1998. Comments on GAP 516 - Further Validation of Bracket Pillar Design Methodology. Anglogold - Vaal River Operations. Letter Ref. SG-22-98, of Aug. 4, 1998.

Ebrahim Trollope, R. and Glazer, S.N., 1996. An assessment of seismic monitoring in a deep level scattered gold mining environment. Extended abstract. ISS, Welkom, SA.

Gay, N.C., Jager, A.J., Ryder, J.A. and Spottiswoode, S.M., 1993. Rock engineering strategies to meet the safety and production needs of the South African mining industry in the 21st century.

Handley M.F., Selfe D.A., Vieira F.M.C.C., Maccelari M.J., and Dede T., 1997. Current position of strike stabilising pillar and bracket pillar design-guidelines for deep level tabular orebodies. S.A.I.M.M. Johannesburg, May 1997.

Hanks T.C. and Kanamori H., 1979. A moment-magnitude scale. J. Geophys. Res., vol. 84 1979. pp. 2348-2350.

Hemp, D.A., 1994a, A literature review and industry survey on the design, use, and implementation of bracket pillars on South African gold mines. CSIR Mining Technology. SIMRAC Interim Project Report. , GAP 034.

Hemp, D.A., 1994b. The classification of dykes and faults on South African Gold Mines. SIMRAC. Dep. Min. Ene. Aff. Interim Project Report, GAP 034, 29 pp. Johannesburg.

McGarr, A., 1984. A scaling of ground motion parameters, state of stress and focal depth. J. Geophys. Res., vol. 89, pp. 6969-6979.

Napier, J. & Ryder, J.A. 1986. Application of excess shear stress concepts to the design of mine layouts. Colloquium .S. Afr. Inst. Mining & Metallurgy, Randburg. June 1986.

Napier, J.A.L., 1987. The application of excess shear stress to the design of mine layouts. J.A. Afr. Inst. Min. Metall., vol. 87, no. 12. Dec. 1987. pp. 397-405.

Napier, J.A.L., 1990. Modelling of fracturing near deep level gold mine excavations using a displacement discontinuity approach. Mechanics of Jointed and Fractured Rock, Rossmanith (ed.), Rotterdam, 1990.

Ryder, J.A., 1988. Excess shear stress in the assessment of geologically hazardous situations J. S. Afr. Inst. Min. Metall. vol. 88, no. 1 Jan. 1988. pp. 27-39.

Spottiswoode, S.M., 1986. Mining in the Vicinity of Geological and Hazardous Structures. Chamber of Mines, paper NS 637.

Spottiswoode, S.M., 1996. Personal communications.

Spottiswoode, S.M., 1998. Personal communications.

Wiles, T., 1996. MAP3D User's Manual. Mine Modelling Limited, Canada.

Vieira, F.M.C.C.; Selfe, D.A.; Dede, T.; Maccelari, M.J.; York, G.; Spottiswoode, S.M.; Esterhuizen, E.; Milev, A.; Johnson, R. A.; Webber, S.J; Handley, M.; Berlenbach, A.; Silva, A. Ruskovich, A. Vlietstra, D., 1998.; Deep mine layout design criteria: Bracket pillars: Volume 2 of 7. SIMRAC Final Report GAP 223.

8 Appendix A

Comparison of two seismic data sets

Seismic data recorded by the dedicated PSS network from the Vaal Reefs 5 Shaft bracket pillar research site were compared with data recorded from the same area during the same period by the mine-wide ISS network, to determine the degree of compatibility between the two systems. This was done in order to assess the extent to which an analysis of a combined data set would be feasible.

The PSS network was in operation from April 1996. Numerous difficulties were encountered from the onset of the monitoring which hindered the consistent operation of the network. A graph of the cumulative number of seismic events recorded by this network is shown in Figure 42. From September 1997 ('A' in Figure 42), the apparent event rate increased, as all of the recording sites were maintained in an operational state more uniformly. Towards the end of 1997 ('B' in Figure 42), the actual event rate decreased, as mining operations in the area were scaled back during a management transition phase. During 1998, most of the mining activity has been focused in a block of ground to the East of the PSS network (i.e. the zone labelled 'II' in Figure 2).

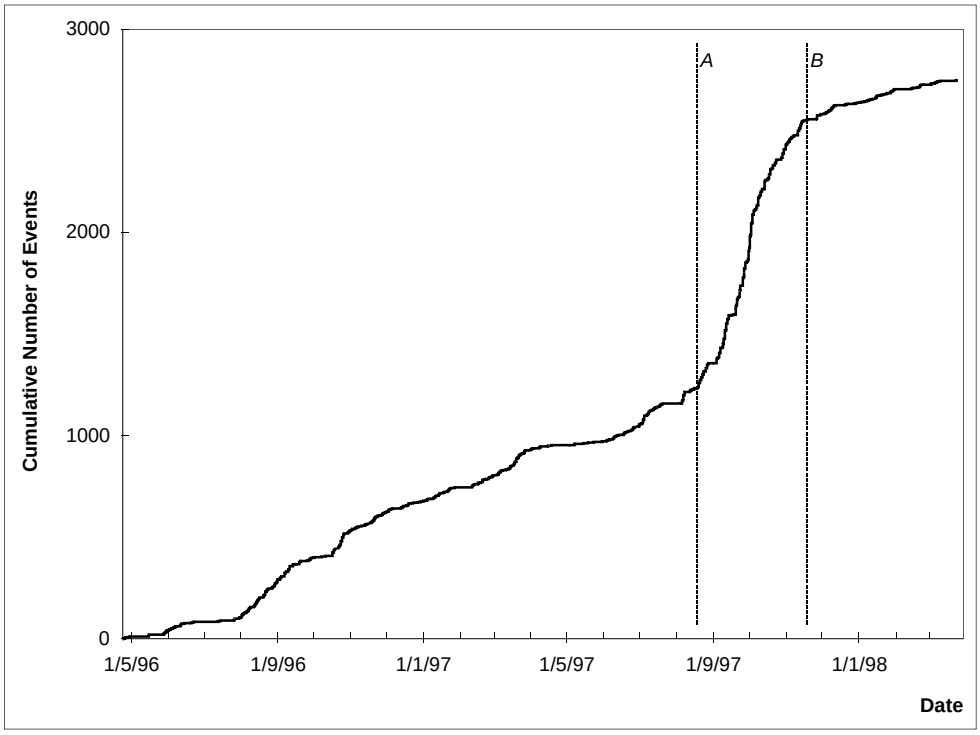

Figure 42 Cumulative number of events recorded by PSS from project site.

The frequency-magnitude distribution for the PSS data is shown in Figure 43. This represents the relationship between the range of event magnitudes determined for the recorded seismic data and the numbers of events occurring in various magnitude intervals within that range. The 'b' value is calculated from the inverse of the slope of the linear portion of the plot (i.e. the portion where magnitudes are greater than the specified minimum magnitude).

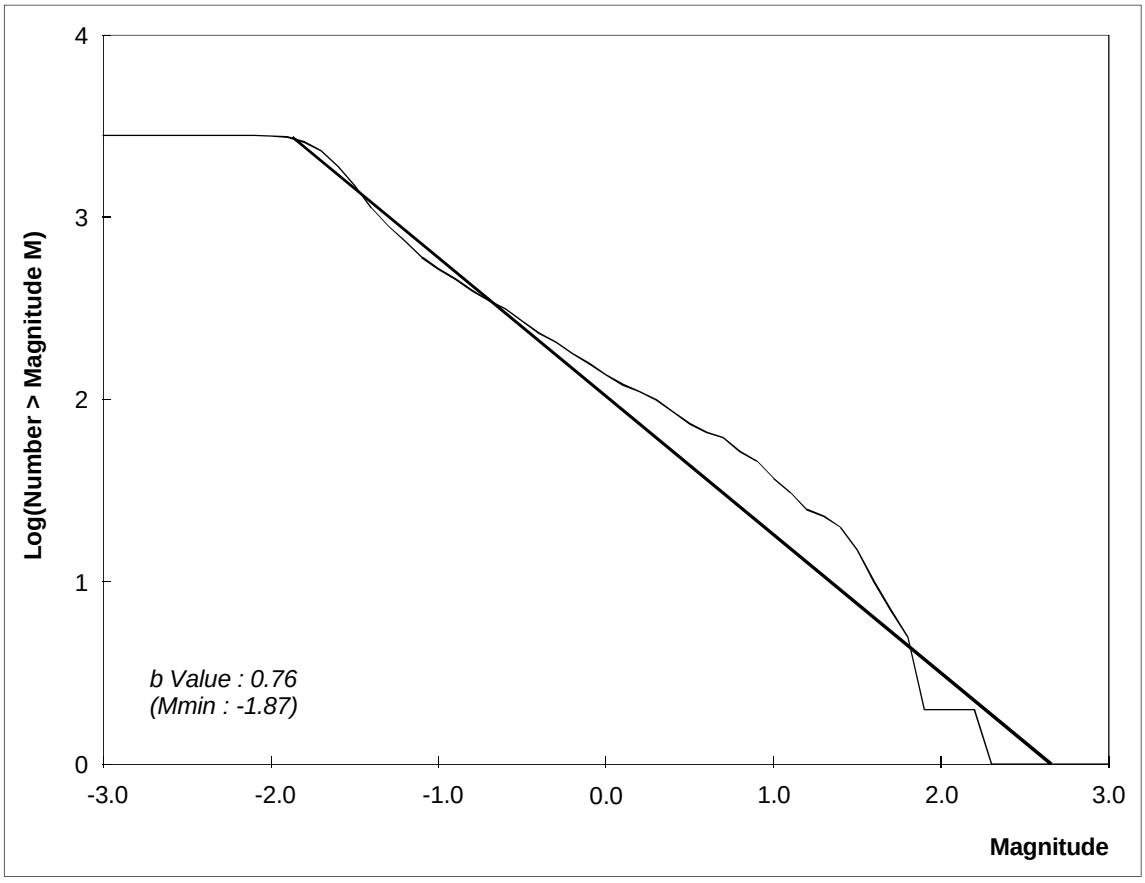

Figure 43 Frequency-magnitude distribution for seismic data recorded by PSS from project site.

Changes made to the ISS software in November 1996 had introduced an inconsistency in the processed data (compared with previous data), but the mine's seismology department had completed a back-calculation exercise which incorporated data recorded from May 1996 onwards. Thus, the ISS data that were used for the comparison with the PSS data were internally consistent. A graph of the cumulative number of seismic events recorded by this network is shown in Figure 44. From January 1998 ('A' in Figure 44), the event rate recorded by the ISS network from the study area increased, with most of the data being recorded from the easternmost part of the area (i.e. to the East of zone 'II' in Figure 2), where mining operations were renewed and the network station density was increased.

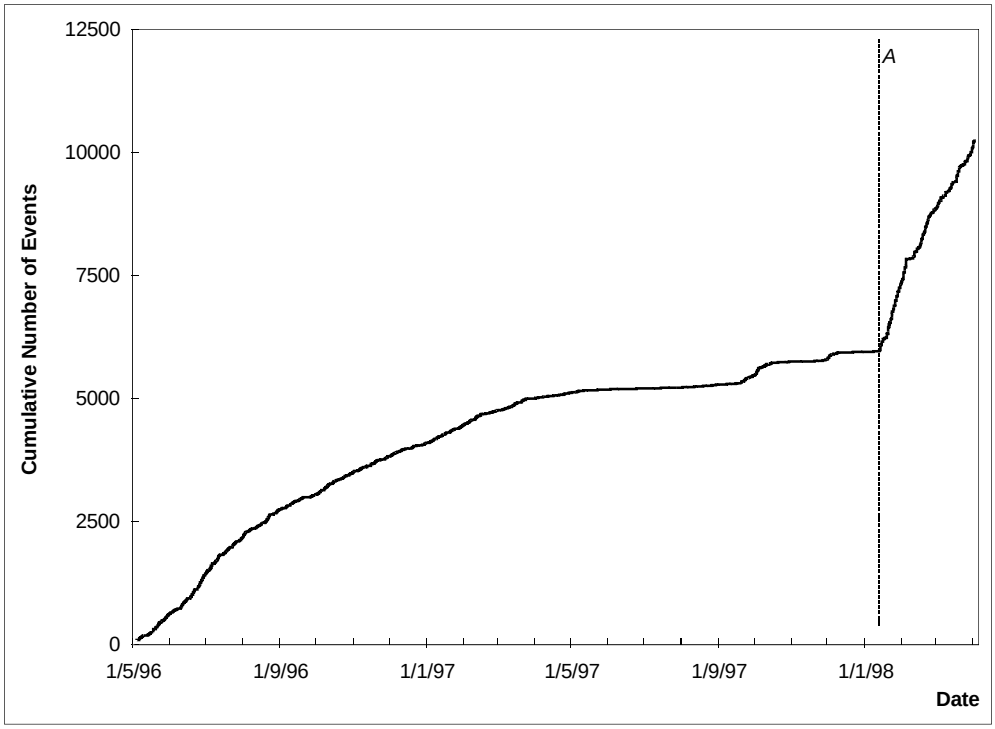

Figure 44 Cumulative number of events recorded by ISS from project site.

The frequency-magnitude distribution for the ISS data is shown in Figure 45. While the 'b' value for this distribution is similar to that for the PSS data, it is evident that the magnitude range is shifted somewhat to the right compared with that for the PSS data (compare this figure with Figure 43). This effect was investigated in greater detail using a subset of common events, as discussed later. It is also apparent that this distribution has a distinctly bilinear form, with a steeper slope (higher 'b' value) for the portion to the left of the minimum magnitude. This portion consists of data recorded from the easternmost part of the study area (mentioned above), where the sensitivity of the mine-wide network was locally enhanced by an increased station density towards the end of the study period.

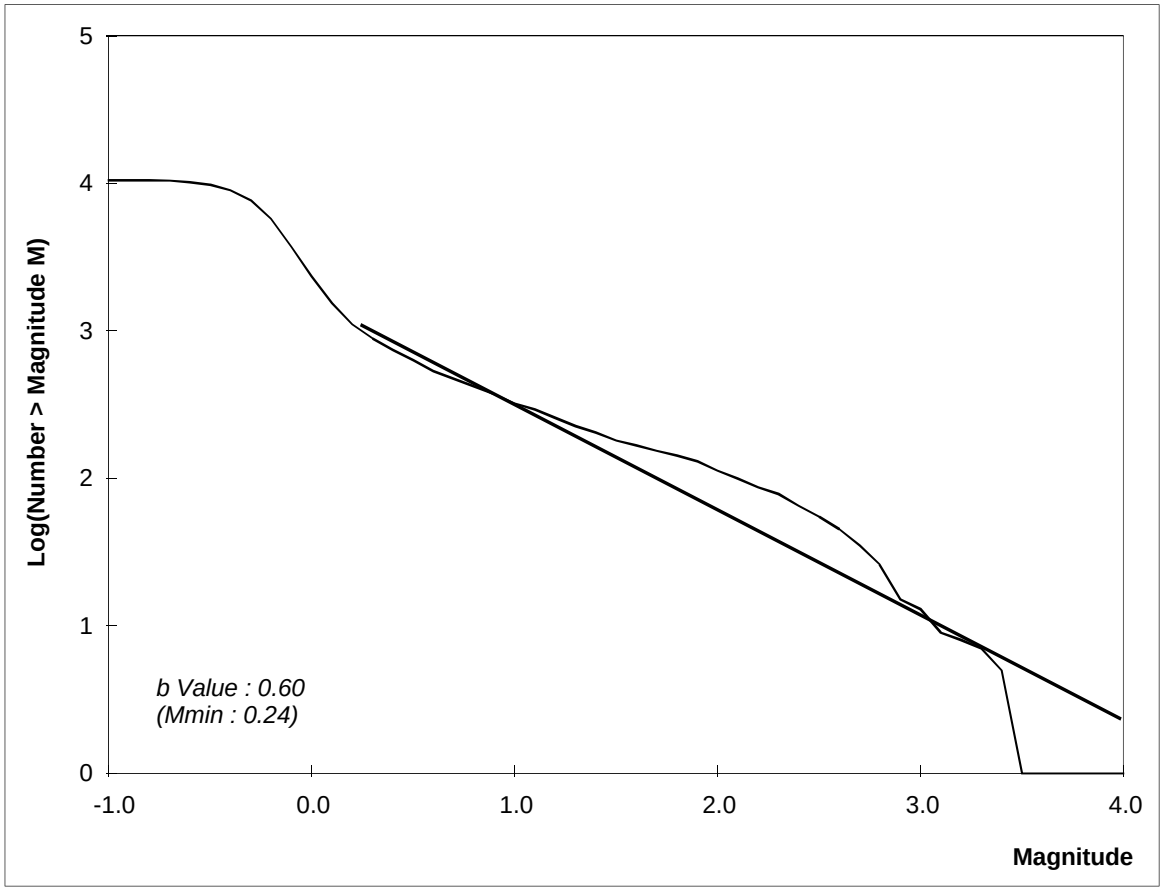

Figure 45 Frequency-magnitude distribution for seismic data recorded by ISS from project site.

A manual search was conducted for events recorded in common by the two networks, and 60 unique record pairs were identified. Only single events isolated in time from other events were considered, as the time bases of the two systems were not linked, so that there was no other way to be sure that the same event had been identified in each data set. The locations and magnitudes of these event records were then compared. The median difference in location of the 60 events was about 50 m, while the median difference in magnitude was 1.5 units. As mentioned in the SIMRAC Project GAP 223 Final Report, the magnitudes are calculated differently for the two systems. It was encouraging that the magnitudes were well correlated (coefficient of 0.92), so that the trends were consistent for the two systems. The magnitudes assigned to the common events by the two systems are compared in Figure 46, from which it can be seen that M_{PSS} -1.5 corresponded to M_{ISS} 0, while M_{PSS} 0 corresponded to M_{ISS} 1.

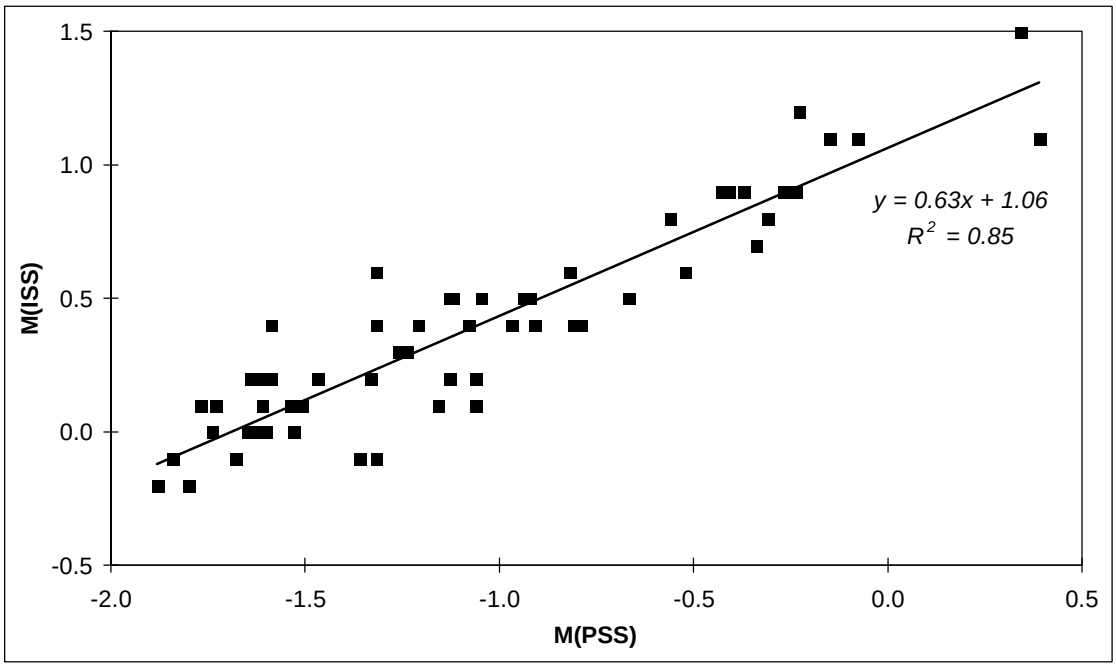

Figure 46 Comparison of magnitudes assigned to 60 events recorded by both PSS and ISS. The results of a linear regression analysis are shown.

The source parameters were then compared for the 52 events for which the PSS quality factors were adequate. The seismic moments (Figure 47) also correlated well (coefficient of 0.97) and tended to align along a one-to-one trend, although the ISS moment values were about 30 per cent greater than the PSS values, on average. The seismic energies (Figure 48) had more scatter (correlation coefficient of 0.57), but tended towards similar values (median difference of less than 10 per cent). This increased scatter was found, on further investigation, to be present in both data sets, compared with the respective moment values.

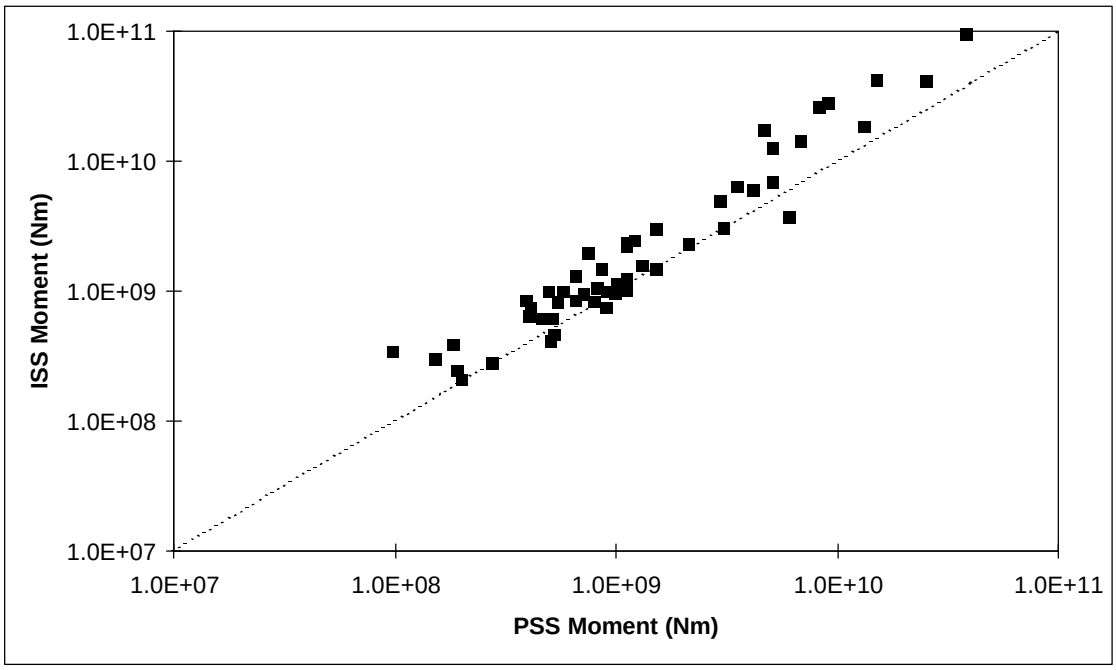

Figure 47 Comparison of moments assigned to 52 events recorded by both PSS and ISS. The diagonal line indicates a one-to-one relation.

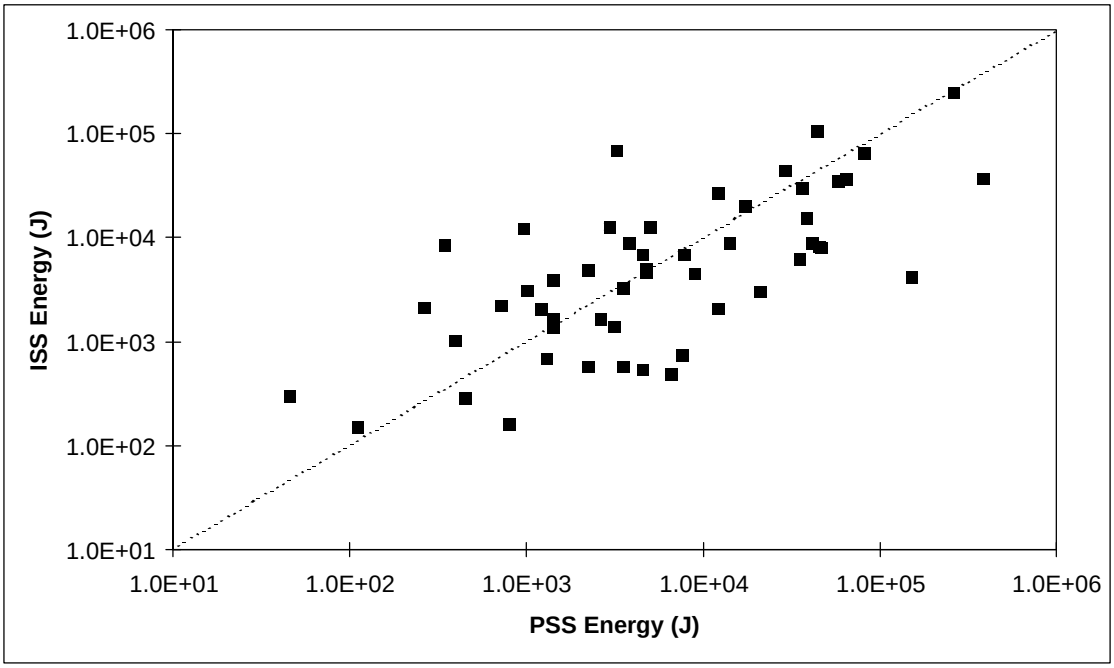

Figure 48 Comparison of energies assigned to 52 events recorded by both PSS and ISS. The diagonal line indicates a one-to-one relation.

9 Appendix B

Comparison between 3D modelling and closure data

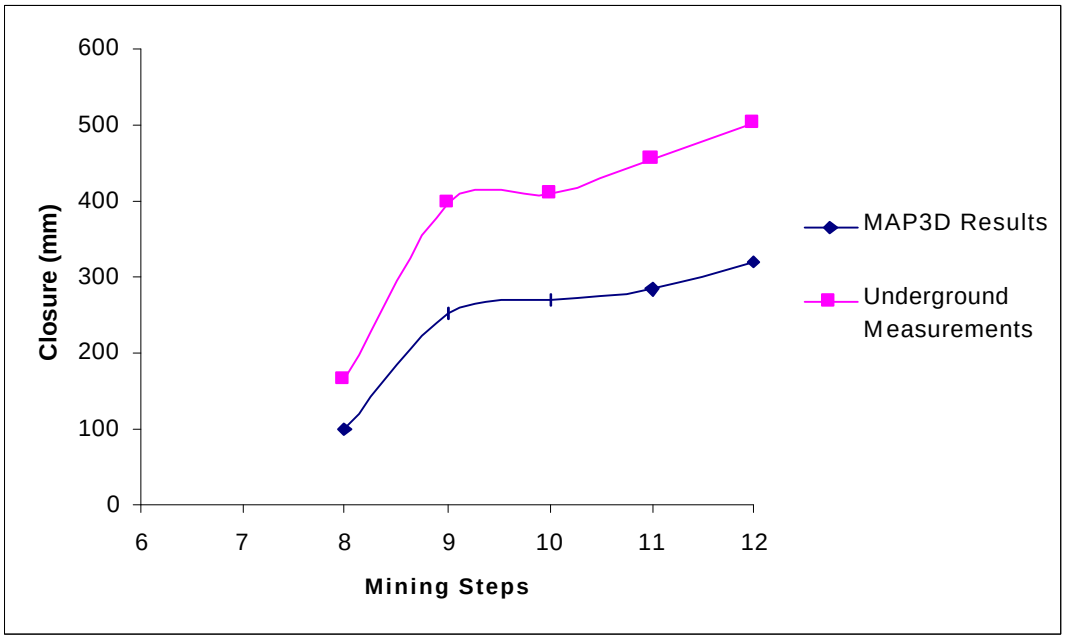

Figure 49 Comparison between 3D modelling results and underground measurements for station A1.

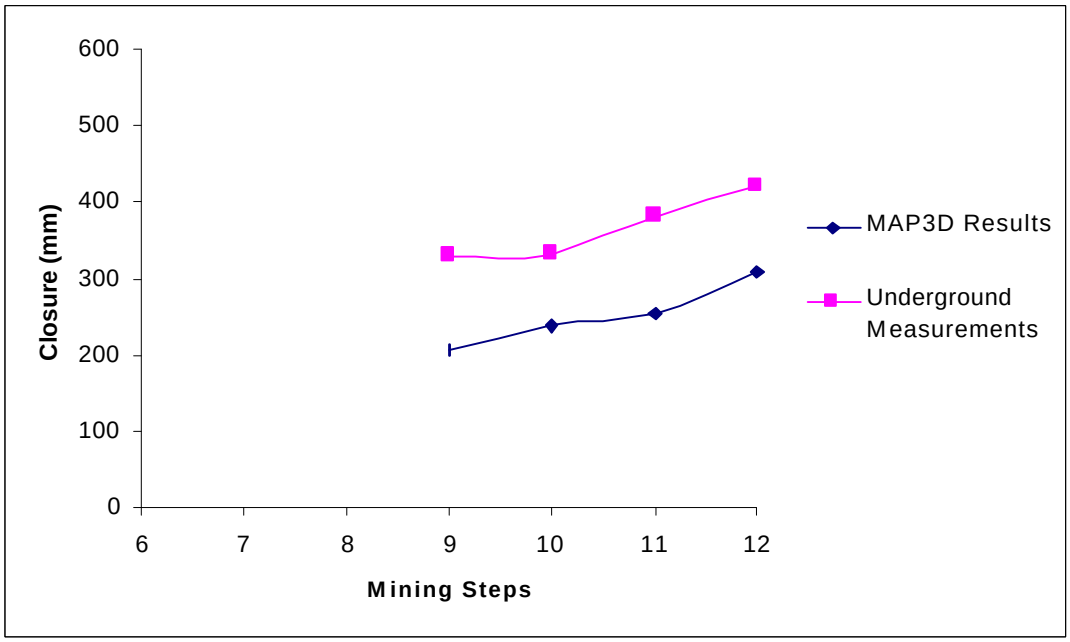

Figure 50 Comparison between 3D modelling results and underground measurements for station A2.

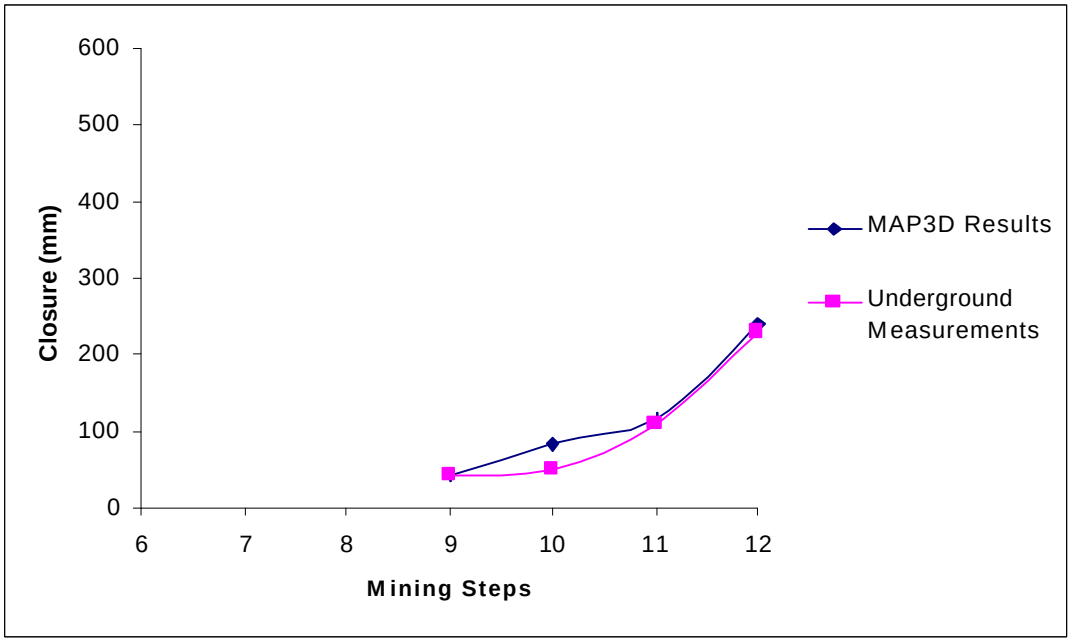

Figure 51 Comparison between 3D modelling results and underground measurements for station A3.

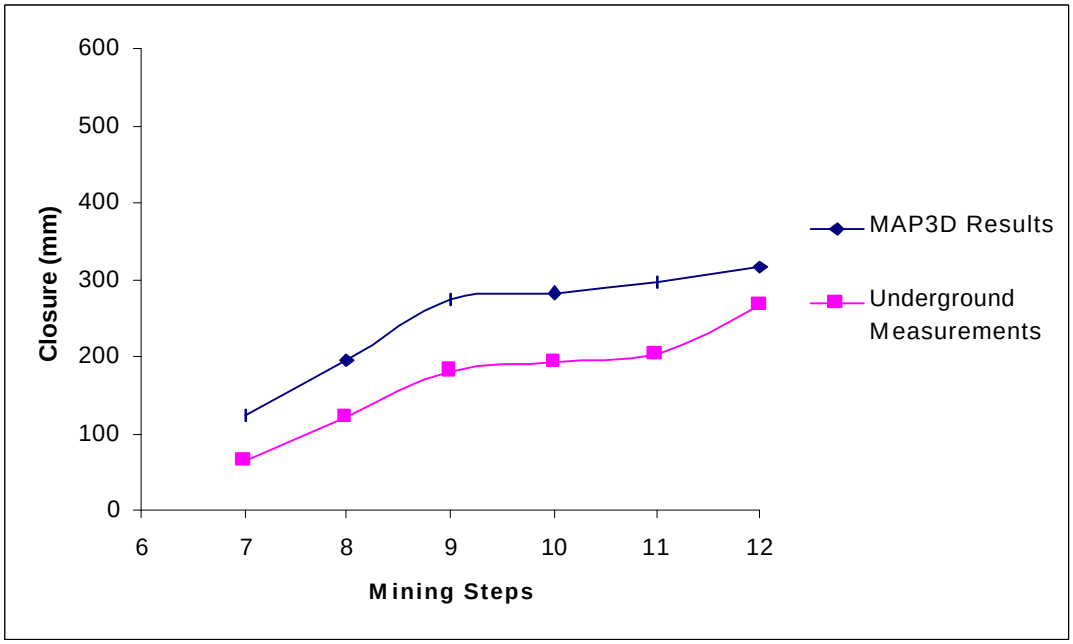

Figure 52 Comparison between 3D modelling results and underground measurements for station B1.

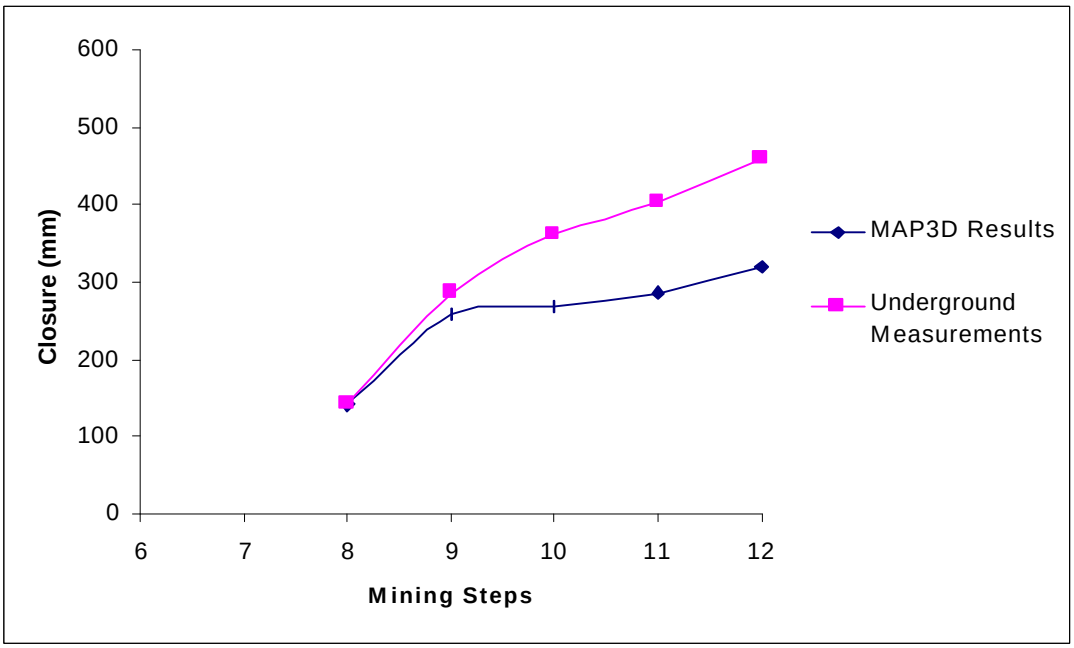

Figure 53 Comparison between 3D modelling results and underground measurements for station B2.

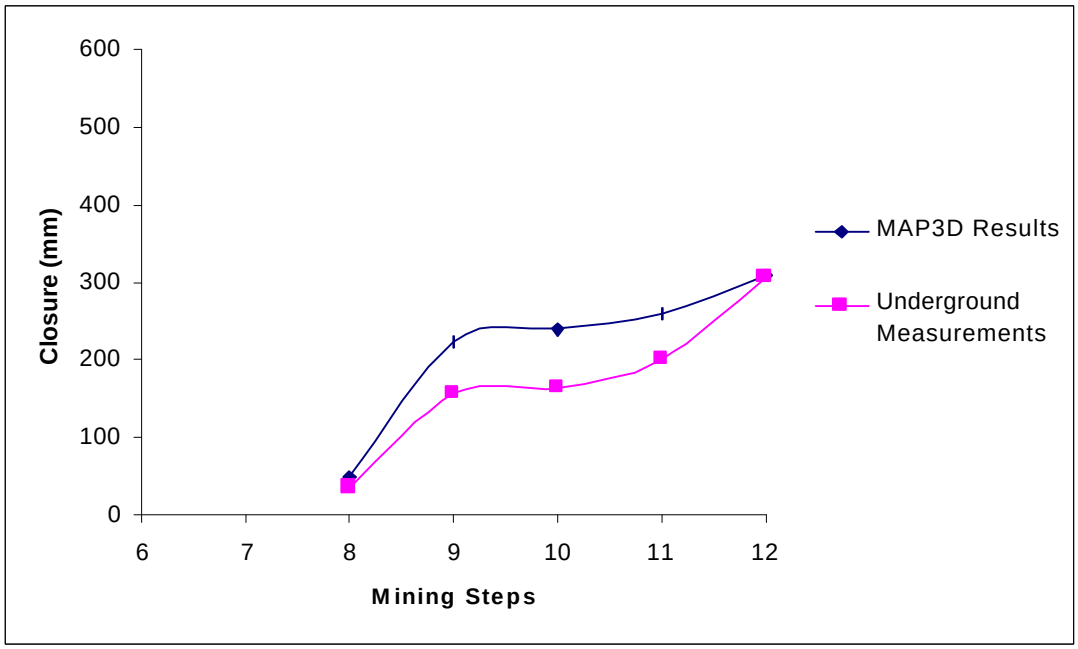

Figure 54 Comparison between 3D modelling results and underground measurements for station B3.

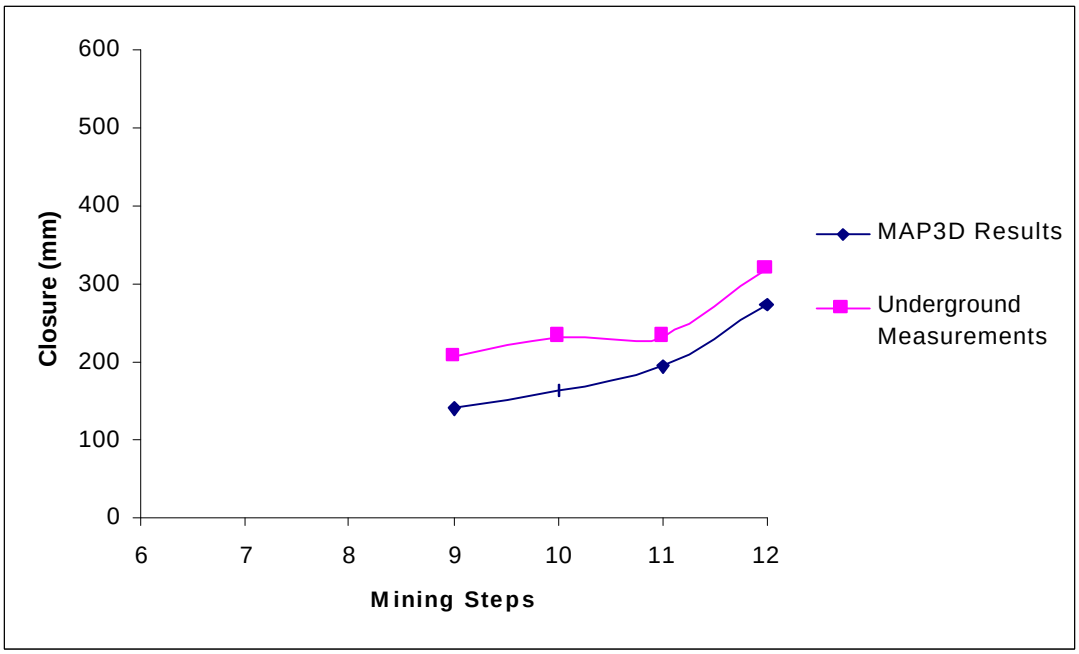

Figure 55 Comparison between 3D modelling results and underground measurements for station B4.

10 Appendix C

Comparison between 3D modelling and seismic data

Note: All seismic moment values from modelling and from the field data in the following charts have units of Nm.

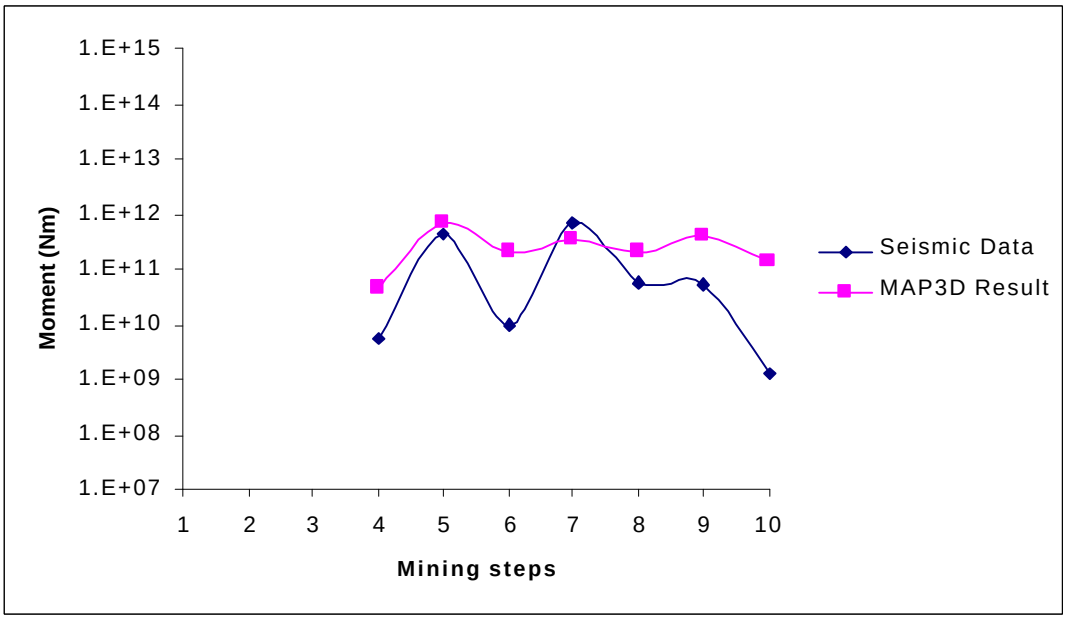

Figure 56 Relationship between 3D modelling and seismic data for the dyke numbered 3 in Figure 31.

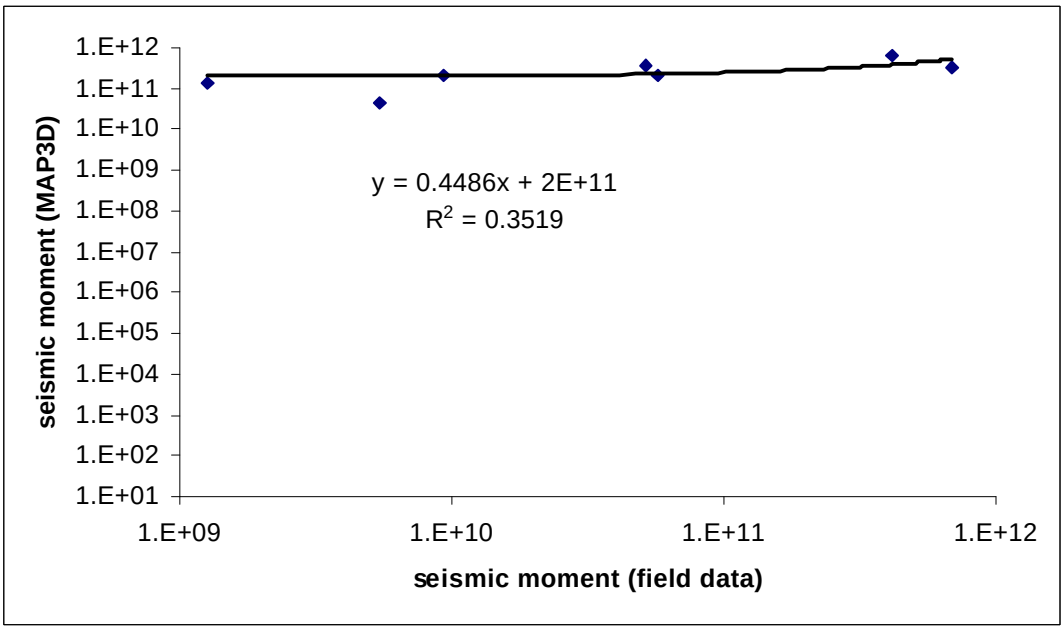

Figure 57 Correlation between field seismic moment and modelling seismic moment (MAP3D) for the dyke numbered 3 in Figure 31.

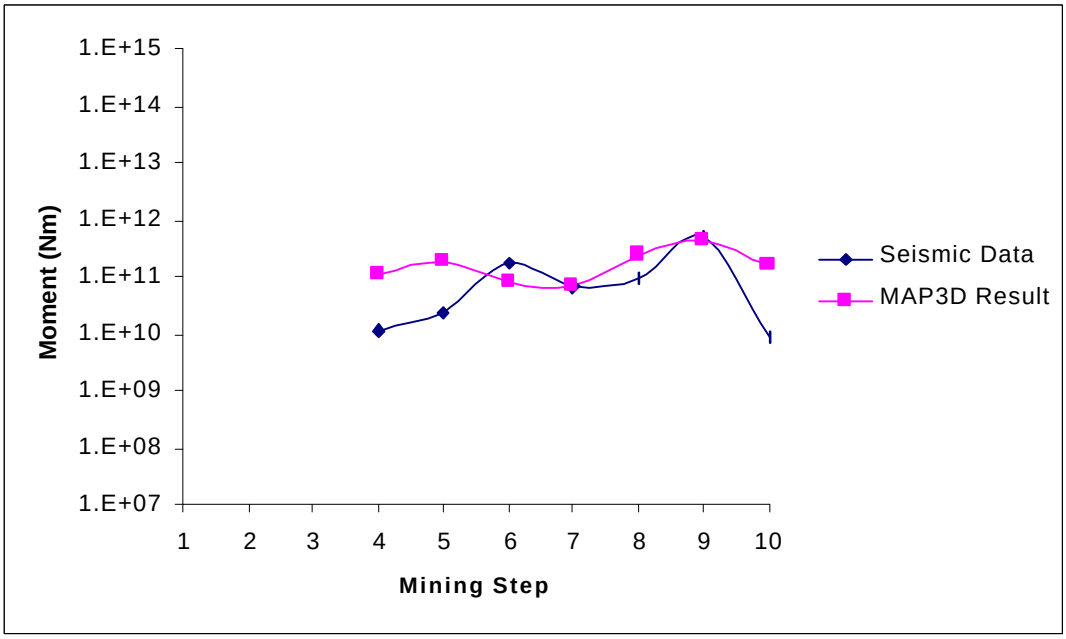

Figure 58 Relationship between 3D modelling and seismic data for the dyke numbered 4 in Figure 31.

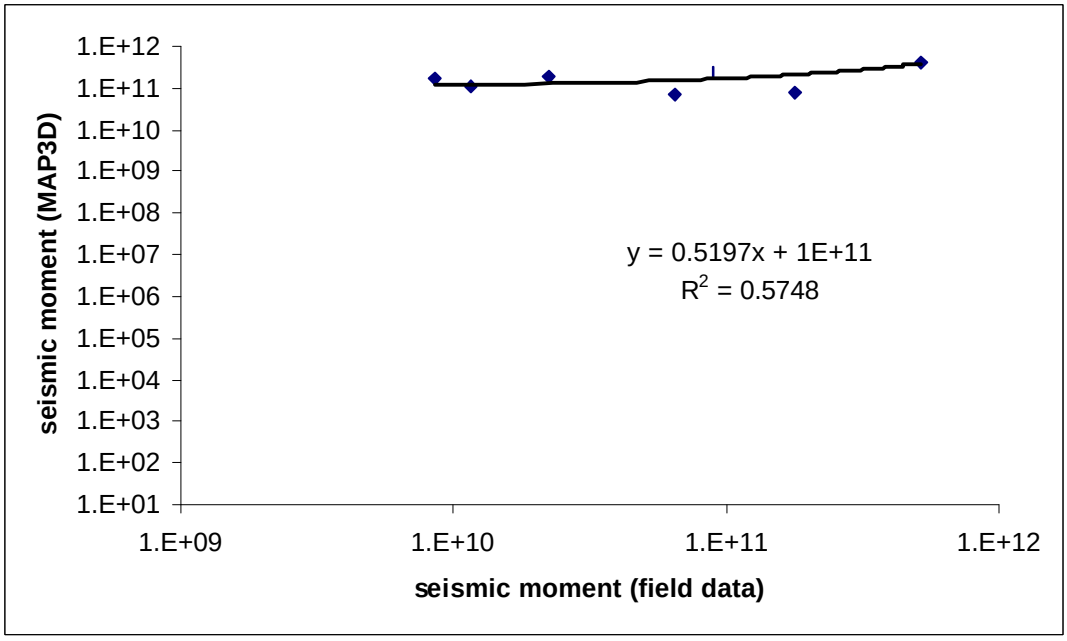

Figure 59 Correlation between field seismic moment and modelling seismic moment (MAP3D) for the dyke numbered 4 in Figure 31.

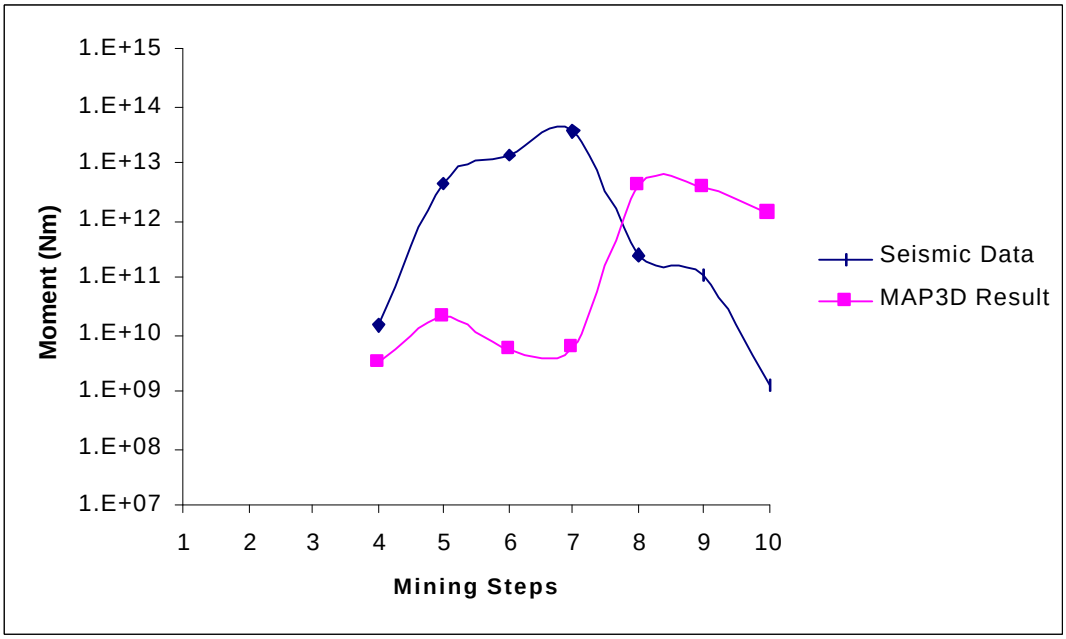

Figure 60 Relationship between 3D modelling and seismic data for the dyke numbered 5 in Figure 31.

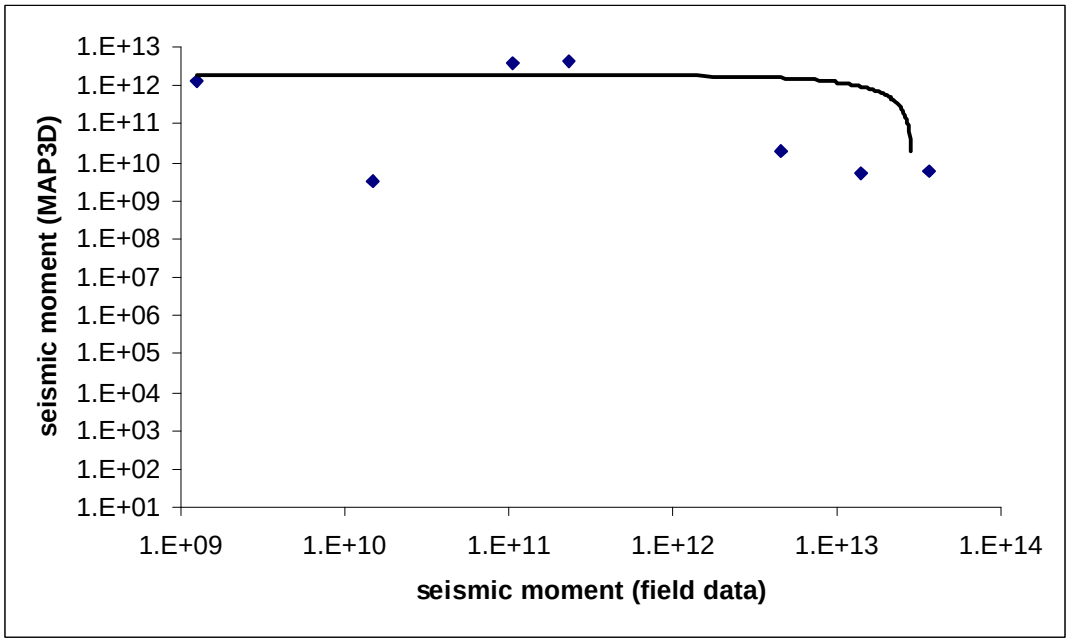

Figure 61 Correlation between field seismic moment and modelling seismic moment (MAP3D) for the dyke numbered 5 in Figure 31.

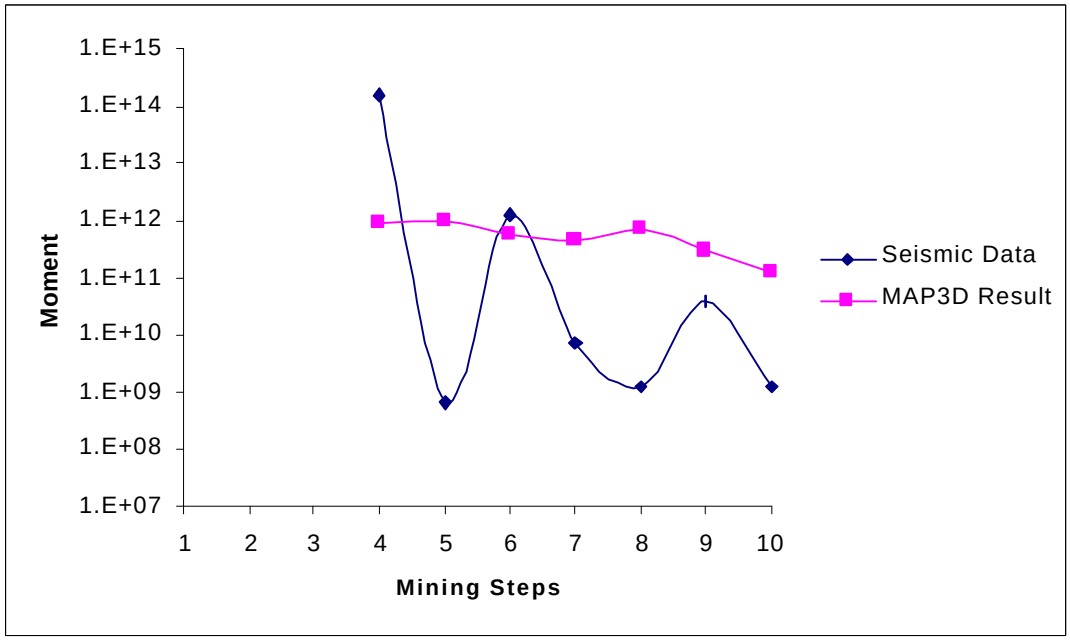

Figure 62 Relationship between 3D modelling and seismic data for the dyke numbered 6 in Figure 31.

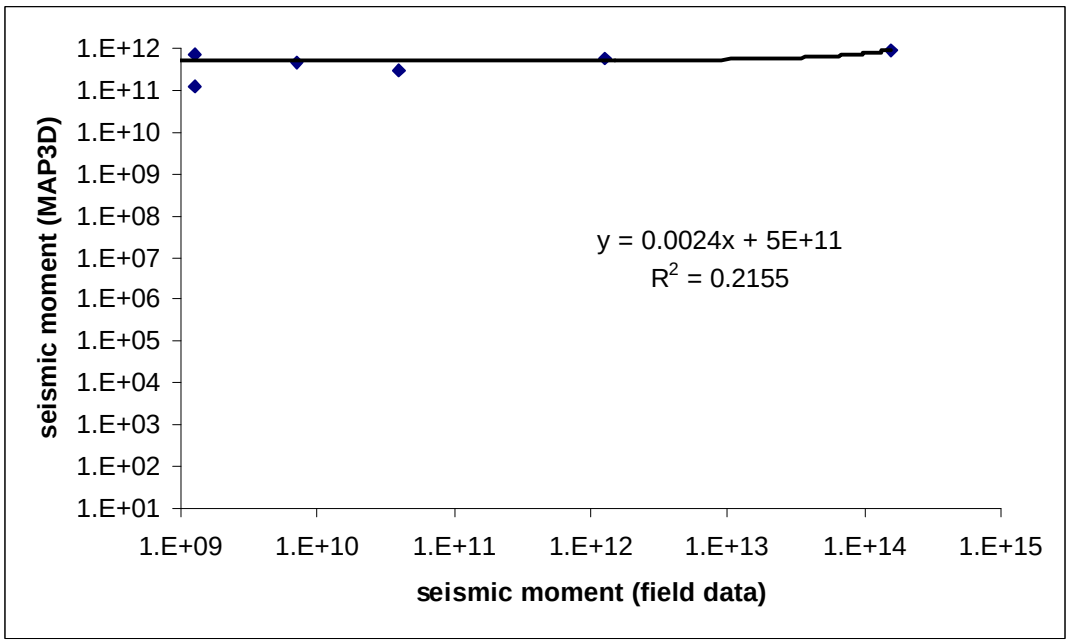

Figure 63 Correlation between field seismic moment and modelling seismic moment (MAP3D) for the dyke numbered 6 in Figure 31.

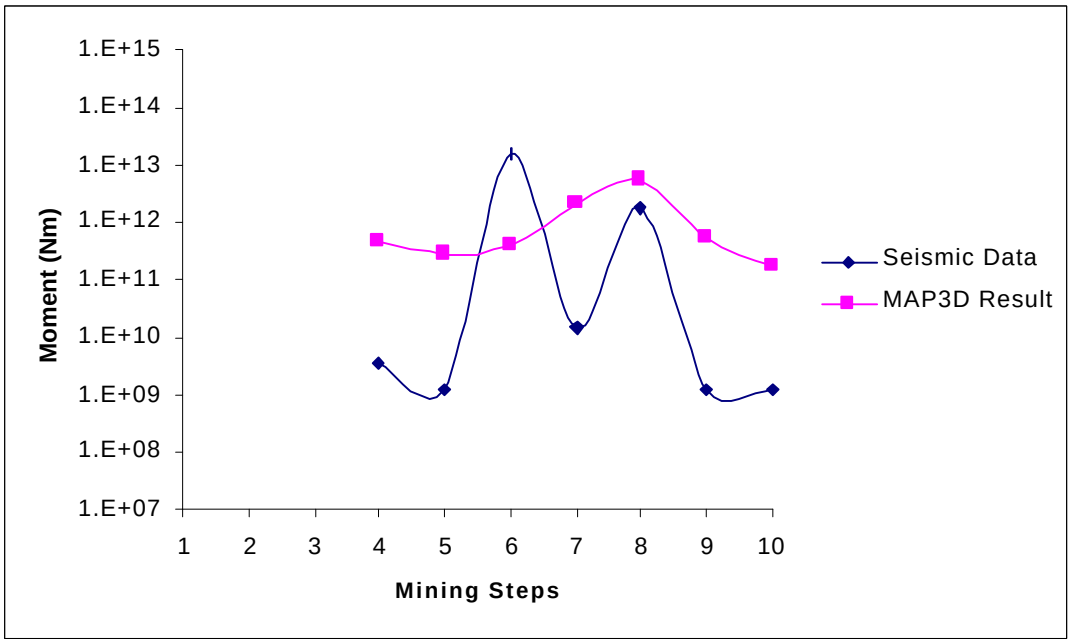

Figure 64 Relationship between 3D modelling and seismic data for the fault numbered 7 in Figure 31.

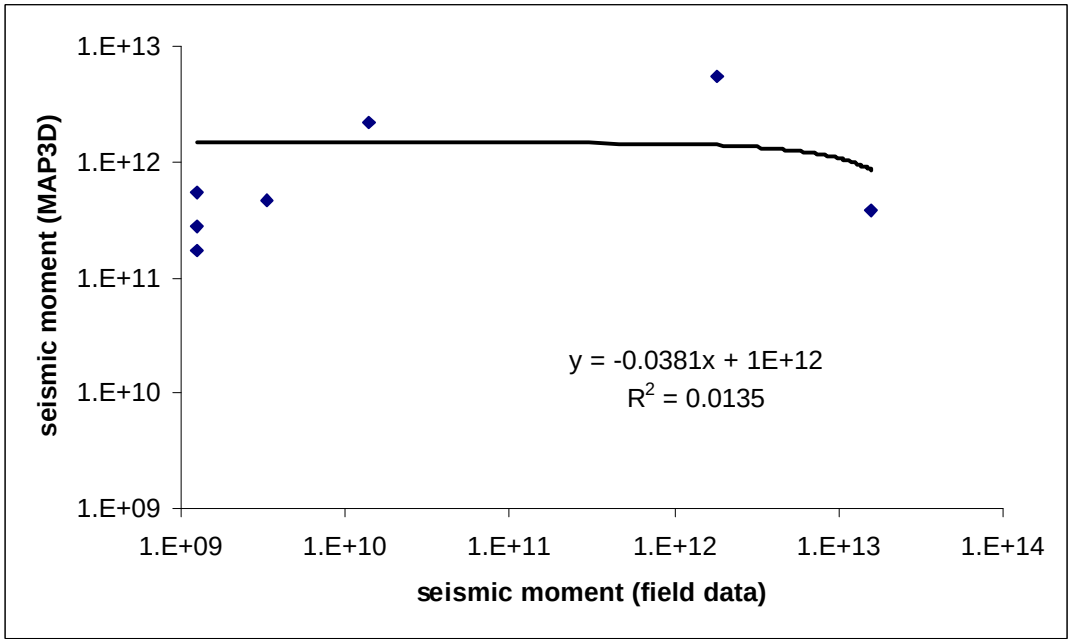

Figure 65 Correlation between field seismic moment and modelling seismic moment (MAP3D) for the fault numbered 7 in Figure 31.

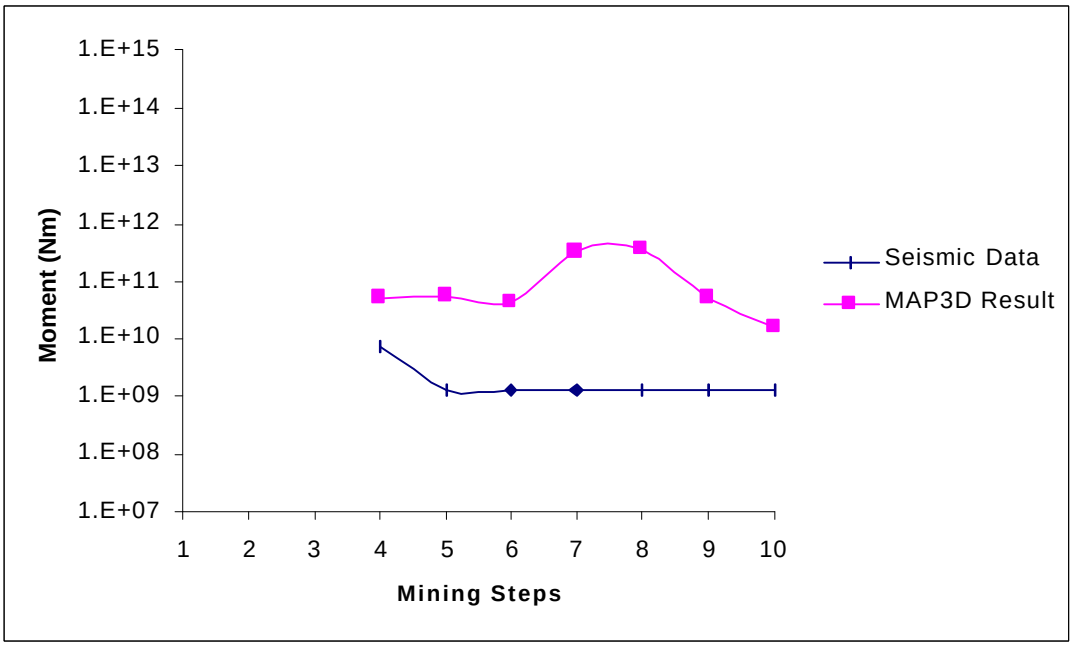

Figure 66 Relationship between 3D modelling and seismic data for the fault numbered 8 in Figure 31.

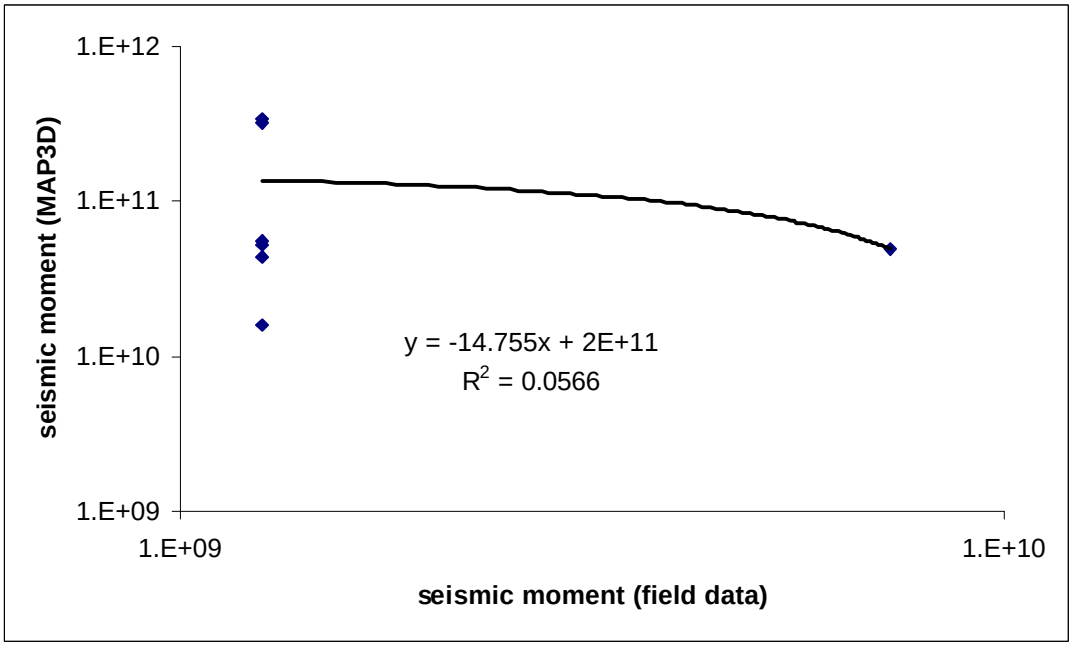

Figure 67 Correlation between field seismic moment and modelling seismic moment (MAP3D) for the fault numbered 8 in Figure 31.

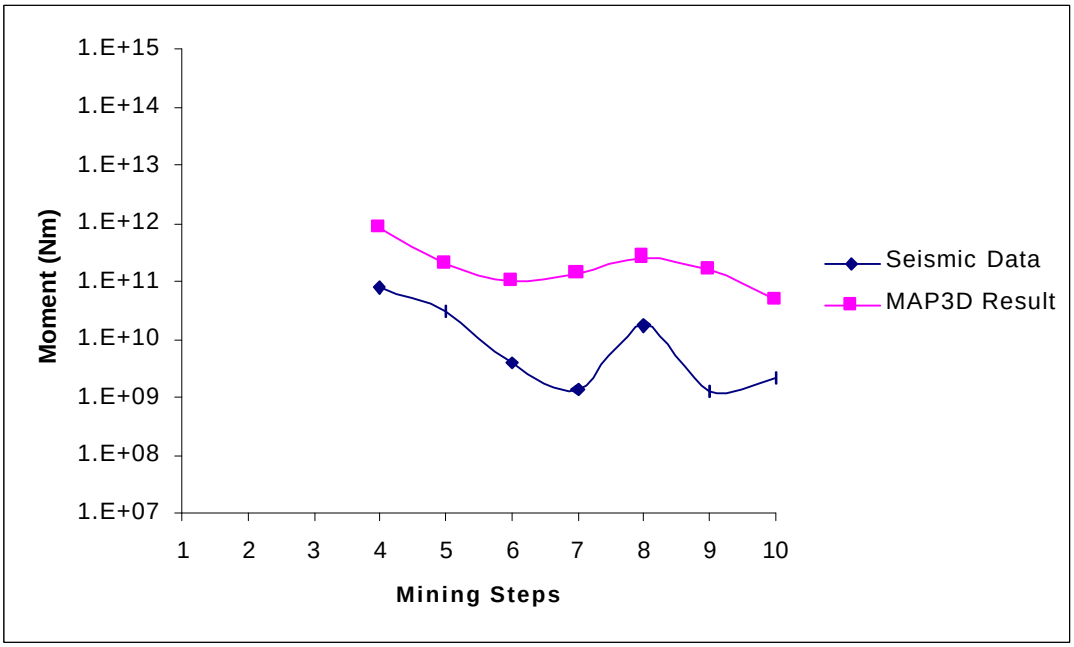

Figure 68 Relationship between 3D modelling and seismic data for the dyke numbered 9 in Figure 31.

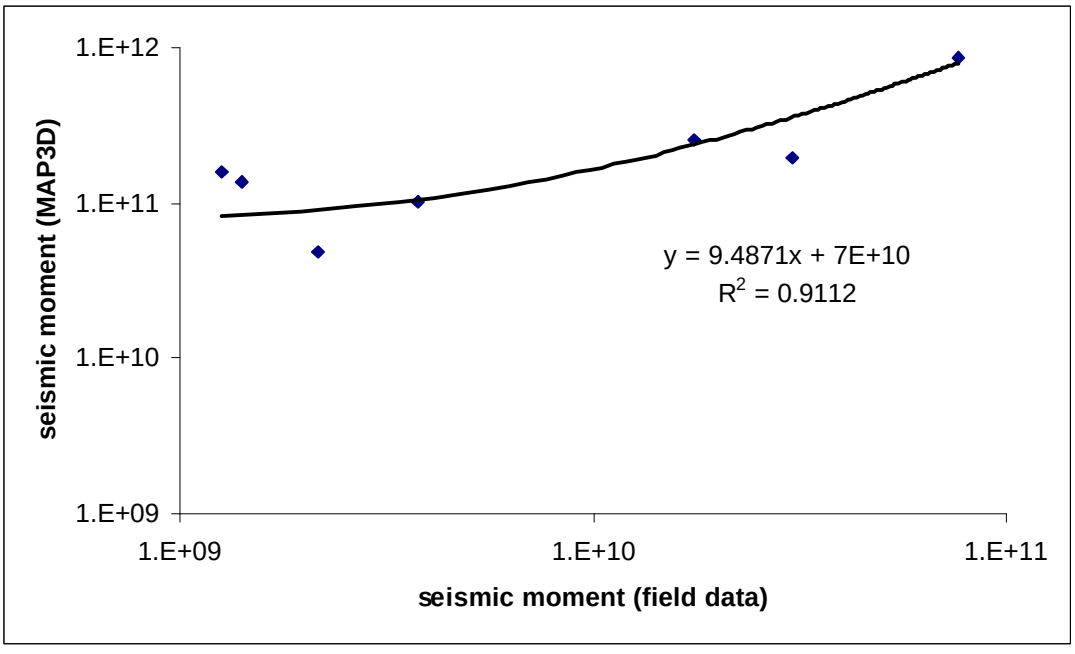

Figure 69 Correlation between field seismic moment and modelling seismic moment (MAP3D) for the dyke numbered 9 in Figure 31.

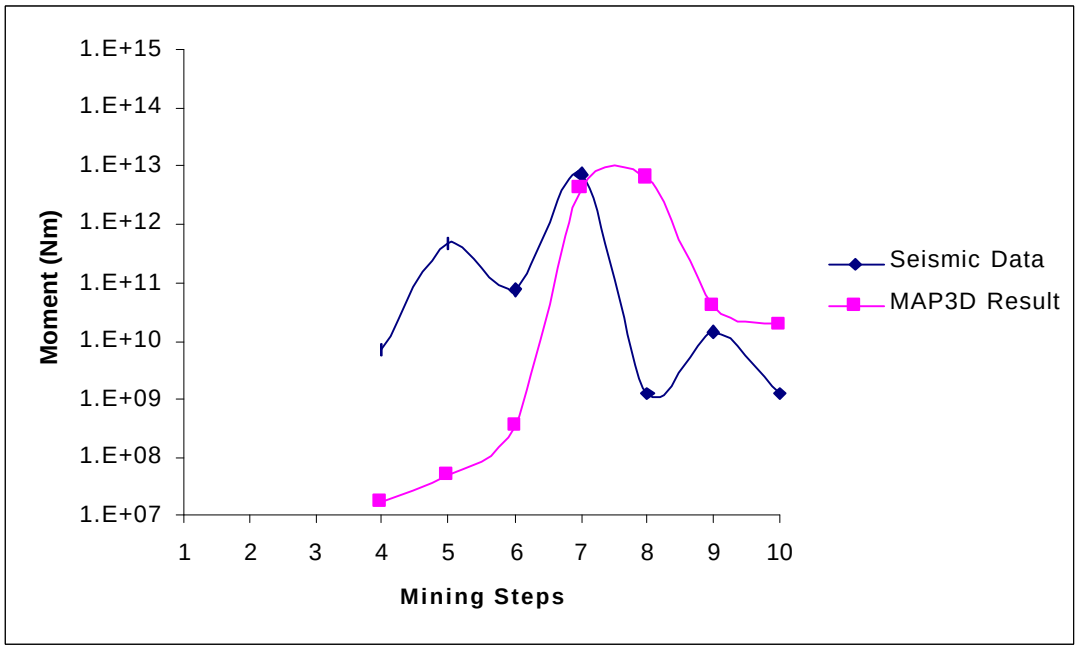

Figure 70 Relationship between 3D modelling and seismic data for the fault numbered 10 in Figure 31.

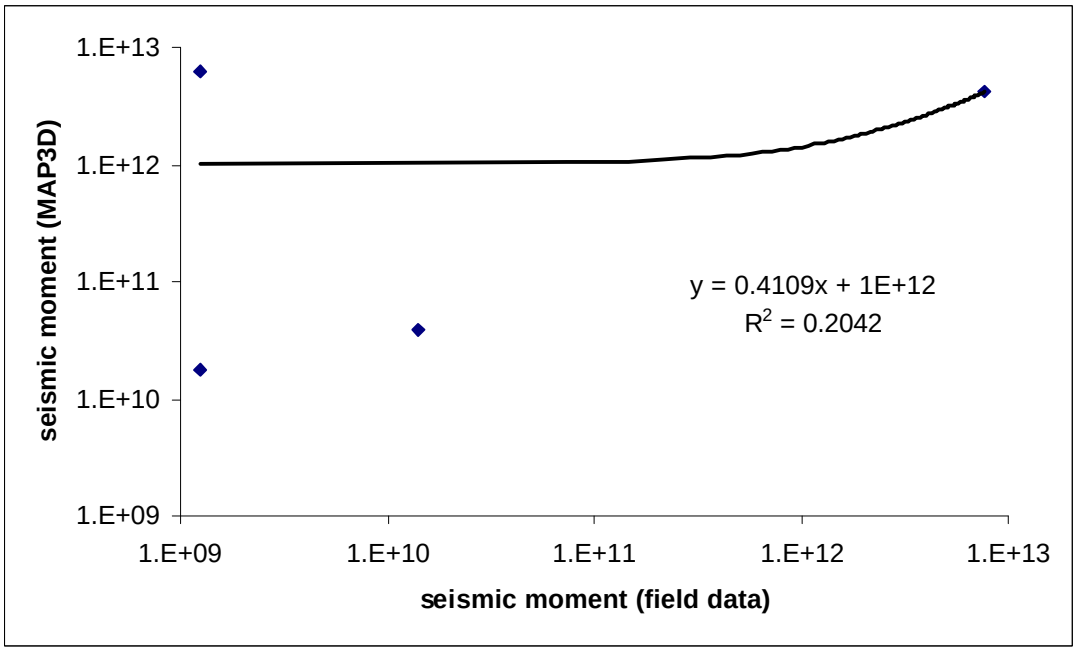

Figure 71 Correlation between field seismic moment and modelling seismic moment (MAP3D) for the fault numbered 10 in Figure 31.

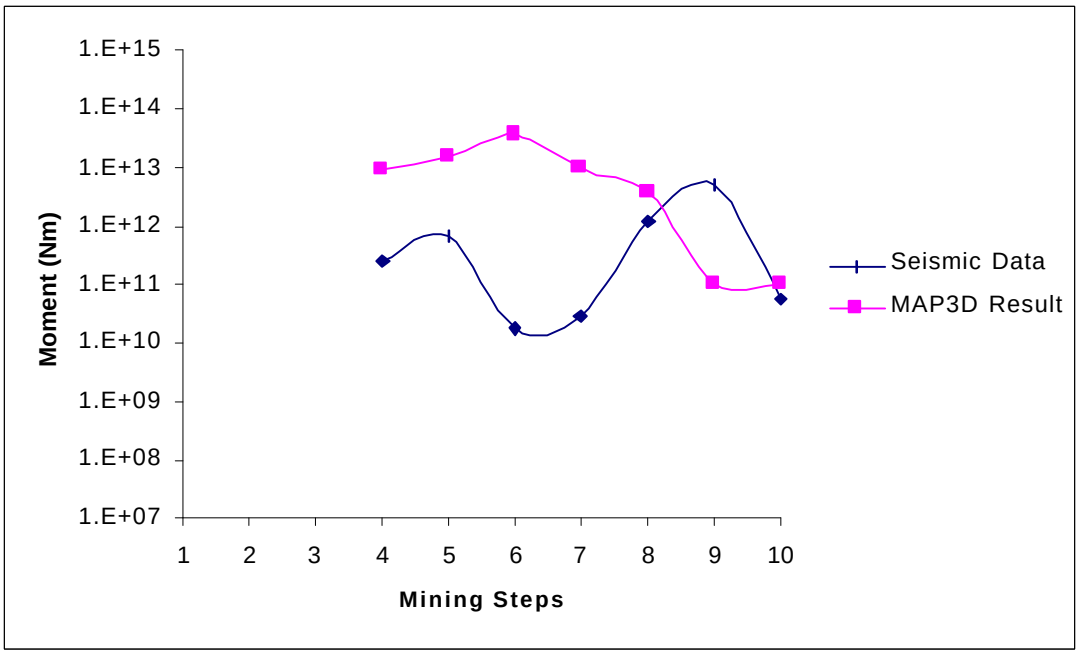

Figure 72 Relationship between 3D modelling and seismic data for the fault numbered 11 in Figure 31.

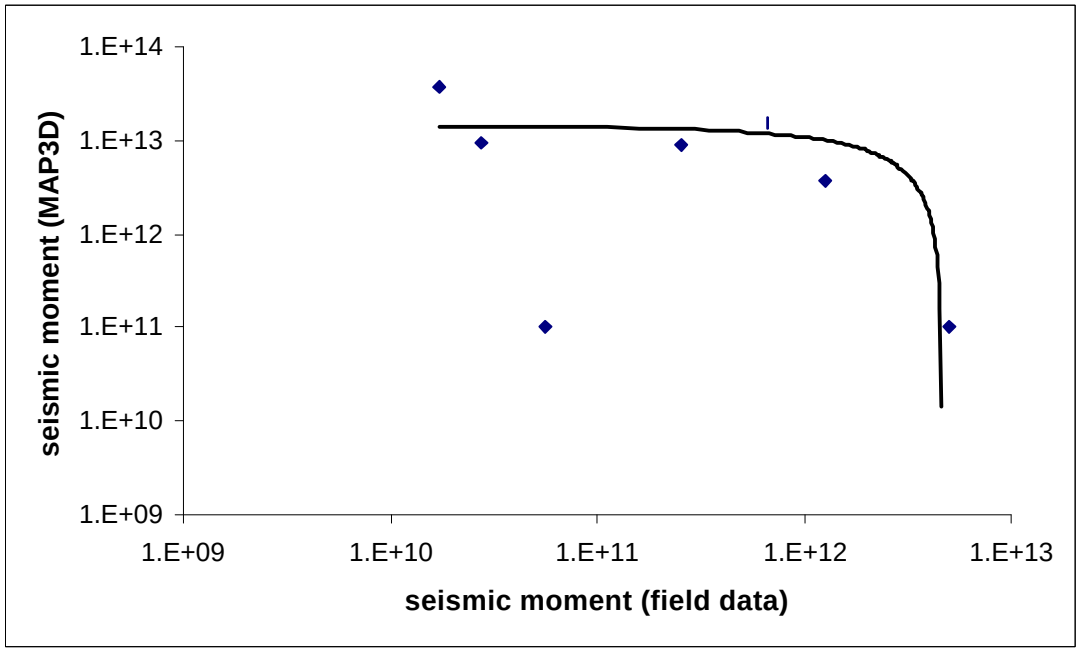

Figure 73 Correlation between field seismic moment and modelling seismic moment (MAP3D) for the fault numbered 11 in Figure 31.

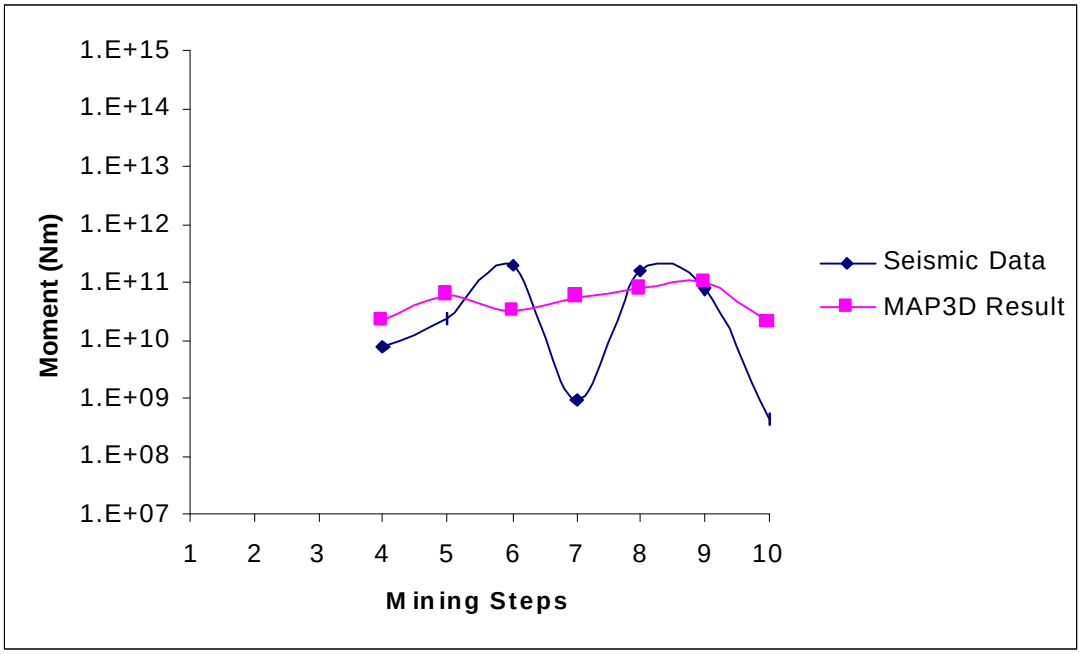

Figure 74 Relationship between 3D modelling and seismic data for the fault numbered 12 in Figure 31.

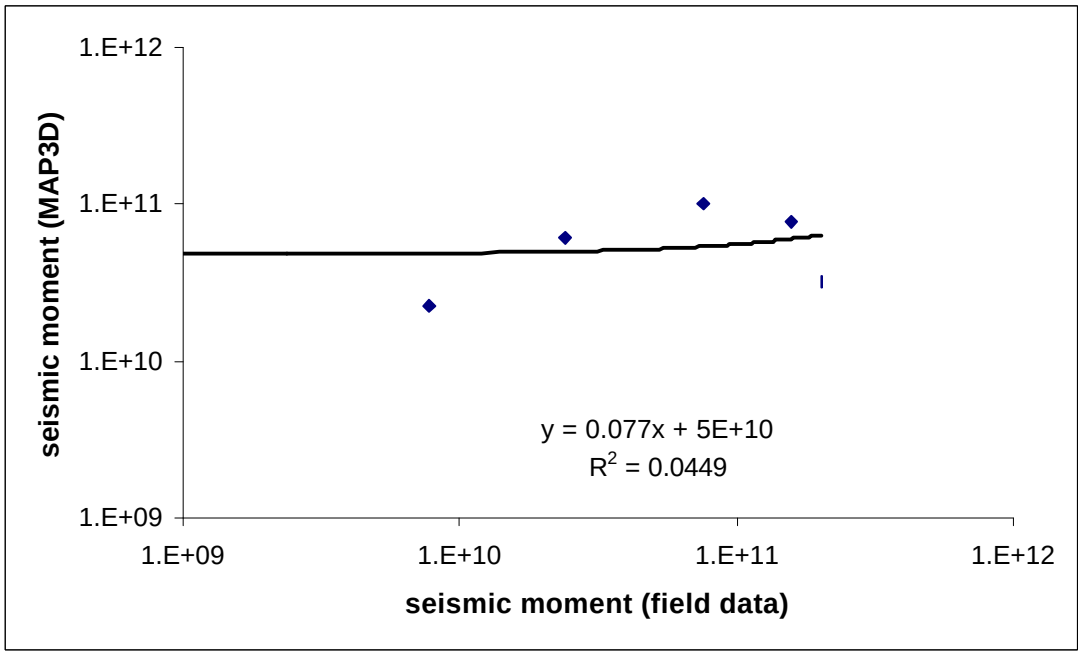

Figure 75 Correlation between field seismic moment and modelling seismic moment (MAP3D) for the fault numbered 12 in Figure 31.

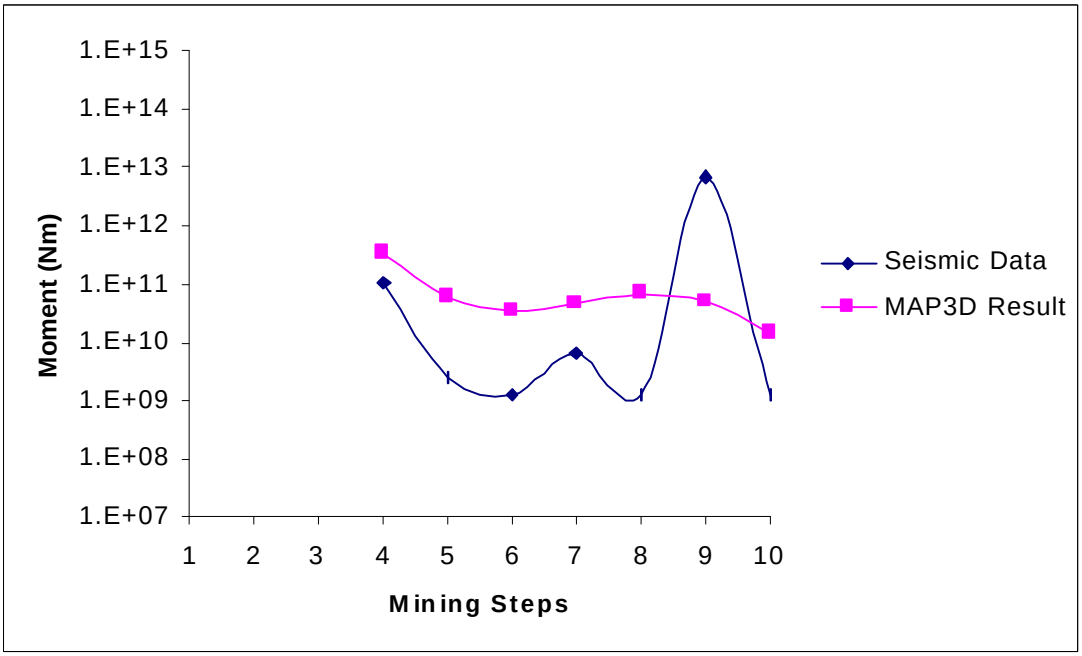

Figure 76 Relationship between 3D modelling and seismic data for the fault numbered 13 in Figure 31.

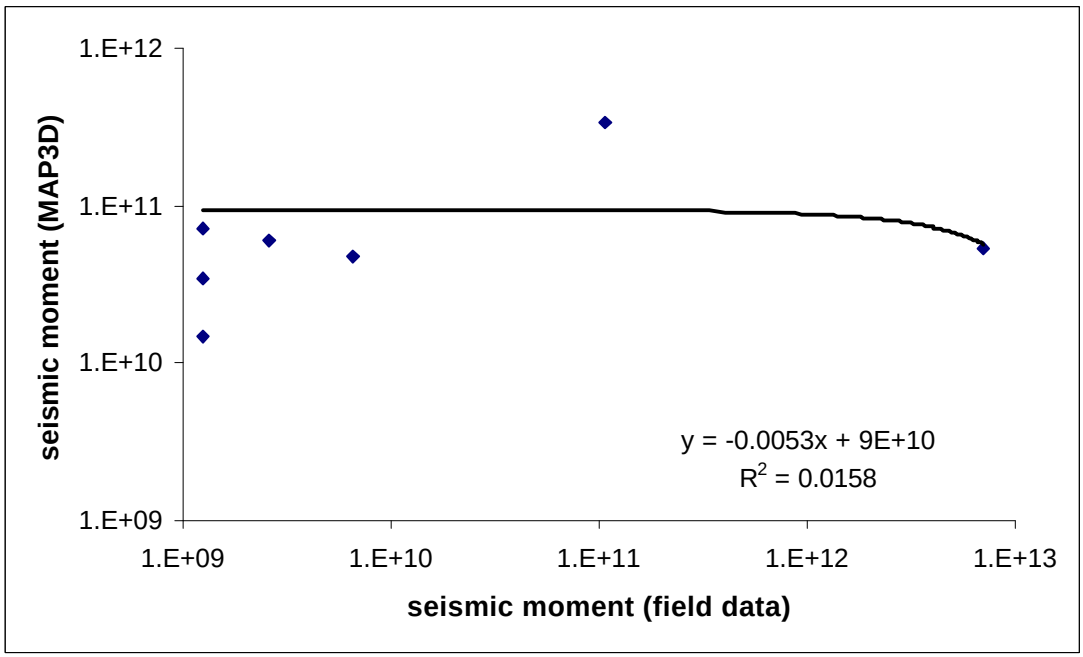

Figure 77 Correlation between field seismic moment and modelling seismic moment (MAP3D) for the fault numbered 13 in Figure 31.

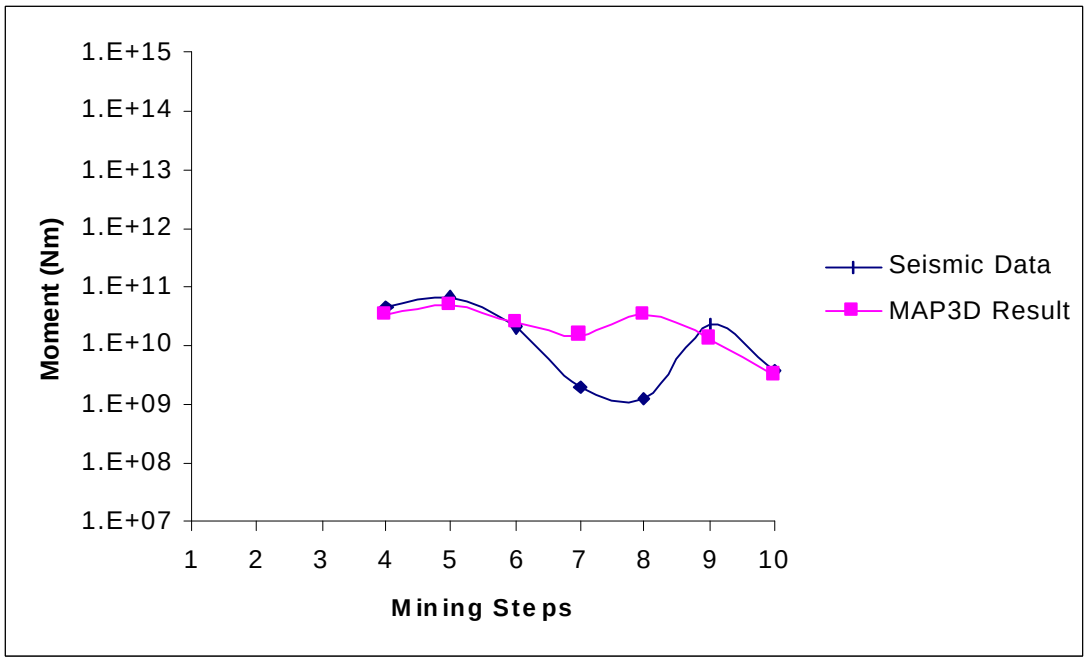

Figure 78 Relationship between 3D modelling and seismic data for the fault numbered 14 in Figure 31.

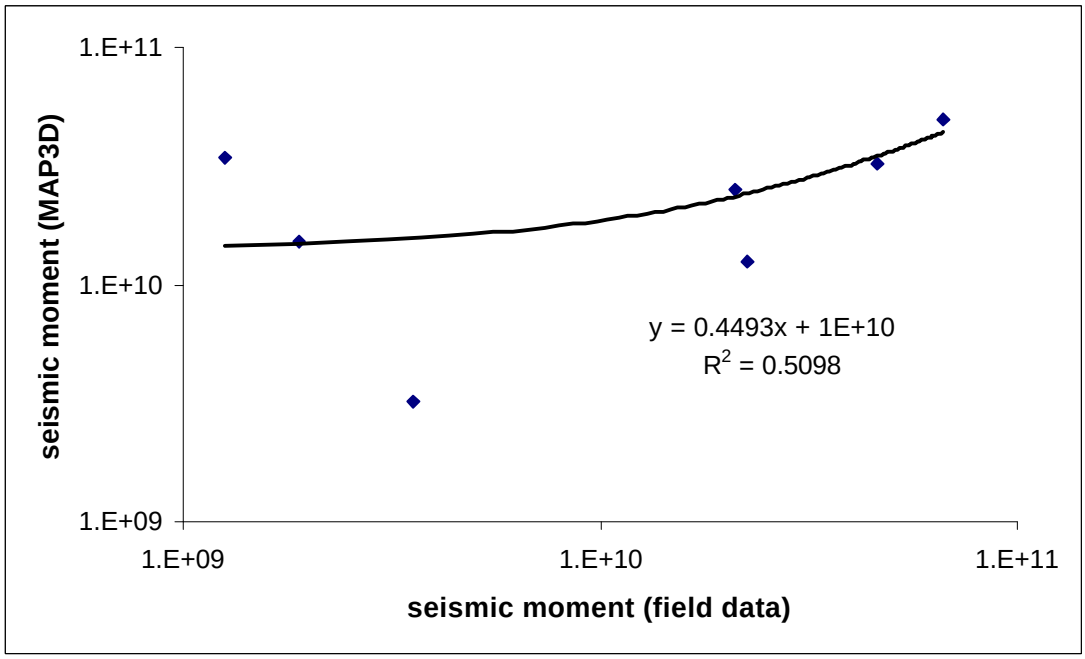

Figure 79 Correlation between field seismic moment and modelling seismic moment (MAP3D) for the fault numbered 14 in Figure 31.

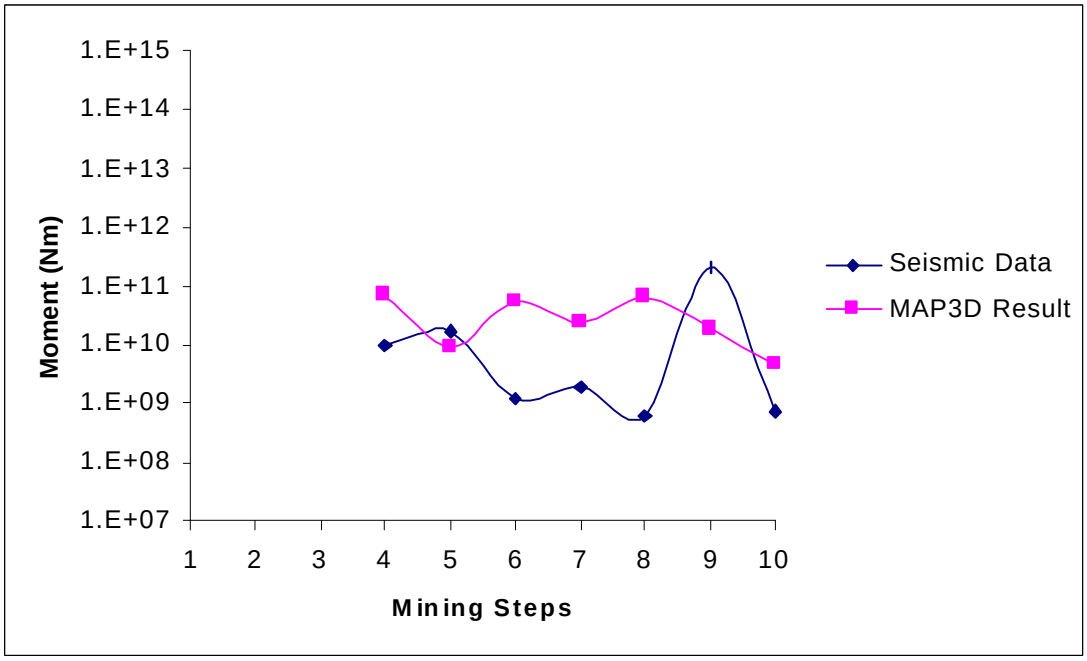

Figure 80 Relationship between 3D modelling and seismic data for the fault numbered 15 in Figure 31.

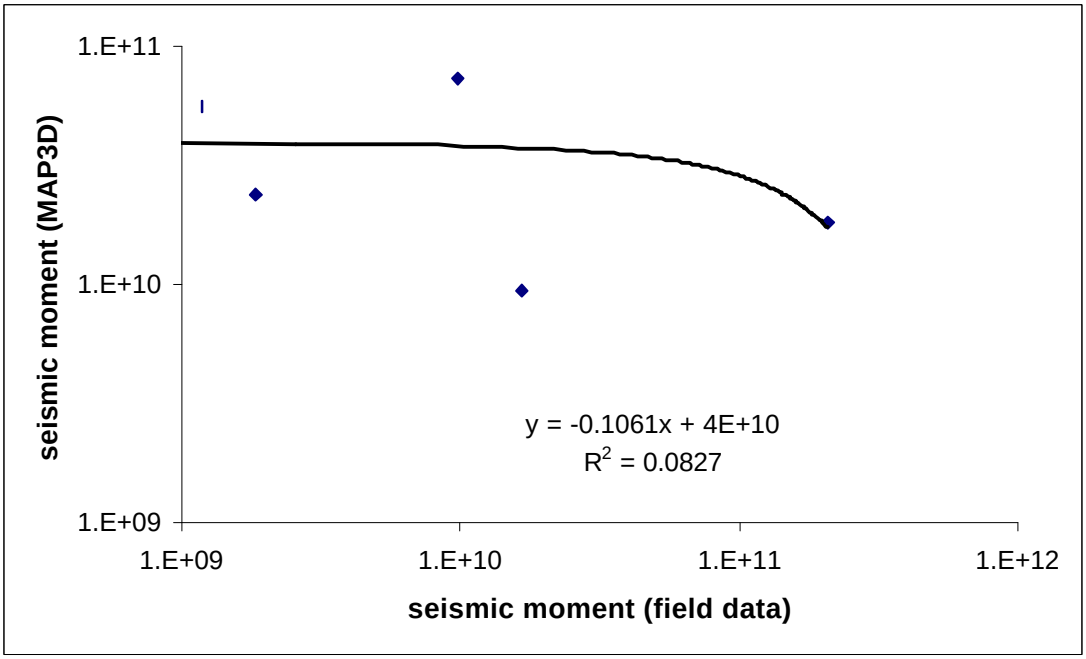

Figure 81 Correlation between field seismic moment and modelling seismic moment (MAP3D) for the fault numbered 15 in Figure 31.

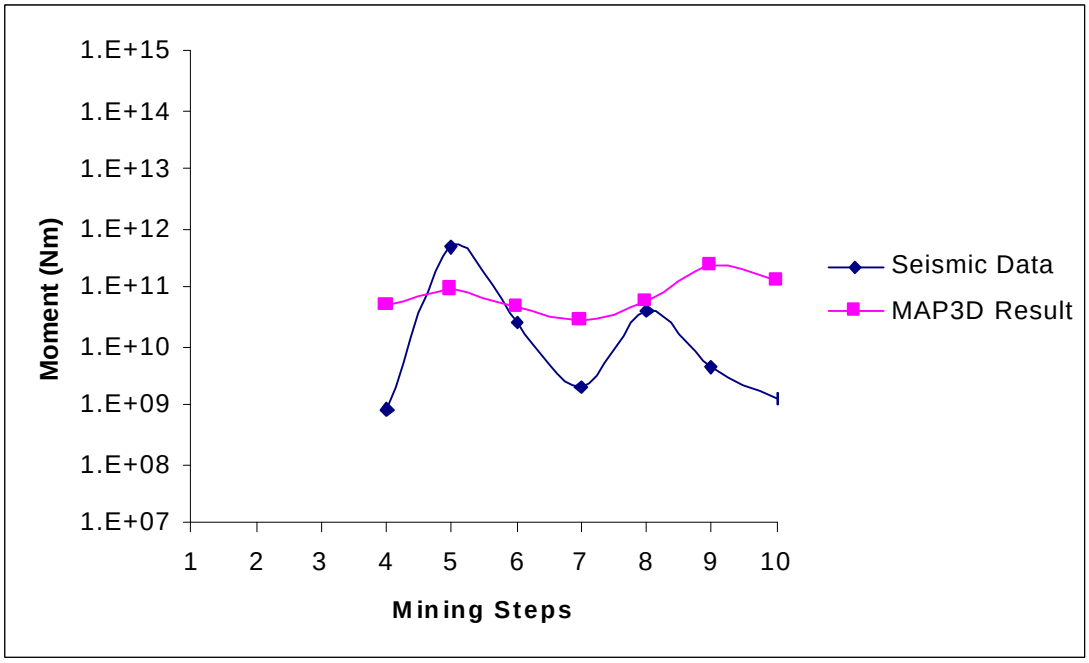

Figure 82 Relationship between 3D modelling and seismic data for the fault numbered 16 in Figure 31.

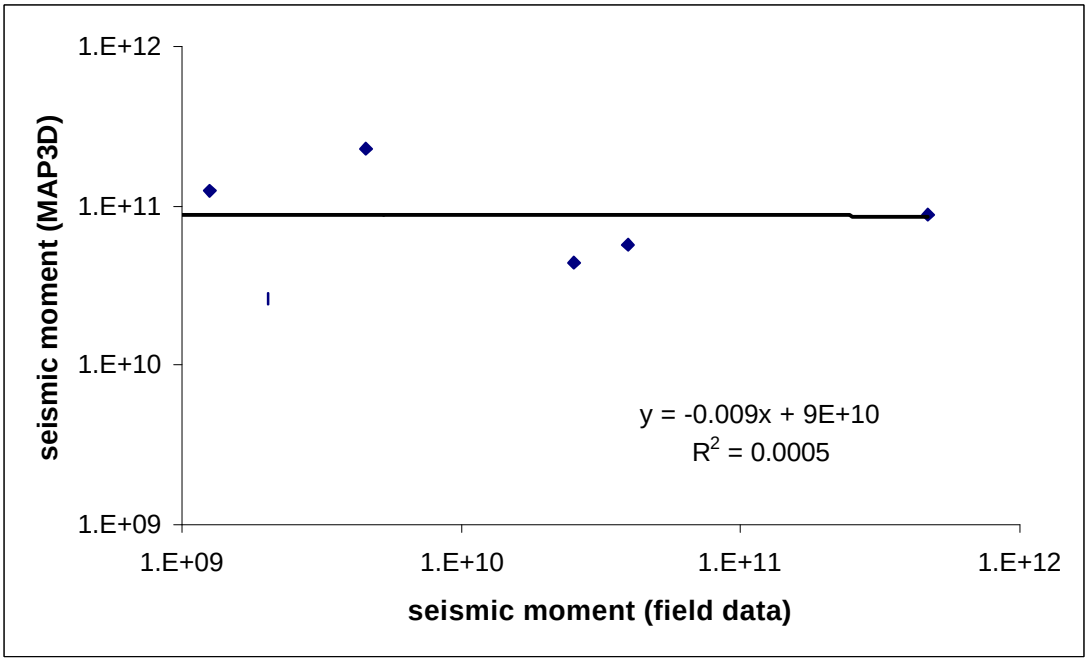

Figure 83 Correlation between field seismic moment and modelling seismic moment (MAP3D) for the fault numbered 16 in Figure 31.

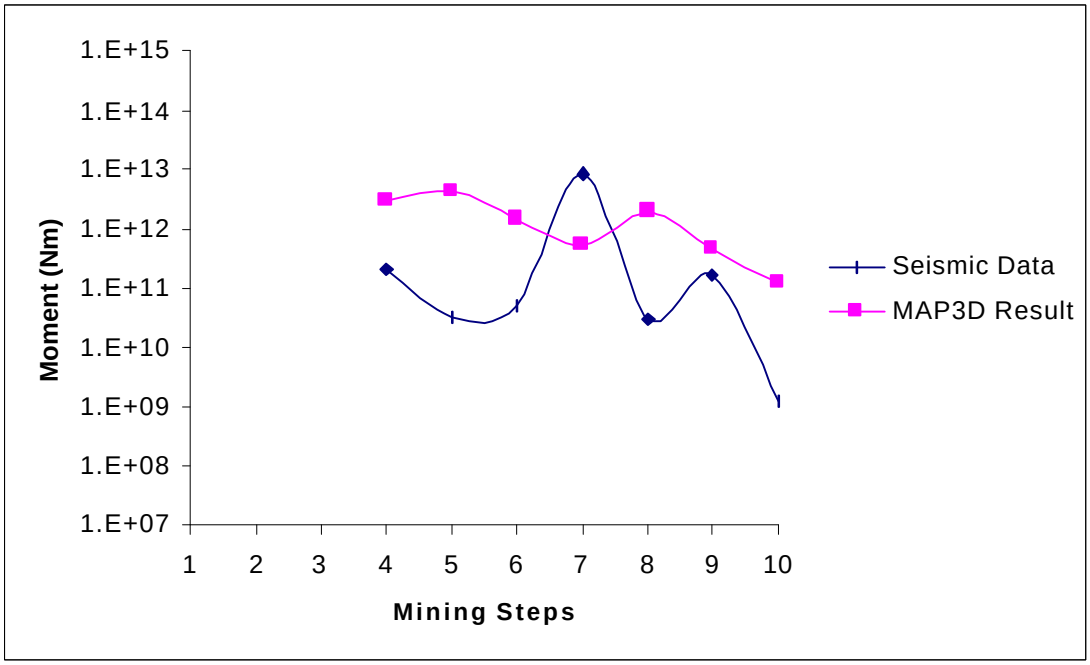

Figure 84 Relationship between 3D modelling and seismic data for the fault numbered 17 in Figure 31.

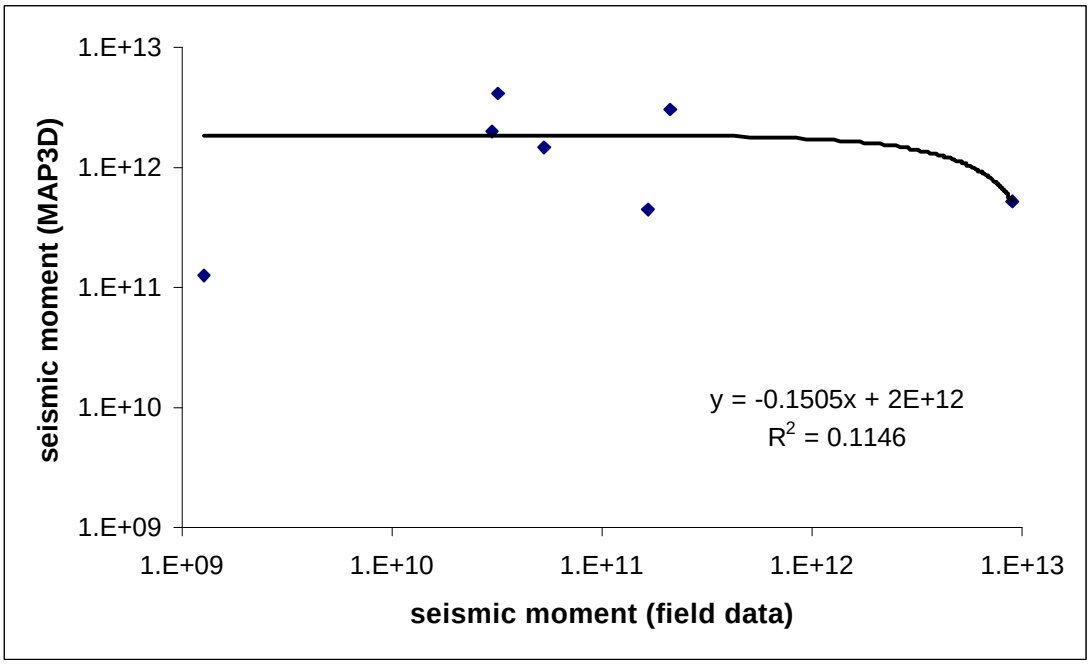

Figure 85 Correlation between field seismic moment and modelling seismic moment (MAP3D) for the fault numbered 17 in Figure 31.

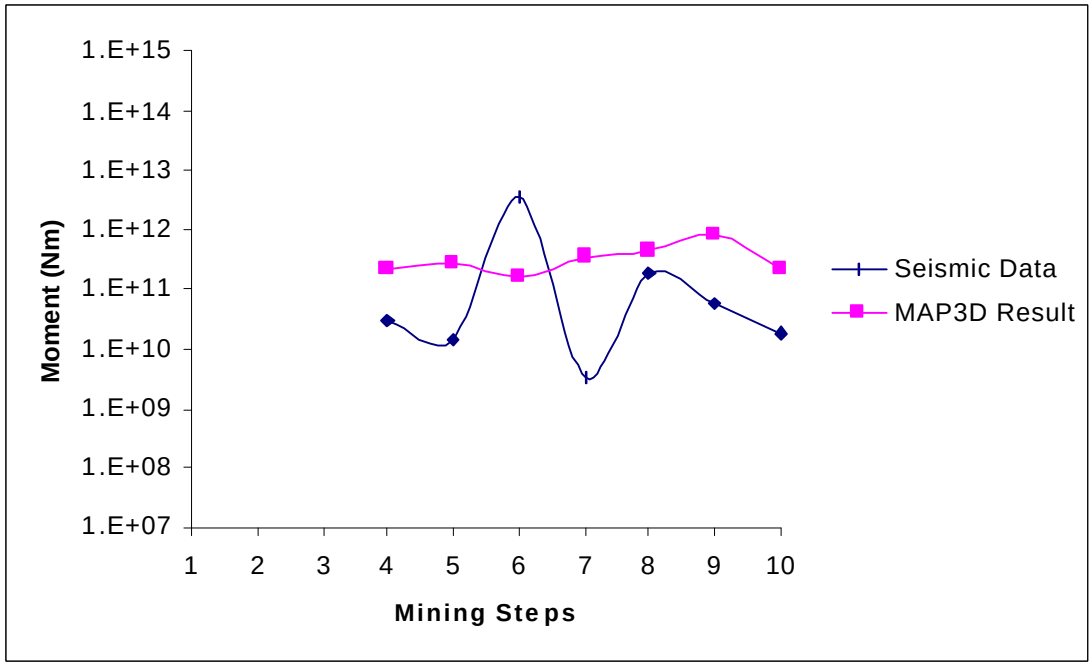

Figure 86 Relationship between 3D modelling and seismic data for the dyke numbered 18 in Figure 31.

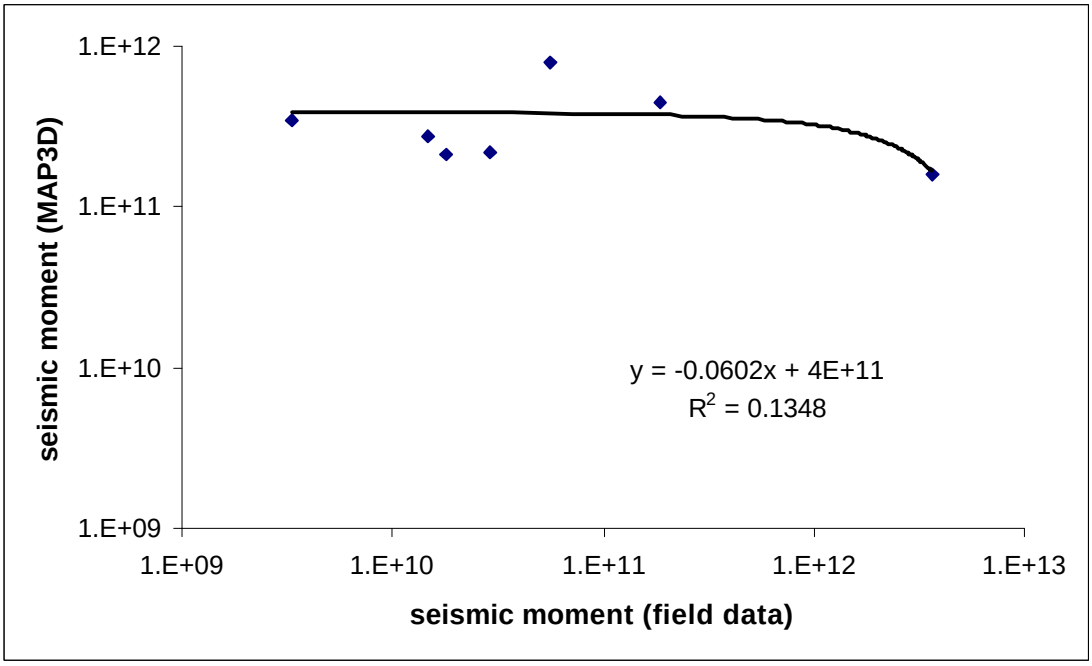

Figure 87 Correlation between field seismic moment and modelling seismic moment (MAP3D) for the dyke numbered 18 in Figure 31.

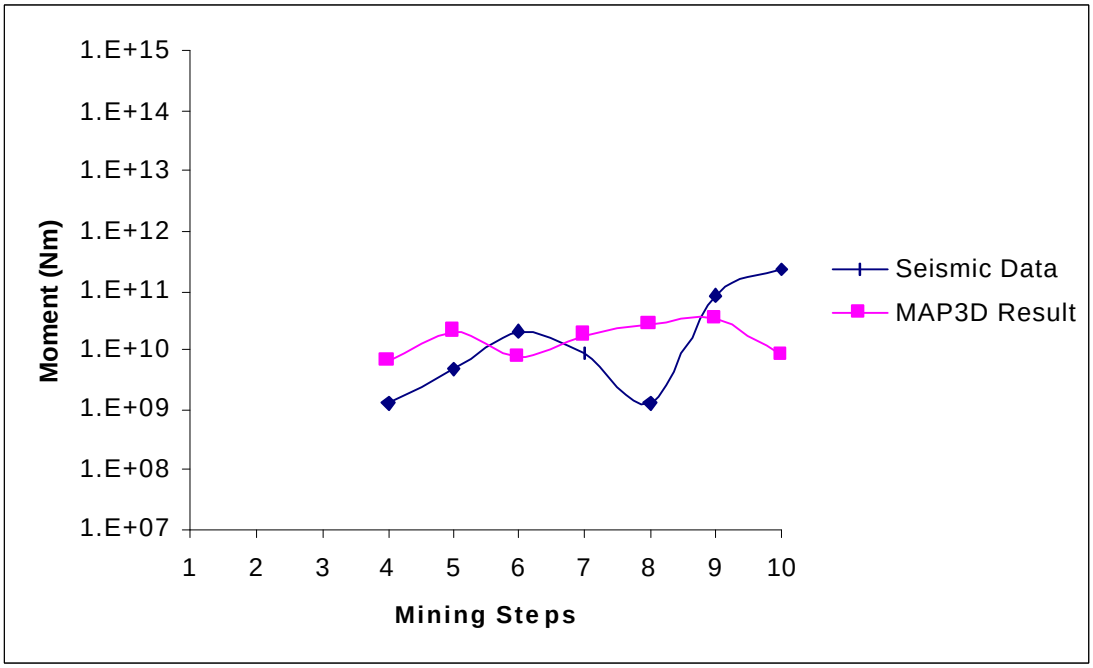

Figure 88 Relationship between 3D modelling and seismic data for the fault numbered 19 in Figure 31.

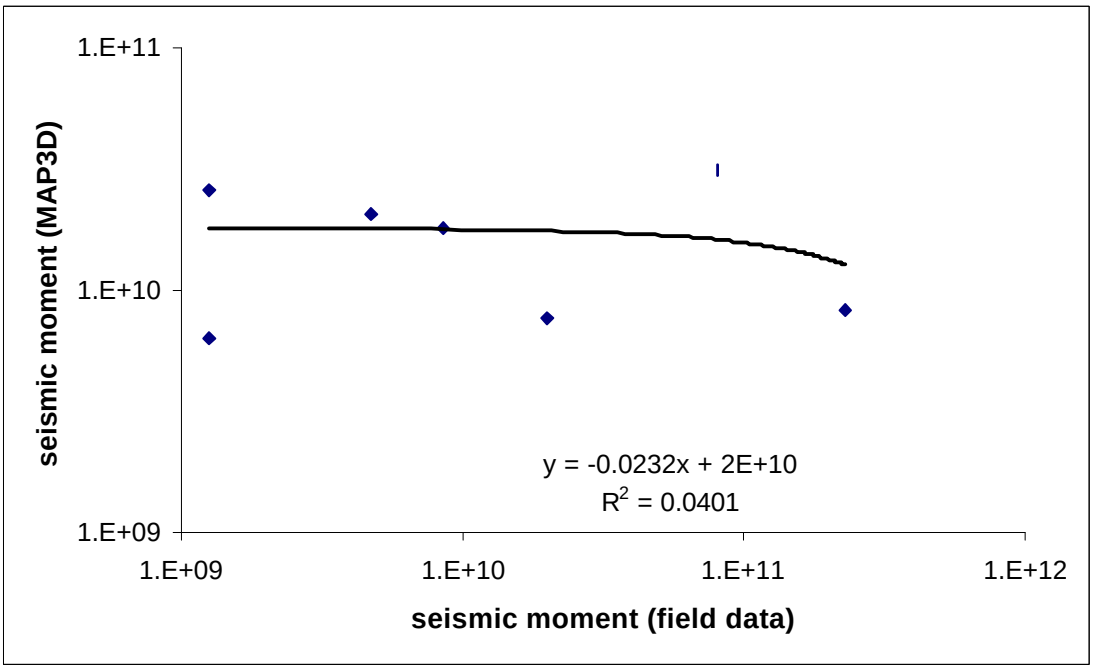

Figure 89 Correlation between field seismic moment and modelling seismic moment (MAP3D) for the fault numbered 19 in Figure 31.

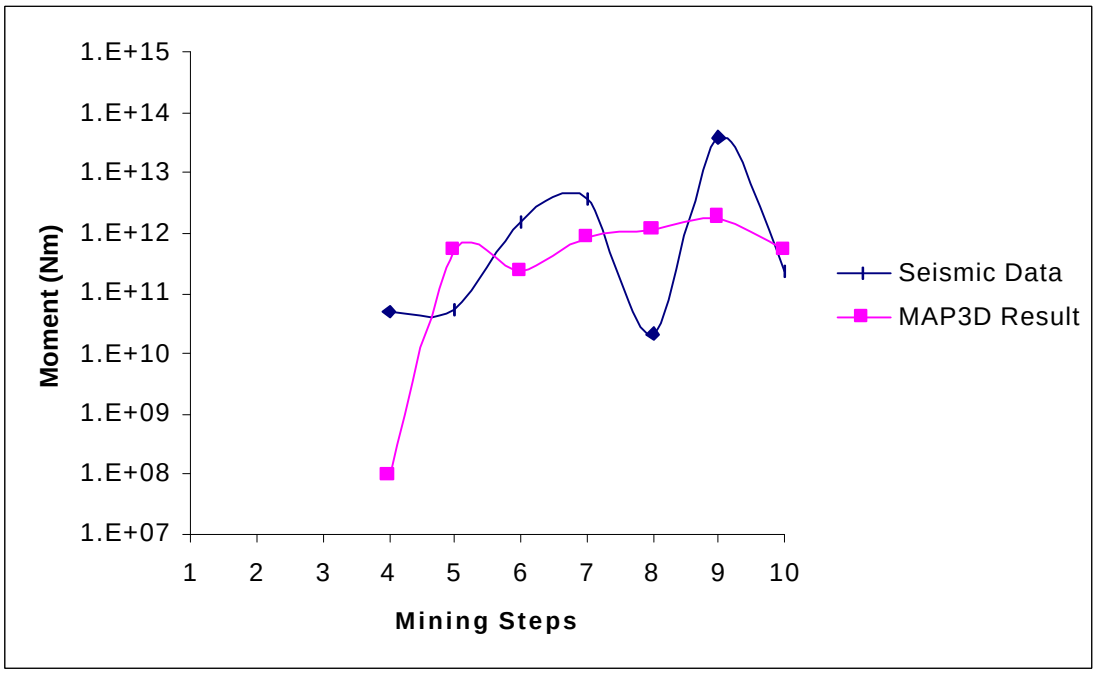

Figure 90 Relationship between 3D modelling and seismic data for the fault numbered 20 in Figure 31.

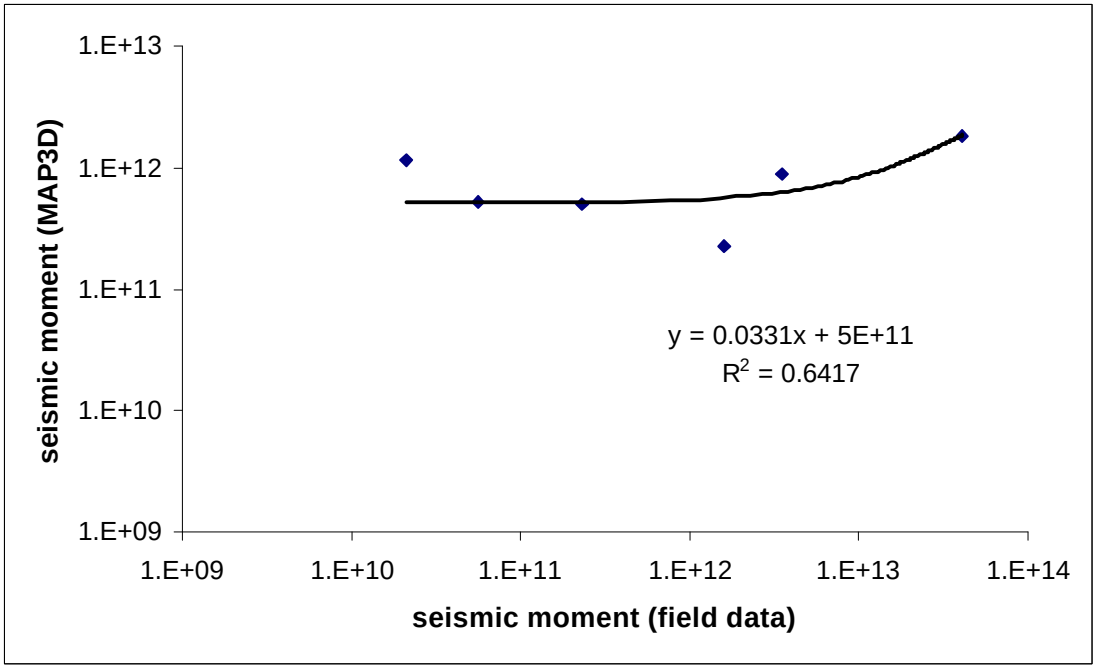

Figure 91 Correlation between field seismic moment and modelling seismic moment (MAP3D) for the fault numbered 20 in Figure 31.

Document Statistics

Today's date: 15/06/00 and current time: 01:55

Path to this document is: D:\DATA STORE\WINWORD\All_PROJECT REPORTS\SIMRAC Reports\GAP 516 FINAL REPORT\FINREP5 (Dec98).doc

Author	Fernando Vieira et al
Document's name	FINREP5 (Dec98).doc
File Size (bytes)	2908160
Created date	11-12-98 11:15 AM
Edit time	369 minutes
Number of characters in the FINREP5 (Dec98).doc	114175
Number of pages in the FINREP5 (Dec98).doc	118
Number of words in the FINREP5 (Dec98).doc	21991
The date FINREP5 (Dec98).doc was last printed	15/06/00 01:55
The date FINREP5 (Dec98).doc was last saved	23-03-99 1:03 PM
Number of times FINREP5 (Dec98).doc has been saved	38

The FINREP5 (Dec98).doc is set to be PRINTED with: HPLaserJet 4V/4MV